A MULTIFUNCTIONAL SOLAR PANEL ANTENNA FOR CUBE SATELLITES

by

Olutosin C. Fawole

A thesis submitted in partial fulfillment
of the requirements for the degree

of

MASTER OF SCIENCE

in

Electrical Engineering

Approved:

Dr. Reyhan Baktur Major Professor	Dr. Edmund Spencer Committee Member
Dr. Jake Gunther Committee Member	Dr. Mark R. McLellan Vice President for Research and Dean of the School of Graduate Studies

UTAH STATE UNIVERSITY
Logan, Utah

2012

Abstract

A Multifunctional Solar Panel Antenna for Cube Satellites

by

Olutosin C. Fawole, Master of Science

Utah State University, 2012

Major Professor: Dr. Reyhan Baktur
Department: Electrical and Computer Engineering

The basic cube satellite (CubeSat) is a modern small satellite that has a standard size of about one liter (the 1U CubeSat). Three 1U CubeSats could be stacked to form a 3U CubeSat. Their low-cost, short development time, and ease of deployment make CubeSats popular for space research, geographical information gathering, and communication applications. An antenna is a key part of the CubeSat communication subsystem. Traditionally, antennas used on CubeSats are wrapped-up wire dipole antennas, which are deployed after satellite launch. Another antenna type used on CubeSats is the patch antenna. In addition to their low gain and efficiency, deployable dipole antennas may also fail to deploy on satellite launch. On the other hand, a solid patch antenna will compete for space with solar cells when placed on a CubeSat face, interfering with satellite power generation. Slot antennas are promising alternatives to dipole and patch antennas on CubeSats. When excited, a thin slot aperture etched on a conductive sheet (ground plane) is an efficient bidirectional radiator. This open slot antenna can be backed by a reflector or cavity for unidirectional radiation, and solar cells can be placed in spaces on the ground plane not occupied by the slot. The large surface areas of 3U CubeSats can be exploited for a multifunctional antenna by integrating multiple thin slot radiators, which are backed by a thin cavity on the CubeSat surfaces. Solar cells can then be integrated on the antenna surface.

Polarization diversity and frequency diversity improve the overall performance of a communication system. Having a single radiating structure that could provide these diversities is desired. It has been demonstrated that when a probe excites a square cavity with two unequal length crossed-slots, the differential radiation from the two slots combines in the far-field to yield circular polarization. In addition, it has been shown that two equal-length proximal slots, when both fed with a stripline, resonate at a frequency due to their original lengths, and also resonate at a lower frequency due to mutual coupling between the slots, leading to a dual-band operation. The multifunctional antenna designs presented are harmonizations and extensions of these two independent works.

In the multifunctional antenna designs presented, multiple slots were etched on a 83 mm x 340 mm two-layer shallow cavity. The slots were laid out on the cavity such when the cavity was excited by a probe at a particular point, the differential radiation from the slots would combine in the far-field to yield Left-Handed Circular Polarization (LHCP). Furthermore, when the cavity was excited by another probe at an opposite point, the slots would produce Right-Handed Circular Polarization (RHCP). In addition, as forethought, these slots were laid out on the cavity such that some slots were close together enough to give Linearly Polarized (LP) dual-band operation when fed with a stripline. This antenna was designed and optimized via computer simulations, fabricated using Printed Circuit Board (PCB) technology, and characterized using a Vector Network Analyzer (VNA) and NSI Far Field Systems.

(98 pages)

Public Abstract

A Multifunctional Solar Panel Antenna for Cube Satellites

by

Olutosin C. Fawole, Master of Science

Utah State University, 2012

Major Professor: Dr. Reyhan Baktur
Department: Electrical and Computer Engineering

This work presented the design of a single antenna structure that can perform the functions of about four antennas. The antenna is to be applied on a new kind of very tiny satellites. These satellites are called CubeSats. In contrast to an ordinary antenna that works at a single frequency band, the antenna designed will be able to work at about three different usable frequencies. In addition, it will be possible to make the waves emitted by the antenna to have multiple senses of rotation or no rotation at all. The multiple functional capability of the antenna will lead to a satellite communication system with enhanced capacity. The antenna presented is based on a class of antennas called slot antennas. Slot antennas are complementary to the popular wire antennas found in many appliances. The wire antenna is a solid conductor hanging in free space, the slot antenna is a thin rectangular space cut out of a thin sheet of conductor. The slot antenna, because of its planar shape, can be easily integrated with a satellite in such a way that solar cells for satellite power generation can be placed side by side with the antenna without the two disturbing each other. In the realization of the multifunctional antenna, already established ideas on the slot antenna were further developed and combined together. This antenna was initally developed using computer software and then manufactured for demonstration.

To my father and my mother, my sister and brother, for their unconditional, unquestionable, and steadfast love.

Acknowledgments

First, I would like to thank my advisor for her unwaivering support from the time I demonstrated interest in working with her, up until the end of my work. I appreciate her understanding, and her belief in me. I believe she will still be there to offer her support even after the completion of my master's program. Her contribution towards the success of my work is invaluable and ineffable. I would also like to thank the other members of my supervisory committee, Dr. Jake Gunther and Dr. Edmund Spencer, for giving the necessary support needed for the successful completion of my work, and for finding the time to make it to my thesis defense despite their very tight schedule on that day.

I also thank Robert Burt of the Space Dynamics Laboratory for providing the insight and materials to make this work of practical sense. I also thank Trent Johnson and Scott Kimber for helping with the software tools needed in making this work. I would also like to thank Heidi Harper of the ECE store for providing the materials needed in the fabrication of this work.

My profound gratitude also goes to the members of my reseach group who lent their insight and assistance in the making of my work, from the begining to the end - Tuerxunjiang Yasin, Ali Khoshniat, Mangalam Chandak, Maryam Jamali, and MaiMaitirebike Maimaiti.

Finally, I will like to thank my friends who support me socially and emotionally throughout my stay in Logan, right from the begining till now - Abdul Zohur, Changwe Ngosa, Mangalam Chandak, Gustavo Estrada, Tejas Jadhav, and Ravi Kant. My days in Logan would not have been that bright without you. From the bottom of my heart, I wish you too the best in all your endeavors.

Olutosin C. Fawole

Contents

List of Tables

List of Figures

Chapter 1

Introduction

Cube satellites (CubeSats) are modern small satellites that are revolutionizing space research because of their small sizes and standardized architectures. The standardized architectures of CubeSats and their small sizes make it easy to manufacture CubeSats at low costs within a short period of time. Furthermore, the small sizes of CubeSats make it possible to place a number of CubeSats as secondary payloads on conventional satellites, making the deployment of CubeSats cheap and easy. CubeSats have numerous space applications - providing aerial geographic images for disaster management, providing a cheap way to test space technology before they are applied in mission-critical space applications, providing a miniature platform that allows students to learn about all systems involved in conventional spacecraft development within the short duration of their studies, providing a setup to perform biological experiment in space, and providing low-cost telecommunication access [1].

An antenna is a critical component of any wireless communication system. An antenna provides the bridge for signal translation between wired circuits and free space. A working antenna on a CubeSat will make it possible for the satellite to be tracked and controlled remotely from a ground station. Furthermore, the payload data (data from measuring space parameters, or result data from a space experiment carried out within the CubeSat) from a CubeSat can only be transmitted to a ground station via an antenna. Therefore, if the antenna system on a CubeSat fails, then the space mission will fail. In addition, antennas are important in space missions which require CubeSats to communicate with other satellites in space. Furthermore, CubeSats have the potential to provide simple low-cost telecommunication access to remote locations if an efficient antenna system could be developed for that purpose [1].

On CubeSats, which have very small sizes, antenna placement is usually a challenge because the solar cells necessary for CubeSat power generation and antennas necessary for communication usually compete with each other for the limited CubeSat surface area. Furthermore, some types of protruding antennas employed on CubeSat require deployment mechanism. An antenna deployment system complicates CubeSat design and introduces some unreliability in the CubeSat system because the deployment mechanism with its moving part is a potential source of failure. A possible solution to these two common problems is the application on a CubeSat of an antenna which could be unobtrusively integrated with the solar panel on a CubeSat, which would not compete for space with the solar cells, and which does not require a deployment mechanism. The type of antenna proposed in this thesis, which is based on the slot antenna, surmounts the aforementioned challenges of CubeSat antenna design. Using this kind of antenna, the available surface area on the CubeSat can be fully exploited to develop an antenna with multifunctional capability without affecting the power generating capacity of the CubeSat. This antenna, with its multifunctional capacity will further improve the communication capacity of the CubeSat. The functions achieved in the proposed antenna are multiple operating frequencies, multiple radiation patterns, and multiple polarizations. Importantly, the proposed multifunctional antenna offers all these desirable functions without negatively impacting solar cell placement on the CubeSat.

This thesis is organized into six chapters. Chapter 1 introduces the research presented in this thesis. Chapter 2 introduces the CubeSat, which is the practical framework of this research, with particular emphasis on the CubeSat antenna subsystem. Chapter 3 introduces the slot antenna, the antenna type upon which the multifunctional antenna is predicated. This chapter explored the elements of the slot antenna which would eventually be applied in the final multifunctional antenna design. Chapter 4 presents three different designs of the multifunctional antenna. Chapter 5 details the fabrication, and full characterization (measurements) of a multifunctional antenna design, integration of solar cells on antenna, and the placement of the antenna on the CubeSat. Chapter 6 summarizes this work and highlights the future work that could be done on the multifunctional antenna.

Chapter 2

CubeSats and their Antennas

2.1 CubeSat Overview

2.1.1 CubeSat Structure

CubeSats belong to the broad class of satellites called small satellites. Small satellites are satellites having wet mass (mass including fuel) less than 500 kg. These satellites embrace the philosophy of "Faster, Better, Smaller, Cheaper" of satellite development, and are therefore built with short lead times using cheap terrestrial Commercial Off-the-shelf Technology (COT) that permits an efficient and miniaturized design. Small satellites are classified according to their wet mass as shown in Table 2.1 [2].

The CubeSat program was started in 1999 as a collaborative effort between California Polytechnic State University's Multidisciplinary Space Technology Laboratory (MSTL) and Stanford's Space Systems Development Laboratory (SSDL). Jordi Puig-Suari of MSTL and Robert Twiggs of SSDL introduced the CubeSat specification. The most recent version of the CubeSat specification [3] defined the basic CubeSat to be a 100 mm x 100 mm x 113.5 mm cube of mass that may not exceed 1.33 kg (a CubeSat of this size is referred to as the 1U CubeSat). The CubeSat specification also allowed for double (2U) and triple (3U) CubeSat configurations with dimension change in the z-axis (227 mm for doubles and 340.5 mm for triples). The mass of the triple configuration may not exceed 4 kg. Furthermore, the CubeSat document specified the structural, electrical, operational, and testing requirements for the CubeSat. The document also specified the requirements for the standard CubeSat deployment system, the Poly Picosatellite Orbital Deployer (P-POD). With these mass specifications, the basic CubeSat belongs to the pico satellite class, while the double and triple CubeSats belong to the nano satellite class of small satellites.

Table 2.1: Classification of small satellites by wet mass.

Group Name	Wet Mass
Mini Satellite	100 - 500 kg
Micro satellite	10 - 100 kg
Nano satellite	1 - 10 kg
Pico satellite	0.1 - 1 kg
Femto satellite	<100 g

Other intermediate CubeSat sizes like 1.5U and 2.5U are also possible. CubeSats of various sizes are depicted in Fig. 2.1 [4, 5].

2.1.2 CubeSat Subsystems

The CubeSat system can be divided into the following subsystems: Power, Command and Data Handling, Altitude Determination and Control, and Communication.

Power Subsystem

The power subsystem of a CubeSat consists of solar cells and rechargeable batteries. Solar cells are placed on the surfaces of the CubeSats to tap sunlight for CubeSat power generation. The batteries are charged by the solar cells to provide power when the CubeSat is in the earth's eclipse, or during high power demands in CubeSats. Typical solar cells used on CubeSats are dual or triple junction GaAs solar cells with an average power generation of 1W each [6].

Spectrolab [7] and Emcore [8] are manufacturers of space-grade triple junction solar cells which are suited for CubeSats. Furthermore, some robust terrestrial solar cells like the Triangular Advanced Solar Cells (TASC) [9], also by Spectrolab, can be used on CubeSats as acceptable trade-offs in situations where the cost of space-grade solar cells is deemed prohibitive. The commercial space-grade solar cells, shown in Fig. 2.2 [10], typically come in dimensions of 26.62 cm squared (3.95 cm x 6.89 cm) and 29.85 cm squared (4.33 cm x 7.63 cm) [11]. Figure 2.3 gives the detailed dimension in inches of a 26.41 cm squared space-grade solar cell.

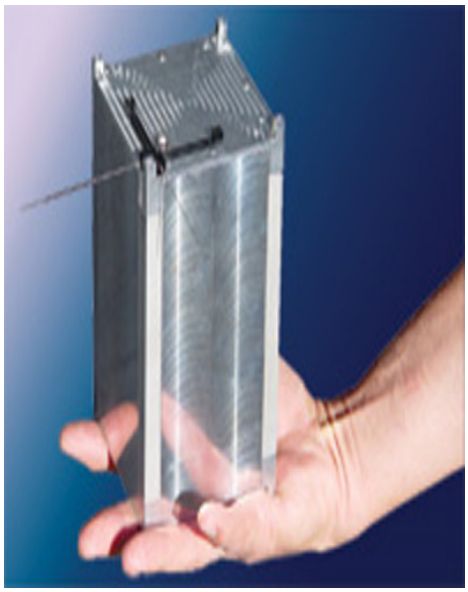

(a) A 1.5U CubeSat.

(b) A 2U and a 3U CubeSat.

Fig. 2.1: CubeSats.

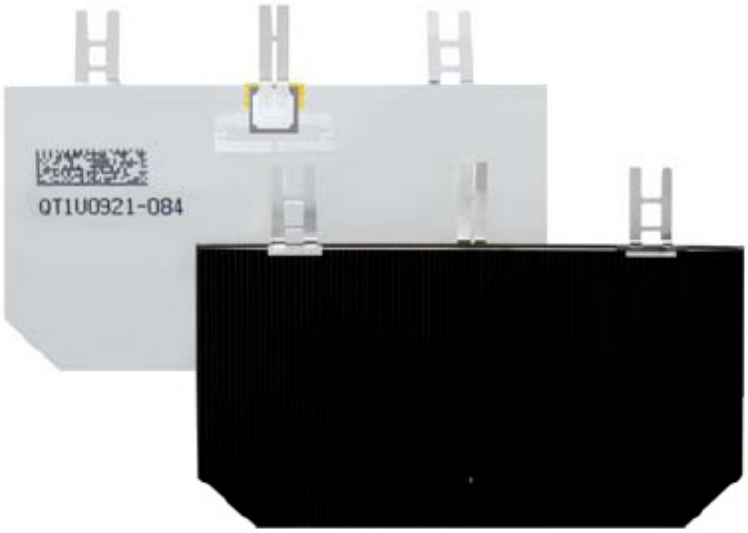

Fig. 2.2: A standard-size space-grade solar cell.

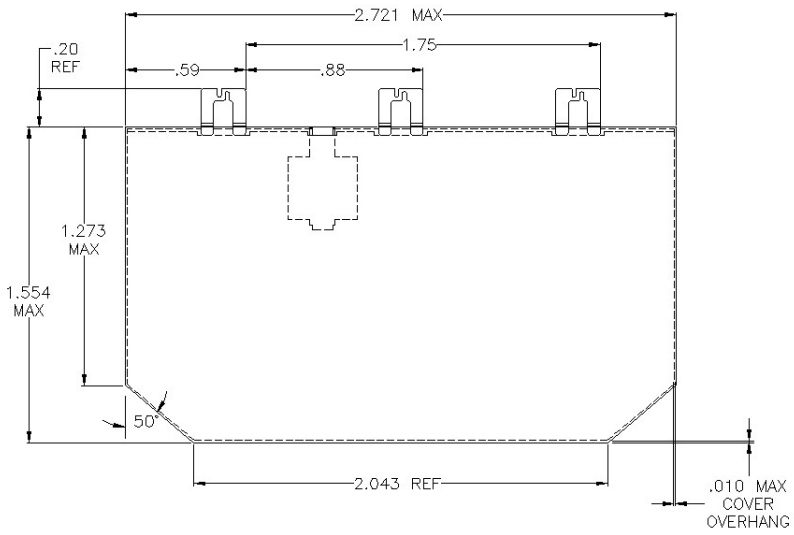

Fig. 2.3: Detailed dimension of a standard space solar cell.

Average power generation and consumption for CubeSats ranges from 2 to 6 W (time averaged) for 1 to 3U nano satellites using "body-mounted" solar panels like those shown on the CubeSats in Fig. 2.1(b) above [1]. The batteries used on CubeSats to store and deliver the generated power are usually of Lithium ion and NiMH types.

Command and Data Handling Subsystem

The Command and Data Handling (C&DH) subsystem is the central place where other CubeSat subsystems are controlled. This subsystem also handles the processing and storage of CubeSat telemetry data prior to transmission. It consists of a microprocessor and memory chips. In a CubeSats, the components of C&DH comprise commercial off-the-shelf components, which are also used in mobile phones and portable computers. This reduces the cost of CubeSat manufacture, and makes it possible for CubeSat design to exploit advances in microelectronics for a cost-efficient subsystem design.

Altitude Determination and Control

The Altitude Determination and Control (AD&C) subsystem orients the CubeSat in a direction that fulfils the mission requirement. The AD&C system employed in a CubeSat

could be passive or active. The passive AD&C uses the space environment (for example, the earth's magnetic field or gravity) to naturally orientate the CubeSat. The active AD&C system, which employs sensors and actuators, is complex to implement and requires a substantial amount of space on the CubeSat. However, it offers a higher degree of accuracy which is needed on CubeSats that requires precision pointing, like CubeSats with highly directive antennas or CubeSat for imaging and remote sensing applications [1].

Communication

The Telemetry, Tracking, and Command (TT&C) is the part of the communication subsystem of the CubeSat that handles the control information from the ground station. The communication subsystem also handles the transfer of payload data to the ground station. This subsystem consists of transceivers and antennas. The communication frequency generally used by CubeSat is in the amateur band. Typical uplink frequency is about 437 MHz in the UHF band, and uplink frequencies about 144 MHz in VHF band. The antennas typically used at these frequencies are wire antennas (dipoles, monopoles, and loops). However, for high data rate applications, like image and video transfer, higher frequency operation is desired. Therefore, some CubeSats are equipped with communication systems that operate in the special license 900 - 915 MHz band, S band (between 2 and 4 GHz) or C-band (5 GHz). This higher frequency band makes it easy to employ other antenna types like patch and slot antennas on CubeSats.

2.1.3 CubeSats in Practice

Since its introduction, CubeSat has been a hot research area. Many universities in the United States have their CubeSat program. Private companies and government agencies are also investing in CubeSat research. This is because the development time for CubeSat is short, between 12 and 18 months. Furthermore, the light weight makes it possible to deploy CubeSat at an affordable rate (commercial deployment cost about $50 000 per kg). This also makes it possible to deploy different CubeSat with different mission objectives at once with the same launch vehicle. CubeSats are deployed in the Low Earth Orbit

(LEO) at a height of less than 1000 km above the earth. Typical lifespan is CubeSat is between six months and one year, although some CubeSats like CUTE-1 of Tokyo Institute of Technology, and XI-IV of University of Tokyo operated beyond five years.

Utah State University (USU) has an active CubeSat program. In October 2011, USU launched a pair of 1.5U CubeSats, build by a USU team, into space from the Vandenberg Air Force Base in California. The CubeSats were for Dynamic Ionosphere CubeSat Experiment (DICE) to investigate the impact of ionospheric effects on communication [12]. The annual conference of small satellites, where players in the small satellite (which includes CubeSat) research and industry convene to discuss advances in the field, is held in August at Utah State University [13].

2.2 Antennas on Small Satellites

On satellites, the way antennas are positioned could determine the feasibility of a mission [14]. Antennas employed on satellites must have good aerodynamic properties. Furthermore, the material selected in designing a satellite antenna must be such that it could withstand the harsh environment of space. Furthermore, the material of the antenna should not be too bulky to add unnecessary weight to the small satellite. In addition, on small satellites that cannot spare the extra space needed for sophisticated pointing mechanism, low directivity or omnidirectional antennas are preferred because directive antennas require accurate AD&C subsystems. Furthermore, due to Faraday rotation in the ionosphere, a transmitted vertically polarized wave from space may arrive at a ground station as a horizontally polarized wave, and vice versa. Therefore, to avoid this uncertainty which will lead to a degradation in signal level due to polarization mismatch, circularly polarized antennas are sometimes preferred on small satellites. Gao et al. [15] presented detailed requirements for antennas applied in space environment. Furthermore, on smaller CubeSats, which have lower power genaration capacity, signal transission is only feasible at low fequencies. However, low frequencies can only support low data rate transmission. However, on bigger small satellites with higher power generating capacity, higher frequency antennas with higher power requirements can be employed.

2.3 Antennas on CubeSats

Below are some reviews of antennas types used or proposed specifically for CubeSats. The geometry, application, and motivation for the selection of such antenna are also discussed.

2.3.1 Linear Wire Antennas on CubeSats

Students at the University of Arizona designed a 1U CubeSat, with its communication subsystem consisting of an array of antennas meant to serve as baseline telemetry system for future CubeSat programs. The antenna system consists of a 2 m receiving dipole with a working frequency of 146 MHz, a 70 cm transceiving dipole working at 437 MHz, and a 70 cm loop antenna for beacon transmission. This beacon antenna provides a redundant means of relaying payload data in analog form if the primary (digital) transmitter fails. The flexible antennas, which are rolled-up on satellite launch, are deployed by means of a Nichrome wire, which when powered through an FET circuit, melts the nylon tying down the wire antennas [16].

The Hermes CubeSat mission by the students at Colorado University employed a monopole antenna [17]. One of the objectives of this mission is to utilize S-Band frequencies to communicate at higher data rates than those possible with traditional Ultra-High Frequency (UHF) of CubeSats [18]. A communication subsystem working at microwave S-band frequency of 2.4 GHz was proposed for higher data transmission rates (image and video transmission) which were impossible with traditional UHF. The communication subsystem antenna consists of a quarter-wavelength monopole antenna working at 2.4 GHz that would be mounted at the center of a face of the 1U CubeSat for broad radiation pattern. The gain of the antenna was below 3 dB. The monopole would be lashed to the CubeSat body using nylon wire before CubeSat launch, and would be released (using a magnetically-latched pin) by a signal from command logic 15 minutes after the satellite is ejected from the launch vehicle. Sadly, the launch vehicle that carried the Hermes CubeSat failed to reach orbit due to a malfunction.

2.3.2 Yagi-Uda Antenna on CubeSats

To improve on the low gain of dipole antennas (wire antennas) used on CubeSats, students at the University of Michigan designed a Yagi-Uda Antenna which could be integrated on an earlier designed deployable solar array prototype [19]. This eXtendable Solar Array System (XSAS) could provide an average of continuous power of 23 W, in contrast to the typical 5W of CubeSats. The XSAS designed for a 3U CubeSat, occupied a 1.5U volume, and had a length of 1.2 m when deployed. This ample space on the solar array was exploited for communication by integrating with it a 6-element Yagi-Uda antenna operating at 435 MHz. The prototyped antenna had a gain of 11.5 dBi with E- and H- plane half-power beamwidths of 46 and 58 degrees, respectively.

2.3.3 Patch Antennas on CubeSats

In order to achieve higher data transmission rates and eliminate the need for antenna deployment, a high frequency commercial off-the-shelf planar patch antenna was selected for use in the NarcisSat [20]. The 2.4 GHz 3 x 5 cm circularly-polarized patch antenna from GRE America was employed. Then antenna has a peak gain of 8.7 dB and a beamwidth of approximately 60 degrees. However, the high gain of the antenna required a pointing mechanism to direct the beam of the antenna to the ground. More importantly, since the planar patch has to be placed on the CubeSat, it will displace some solar cells, thereby reducing the amount of power available on the CubeSat.

The USUSAT nano satellite (not a CubeSat) built by students at Utah State University, weighed 15 kg, It was one of the three-constellation satellite to study density structures and irregularities in the ionosphere. For the communication subsystem, two patch antennas were designed, one for uplink at 0.45 GHz and another for downlink at 2.2 GHz. The antennas used are square patch antennas loaded with dielectric for miniaturization, and trimmed at the edges for circular polarization. The uplink antenna had a dimension of 4.2 x 4.2 inches square. The downlink antenna had dimensions of 0.8 x 0.8 inches square and a measured gain of 4.9 dB [21]. These nano satellite antennas could easily be adapted for CubeSat applications. As usual, these patch antennas would displace the solar cells,

reducing CubeSat power generating capacity.

Furthermore, transparent meshed patch antennas for use on CubeSats have been investigated [22, 23]. These antennas consist of a grid of conductive lines (meshes) printed on transparent substrates. These antennas achieved a transparency of more than 90 percent while maintain radiation properties comparable to that of a solid patch antenna. Commercial solar cells can be easily integrated with such antennas with no substantial reduction in the power generating performance of the solar cells. This antenna type can be easily applied on a CubeSat.

2.3.4 Helical Antenna on CubeSats

Muri et al. [24] proposed a deployable helical antenna for CubeSat application. The 2.45 GHz antenna is 21.8 cm tall, has a reflector diameter of 12.5 cm, has 7 turns, and a gain of 13.2 dBi and a half-power beamwidth of 60 degrees. This antenna, been helical, is naturally circularly polarized.

2.3.5 Slot Antennas on CubeSats

Mahmoud [25] studied the feasibility of using solar cells integrated with cavity-backed slot antennas on the same solar panel of a CubeSat. The slot antenna consists of a thin slot etched on a ground plane. The face of a solar panel could doubled as the ground plane of the slot antenna. Solar cells could then be placed on the ample space on the ground plane not occupied by the slots. Mahmoud demonstrated how the cavity-backed slot antenna could be arranged and excited to achieve linear polarization, circular polarization, dual-band operation, and reconfigurability.

2.4 Limitations of Traditional CubeSat Antennas and Possible Solutions

The deployable CubeSat antenna systems (linear wire antenna, the Yagi-Uda antenna, and helical antenna) discussed above have the drawback of being difficult to produce mechanically because of the deployment system. These deployable antennas are usually held down or folded to the CubeSat body before launch by a nylon tape. The nylon tape is then

melted by passing an electric current through a Nichrome wire. This deployment mechanism is a potential source of unreliability in the CubeSat system. On the other hand, the use of solid patch antenna means that it is impossible to place solar cells in places occupied by the opaque patch antennas. Therefore, the patch antenna option will reduce the power generating capacity of the CubeSat system. Also, the discussed optically transparent patch antennas have very low efficiency and gain, and research of this type of antenna is still in its infancy. Moreover, complex antenna configuration for enhanced communication capacity is very challenging using these transparent antennas.

This thesis explores a new kind of antenna structure for an enhanced CubeSat performance - a slot antenna-based multifunctional radiator. The slot antenna is an excellent antenna type for CubeSat application because solar cells and slot antennas could be integrated on the same panel with negligible interaction between the two. Furthermore, ample space on the cavity-backed slot antenna could be further exploited to realize a complex antenna configuration with multifunctional capacity. Also, a slot antenna backed by a thin cavity has good aerodynamic properties making it suitable for space applications.

Chapter 3

Slot Antennas

3.1 Slot Antenna Fundamentals

The Babinet principle from optics laid the foundation for the relationship between wire antennas and slot antennas (aperture antennas). This optical principle stated that when the field due to a source behind a screen with an opening is added to the field of a complementary structure, the sum is equal to the field when there is no screen [26]. For example, consider a non-reflecting black screen with holes and obstruction, and another screen with the holes and obstructions in the first screen interchanged (the complementary screen), the disturbance produced behind each of the two screens by the same optical source will add up to give a disturbance that equals the case in which no screen is present [27].

Booker extended this optical theorem to radio engineering by considering radiating conducting screens and the polarization of their radiations. Booker's extension established that an electric current source in front of an infinite sized perfectly conducting sheet with an aperture (slot) and a magnetic source in front of a perfecting conducting wire (the complementary screen) produce fields that sum up to give a disturbance as if no screen were present. Booker extension established that the wire antenna (dipole) is complementary to the slot antenna. This extension also established the impedance and radiation pattern relationship between an aperture in a thin perfect electric conductor sheet (the slot antenna) and its complementary screen (the wire antenna).

The radiation pattern for a slot antenna is similar with that of the complementary dipole; however the E plane for a dipole is the H plane for the slot, and vice versa. Furthermore, when a slot is mounted vertically, its electric field is horizontally polarized, while the polarization of a vertically-mounted dipole is vertically polarized.

3.2 The Open Slot

However, the Babinet principle and the Booker extension do not apply when finite-sized screens are involved. For example, when a finite-sized screen with an aperture is illuminated by a source, the edge of the screen acts as diffraction sources, and contributes substantially to the field behind the screen. Therefore, the sum of the fields behind the screen and that behind the complementary screen would not add up to give the field as if no screens were present.

Therefore, as a result of this diffraction effects, the half-wavelength slot on a finite ground plane is observed to be a high-gain high-efficiency bidirectional radiator with gains in excess of 5 dB [28]. This is disparate from the expected gain of about 2.15 dB, which is the gain of a complementary half-wavelength dipole.

Figure 3.1 shows a half-wavelength slot antenna at 2.5 GHz on a square ground plane of size one lambda squared (120 mm x 120 mm). The antenna, like all subsequent designed antennas in this thesis, was modeled and simulated with High Frequency Structural Simulator (HFSS), a commercial Finite Element/ Integral method Solver provided by ANSYS [29]. The slot is 60 mm long, and 1 mm thick, and it is fed with a 50 Ohm lumped port (to mimic a coaxial excitation) at an offset position of 25 mm (rather than at the center) to match the slot antenna to a 50 Ohm line [30].

The return loss and the radiation pattern of the slot are given in Fig. 3.2 and Fig. 3.3, respectively. The slot has a bidirectional radiation with a gain of 5 dB, and with H-plane and E-plane beamwidth of 60 degrees and 48 degrees, respectively. The effects of varying the physical parameters of the open slot on its impedance and radiation characteristics have been investigated [28].

The slot antenna setup is further investigated, now with a microstrip feed line as shown in Fig. 3.4. The microstrip feed, in contrast with coaxial excitation, is preferred in some antenna structures because it can be easily fabricated using planar technology. The slot antenna in Fig. 3.1 is now excited using a microstrip line. The microstrip line is printed on the bottom surface of a dielectric material. In this simulation setup, the material used

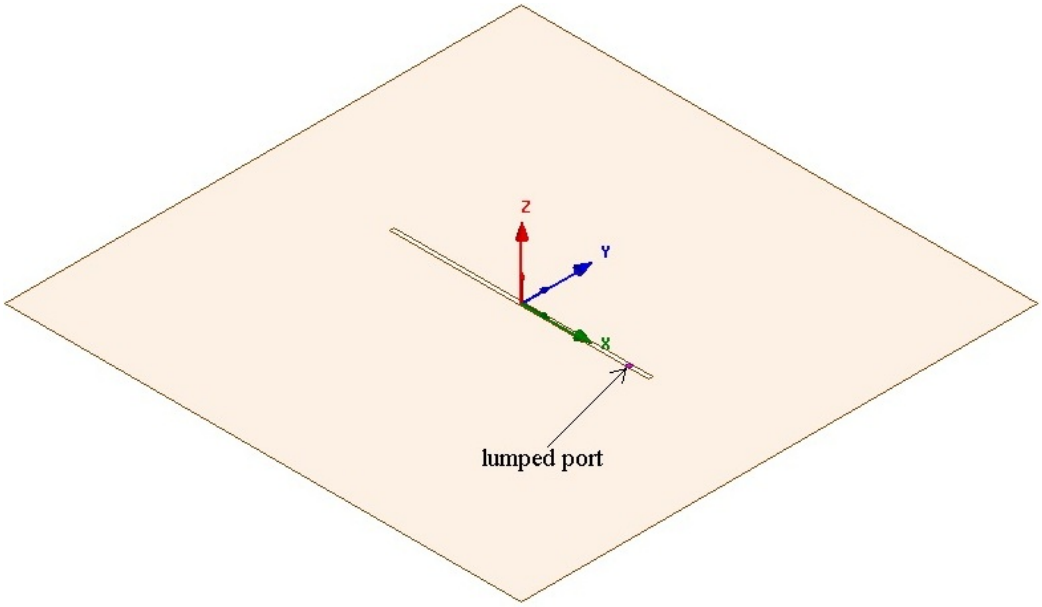

Fig. 3.1: A simple slot antenna.

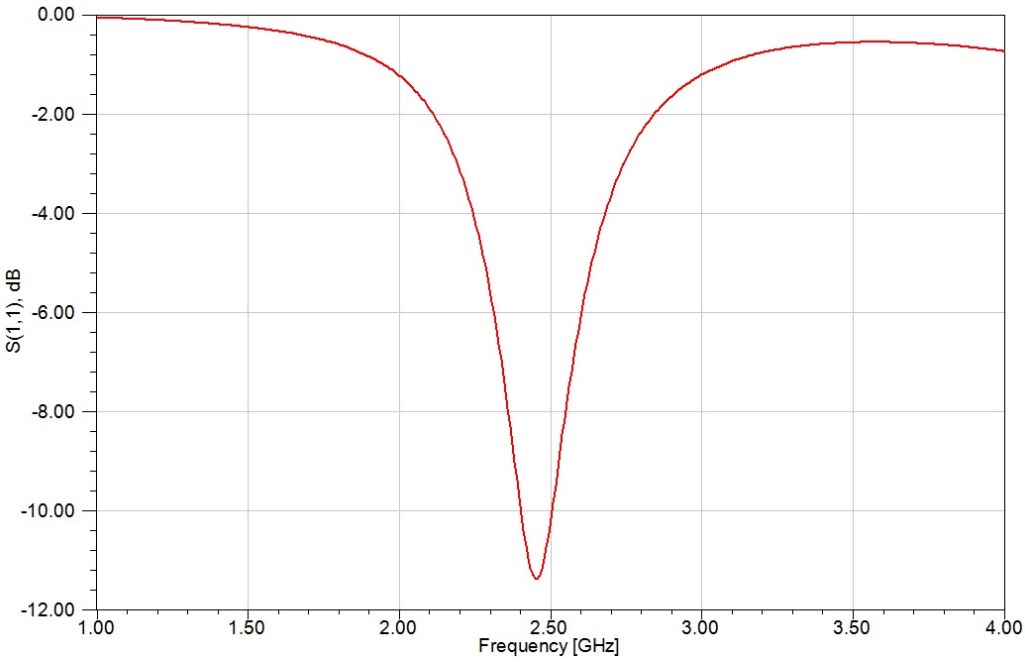

Fig. 3.2: The return loss of a simple slot antenna.

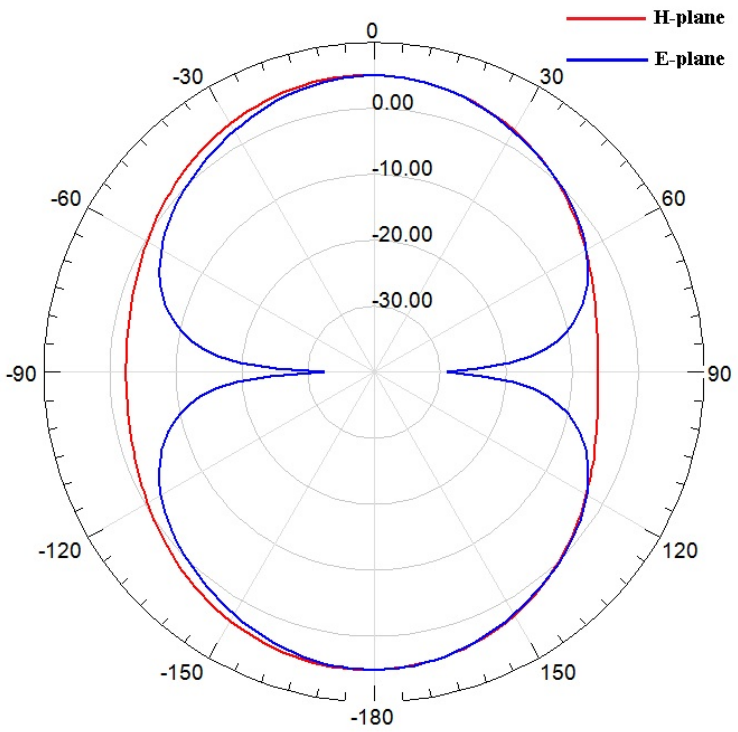

Fig. 3.3: The radiation pattern of a simple slot antenna.

is Rogers RT/duroid 5880 with relative permittivity 2.2 and thickness 1.575 mm [31]. The microstrip line was simulated with ADS linecalc [32] for an impedance of 50 Ohm. The width of the microstrip that gives a 50 Ohm impedance at 2.5 GHz is 4.3 mm. The half-wavelength slot antenna was cut out of the Perfect Electric Conductor (PEC) ground plane on the substrate. The half-wavelength in this case is calculated by factoring in the dielectric substrate effect into the free space effect. The substrate increases the effective dielectric constant of the antenna setup, resulting in a lower wavelength at 2.5 GHz. Therefore, the half wavelength slot is now 50 mm long, its thickness is still 1 mm. The center of the microstrip line is offset from the center of the slot by 20 mm, and the length of the microstrip line extends 20 mm beyond the edge of the slot to ensure matching the slot to the microstrip line. The ground plane is 120 mm by 120 mm square PEC. The simulation result for this structure is presented in Fig. 3.5 and Fig. 3.6 below. The gain of the antenna is 6 dB, with H-plane and E-plane beamwidth of 92 degrees and 72 degrees, respectively.

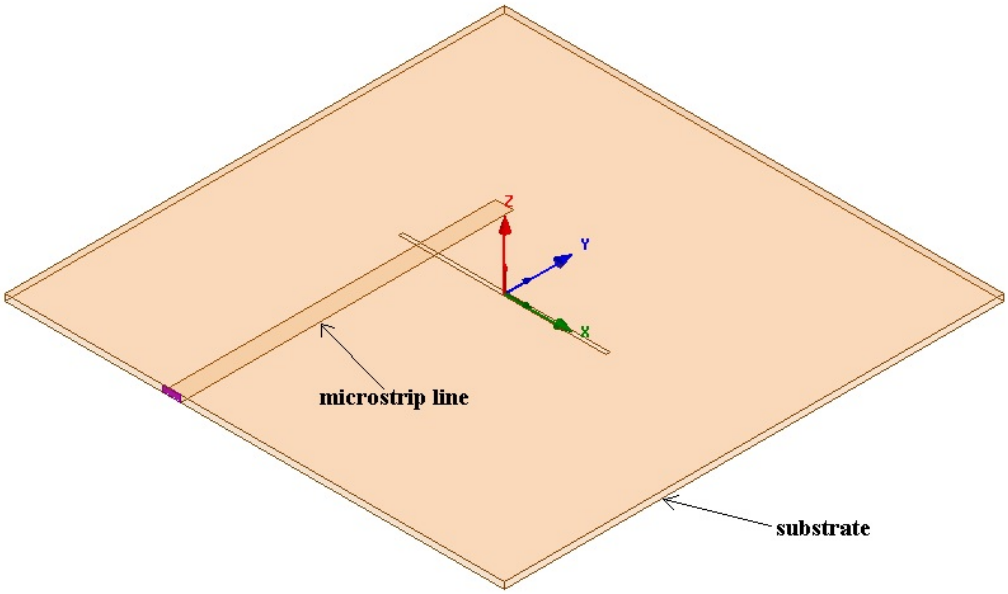

Fig. 3.4: A microstrip line-fed slot antenna.

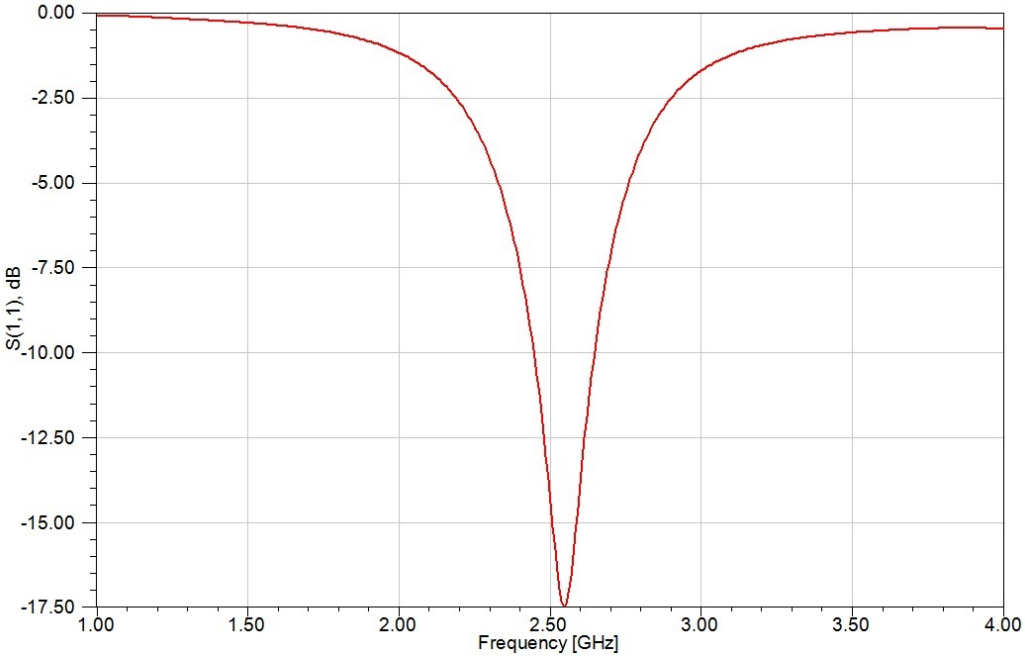

Fig. 3.5: The return loss of a microstrip line-fed slot antenna.

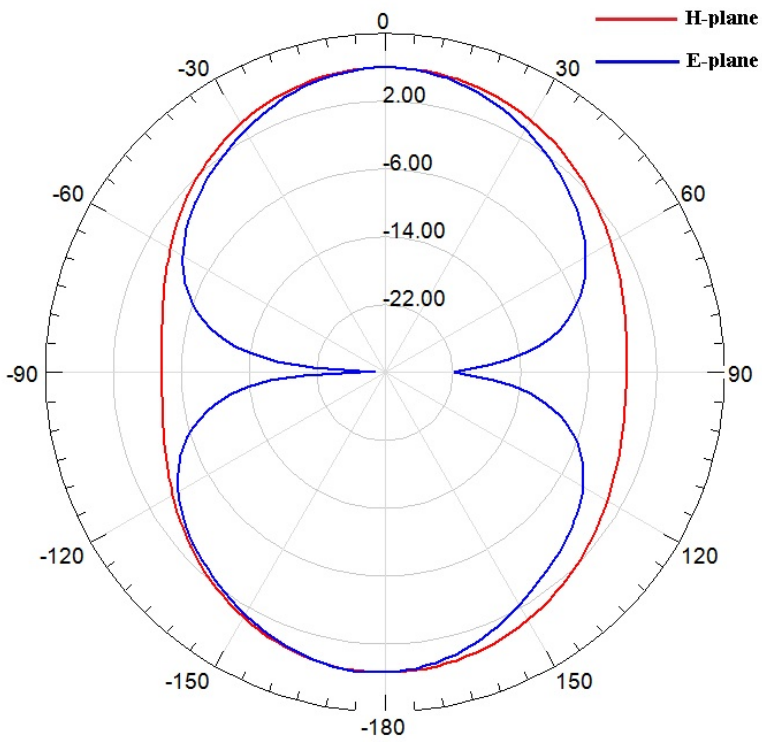

Fig. 3.6: The radiation pattern of a microstrip line-fed slot antenna.

3.3 The Reflector-Backed Slot Antenna

Sometimes, it is undesirable to have a slot antenna radiate bidirectionally. For example, when a slot is placed on a CubeSat surface, it is desired that the radiation goes out into space, and not into the electronics inside the CubeSat. Moreover, an antenna that radiates bidirectonally will have its radiation blocked when mounted near or on metallic surfaces. This obstruction would affect an antenna's impedance. Therefore, to make the slot antenna suitable for numerous practical applications, the slot antenna has to be backed by a reflector or a cavity.

According to Yoshimura [33], the reflector for a slot antenna should be placed at a distance of a multiple of one- or three-quarter wavelength of the operating free space wavelength of the slot antenna for easy matching, maximum beamwidth, and maximum front-to-back ratio. [1]

[1] The power gain ratio between the forward gain and backward gain of a directional antenna.

The properties of the antenna, shown earlier in Fig. 3.1 above, is investigated with respect to different reflector spacings. Figure 3.7 shows the matched slot antenna above but with a reflector added at a spacing of one-quarter wavelength below the slot ground plane. The simulation results are presented in Fig. 3.8 and Fig. 3.9. The structure has a forward gain of 7.94 d, with front-to-back ratio of 11 dB. The E-plane and H-plane beamwidth are 46 and 84 degrees, respectively.

A reflector spacing of half-lamba was also simulated. It was observed that the resonance frequency shifted from 2.5 GHz to 2.38 GHz. The forward gain was 4.57 dB, the front-to-back ratio was 3.37 dB. The H-plane and E-plane beamwidths were 128 degrees and 112 degrees, respectively.

Figure 3.10 and Fig. 3.11 show the simulation result with one-lambda spacing. The resonance frequency is now 2.425 GHz, the forward gain is 5.75 dB, with front-to-back ratio 1.81 dB. The H plane and E-plane beamwidths are about 90 degrees.

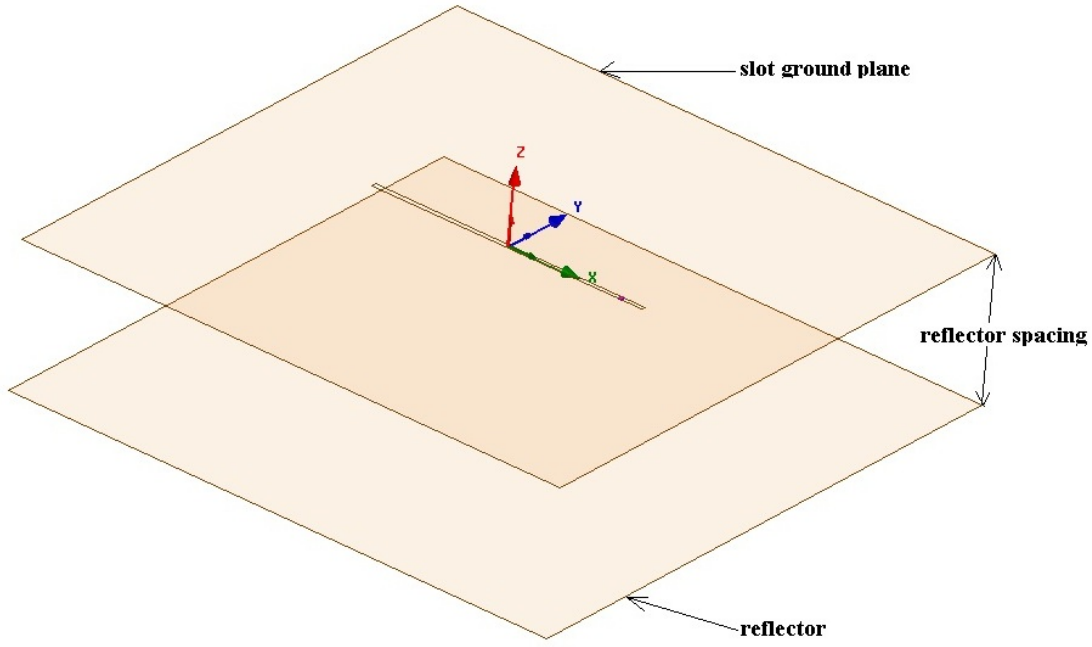

Fig. 3.7: A simple slot antenna with a quater wavelength reflector spacing.

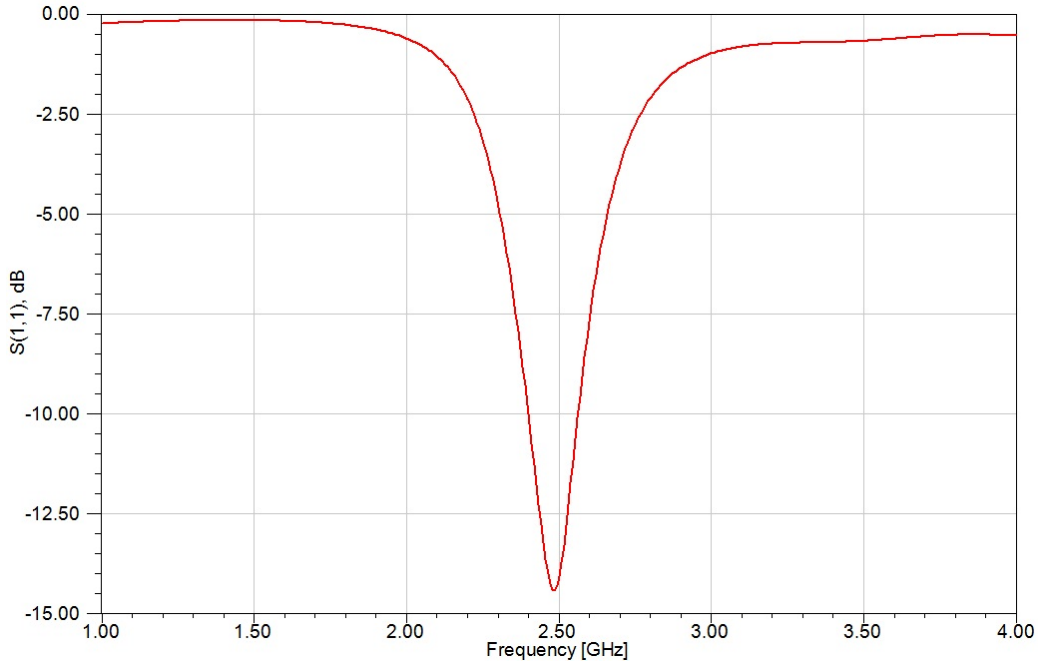

Fig. 3.8: The return loss of a simple slot antenna with a quater wavelength reflector spacing.

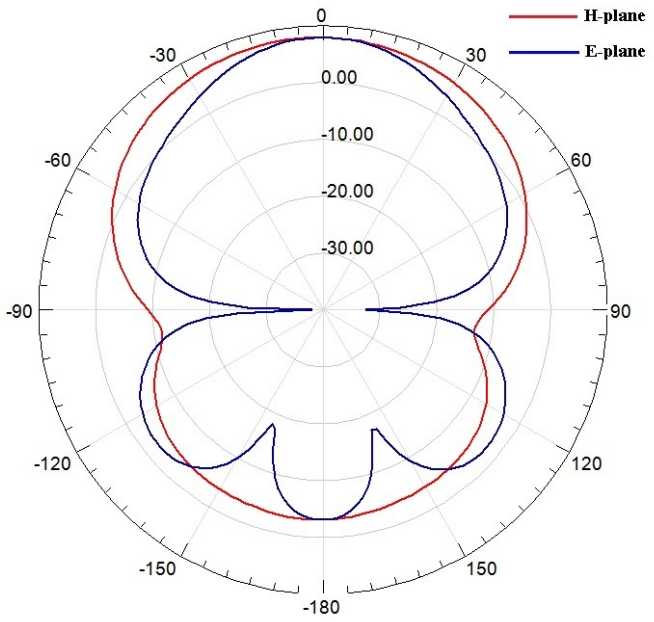

Fig. 3.9: The radiation pattern of a simple slot antenna with a quater wavelength reflector spacing.

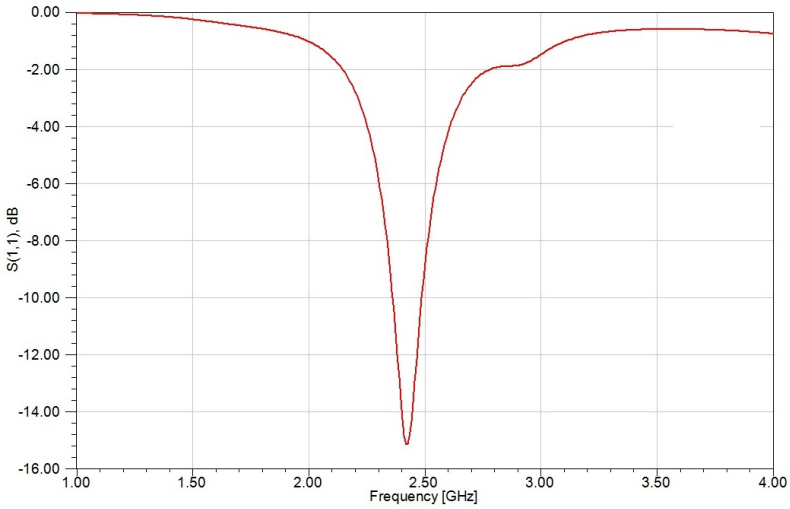

Fig. 3.10: The return loss of a simple slot antenna with one wavelength reflector spacing.

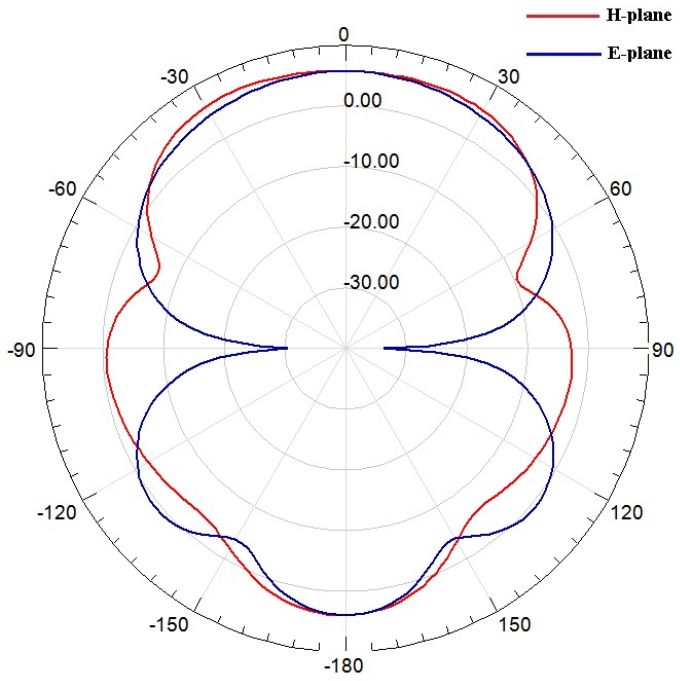

Fig. 3.11: The radiation pattern of a simple slot antenna with one wavelength reflector spacing.

It can be seen from this study that the further away the reflector is from the ground plane, the less its capability to reflect the back radiation forwardly. In addition to this drawback, the widely space reflector would result in a bulky antenna. Therefore, a practical slot antenna, with a reflector, that occupy minimal space was also investigated. The antenna structure with a reflector spacing of 3 mm (0.025 lambda) is shown in Fig. 3.12. The simulation results are presented in Fig. 3.13 and Fig. 3.14. Decreasing the reflector spacing to lambda 0.025 increases the forward gain to 9.3 dB, the front to back ratio of 16.3 dB. The beam width (both E-plane and H-plane) is 48 degrees. However, the very close reflector introduces extra resonances in the antenna return loss, and the frequency bandwidth of the antenna resonance is also reduced. Nevertheless, the increased gain and the conformal nature of this structure make it an attractive antenna type.

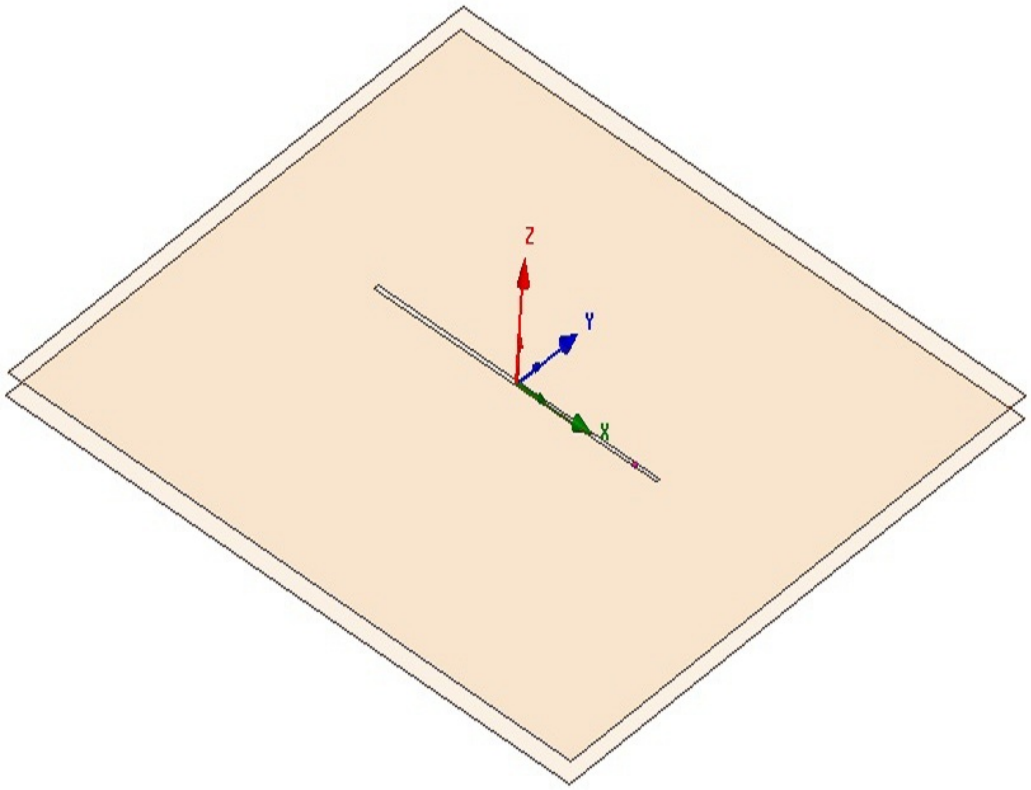

Fig. 3.12: A simple slot antenna with 0.025 wavelength reflector spacing.

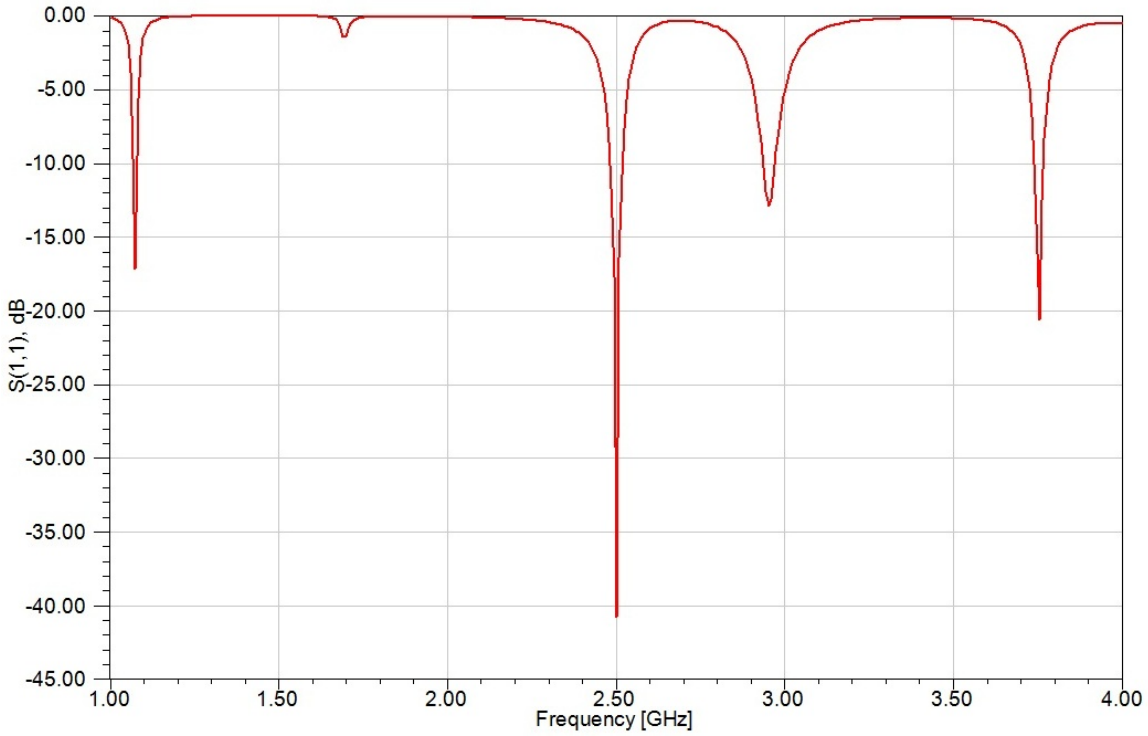

Fig. 3.13: The return loss of a simple slot antenna with 0.025 wavelength reflector spacing.

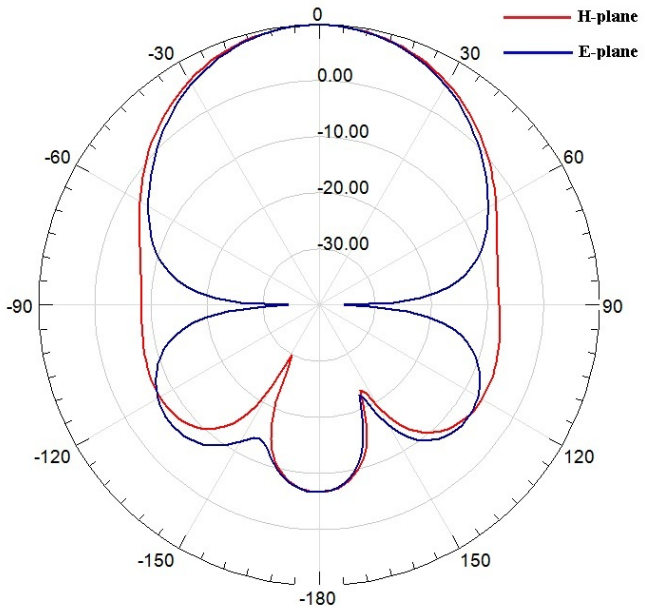

Fig. 3.14: The radiation pattern of a simple slot antenna with 0.025 wavelength reflector spacing.

The microstrip-fed slot antenna backed by a reflector was also investigated. For a quarter-wavelength reflector spacing, the forward gain is 7.7 dB and the front-to-back-ratio is 10.5 dB. The H-plane and E-plane radiation patterns have 96 degrees and 48 degrees beamwidths, respectively. For half-wavelength reflector spacing, the forward gain is 2.63 dB, the front-to-back ratio is 0.83. The E-plane and H-plane beamwidth are 148 degrees and 132 degrees, respectively. For one-wavelength spacing, the forward gain is 4.3 dB, the front to back ratio is 0.7dB. Both E- and H-plane beamwidths are both around 106 degree. The case of a very close spacing reflector shown in Fig. 3.15 is also investigated. The reflector has a spacing of 0.025 lambda (3 mm). The simulated results are shown in Fig. 3.16 and Fig. 3.17. The forward gain was 9.3 dB, the front-to-back ratio is 11 dB. The E-plane and H-plane beamwidths are 80 degrees and 42 degrees, respectively.

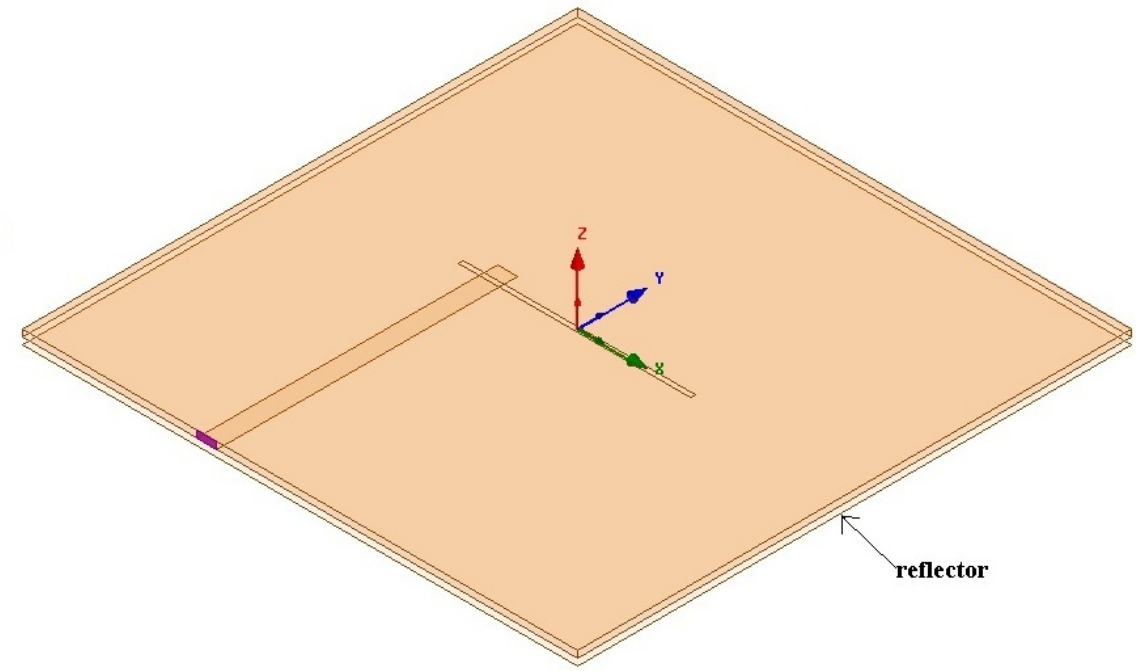

Fig. 3.15: A simple microstrip line-fed slot antenna with 0.025 wavelength reflector spacing.

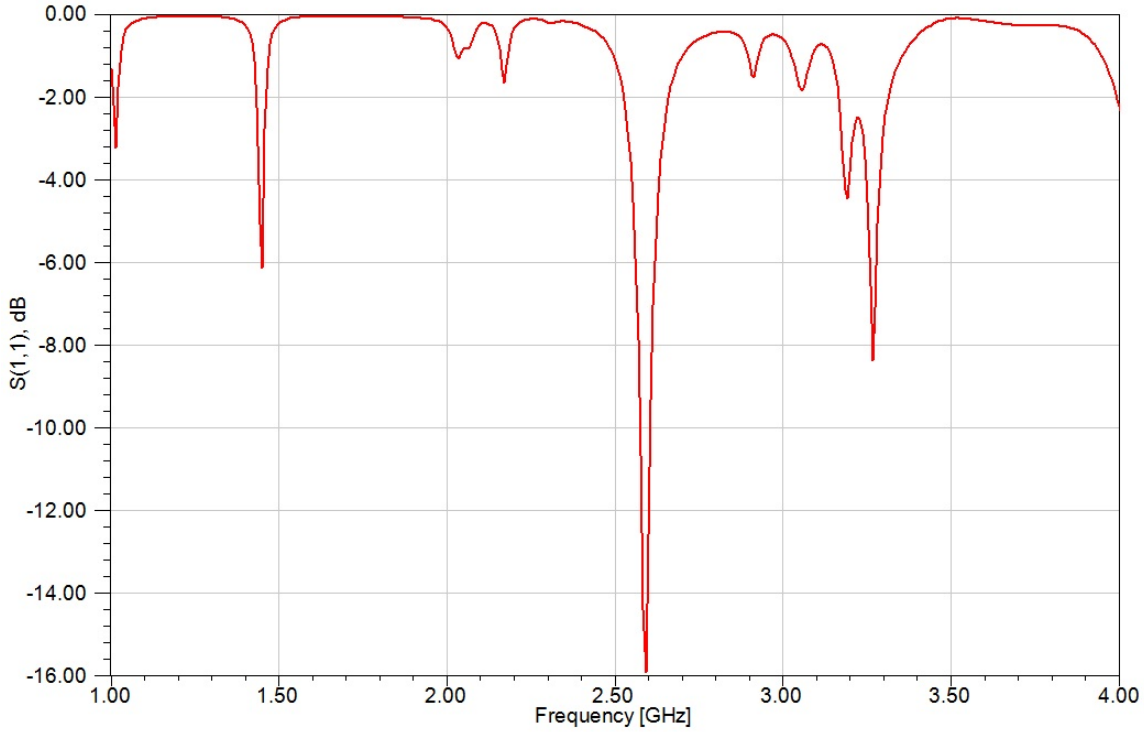

Fig. 3.16: The return loss of a simple microstrip line-fed slot antenna with 0.025 wavelength reflector spacing.

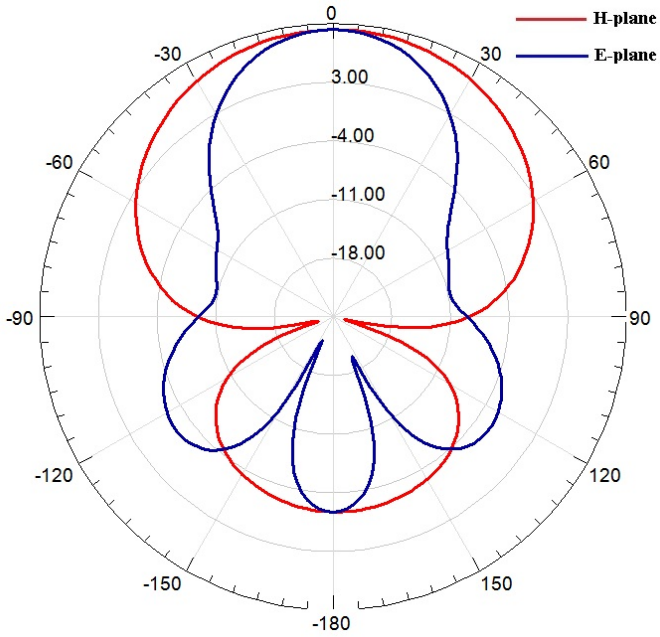

Fig. 3.17: The radiation pattern of a simple microstrip line-fed slot antenna with 0.025 wavelength reflector spacing.

The effect of reflector spacing for a microstrip-fed is like that of a wave-port fed slot. It is worth mentioning that the feed offset length was 5 mm for the 0.025 wavelength reflector spacing to achieve matching. For the other above mentioned reflector spacing variations, other antenna parameters were left the same. Therefore, a reflector backed slot antenna with good properties can be obtained using very close reflector spacing.

3.4 The Cavity-Backed Slot Antenna

A slot antenna can be backed by a cavity instead of a reflector for a structually robust design. Figure 3.18 shows the slot antenna in Fig. 3.4 above now backed with a metallic cavity that is a quarter-wavelength lambda deep. The slot antenna is excited by a stripline supported by a dielectric substrate. Then the slot with the substrate is surrounded by metallic sidewalls and a base to form a quarter-wavelength-deep air-filled cavity as shown in Fig. 3.18. The simulated return loss and radiation pattern of this structure is presented in Fig. 3.19 and Fig. 3.20. At 2.18 GHz, the structure has a forward gain of 6.8 dB, a front-to-back ratio of 13.6 dB. The E- and H-plane beamwidth are 90 degrees and 75 degrees, respectively.

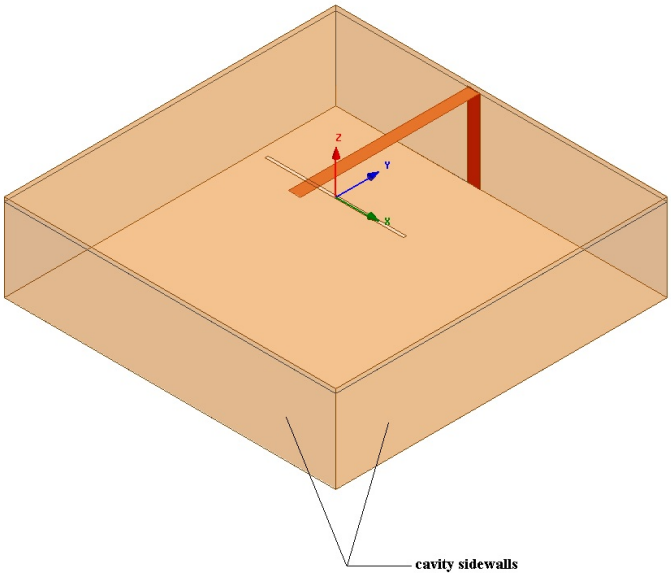

Fig. 3.18: A cavity-backed slot antenna with a quater wavelength deep cavity.

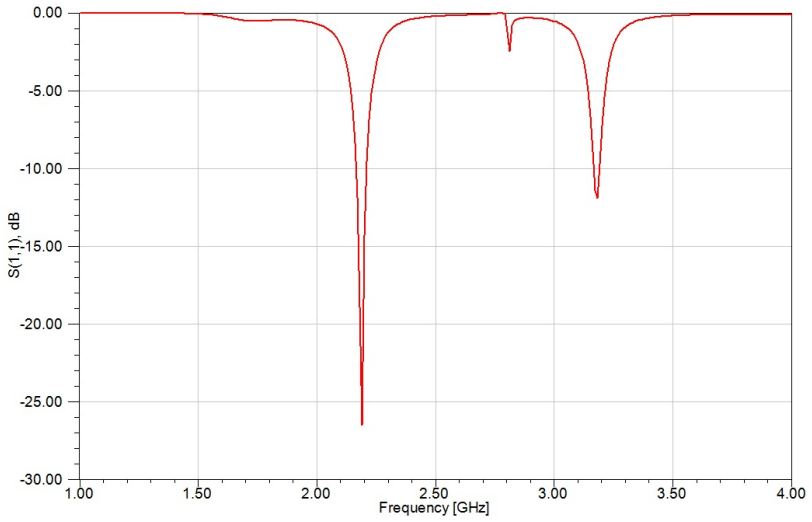

Fig. 3.19: The return loss of a cavity-backed slot antenna with a quater wavelength deep cavity.

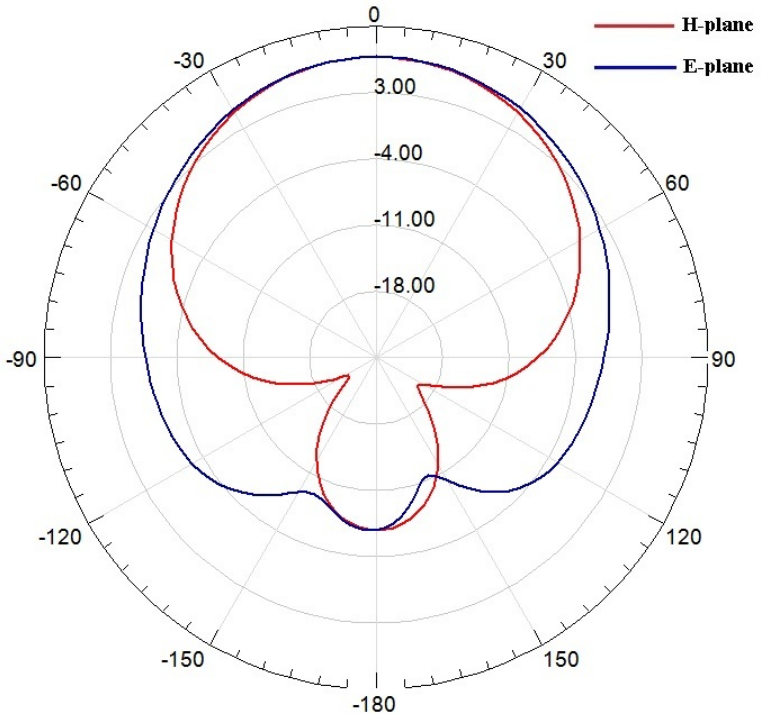

Fig. 3.20: The radiation pattern of a cavity-backed slot antenna with a quater wavelength deep cavity.

In order to obtain a structure that is robust and that could be fabricated easily using planar technology, an all dielectric-filled cavity was investigated. It would consist of two layers of dielectric material. The slot would be etched on the standard top copper layer of substrate one, and the bottom copper layer of this substrate will be removed. The feed line (stripline) will be printed on the top copper surface of substrate two, the bottom copper of this substrate would be left intact. The two substrate would then be firmly pressed together, and their sides surrounded with a conductive tape to form a full cavity-backed structure. The model of this conformal dielectric-loaded cavity-backed slot antenna is shown in Fig. 3.21. The simulation results are presented in Fig. 3.22 and Fig. 3.23. At 2.52 GHz, the structure has a forward gain of 7.2 dB, a front-to-back ratio of 13 dB, and E- and H-plane beamwidths of 90 degrees and 72 degrees, respectively.

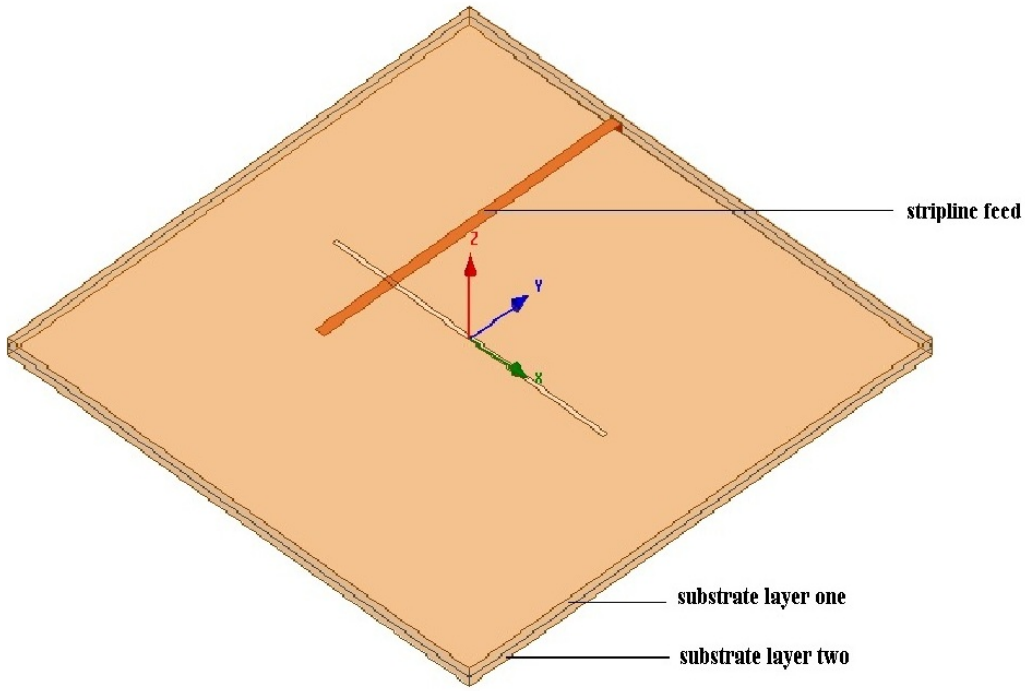

Fig. 3.21: A thin cavity-backed slot antenna.

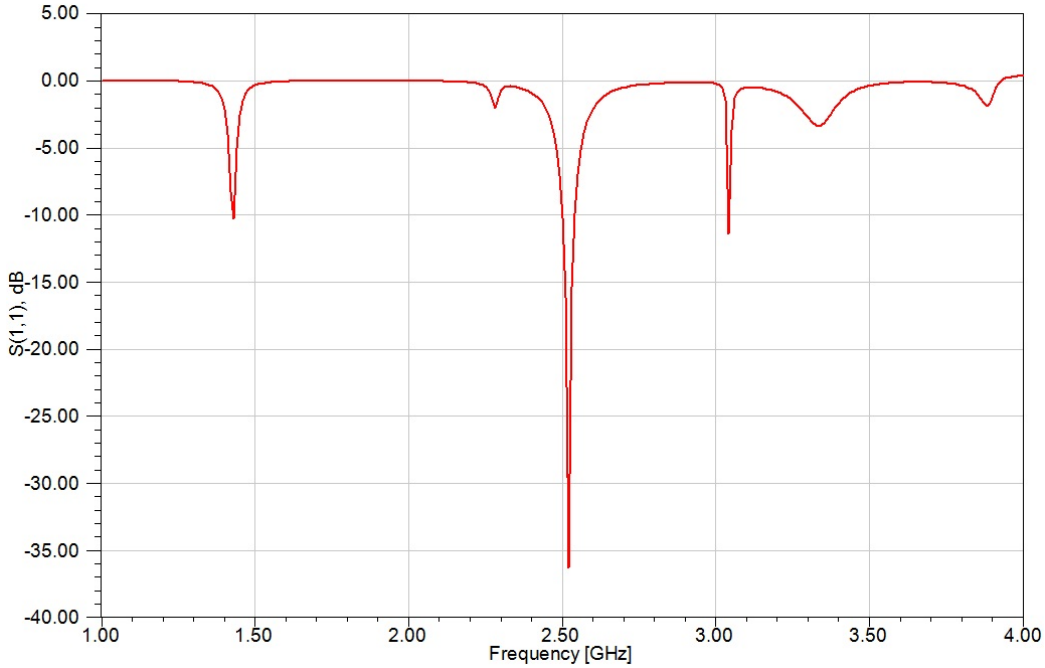

Fig. 3.22: The return loss of a thin cavity-backed slot antenna.

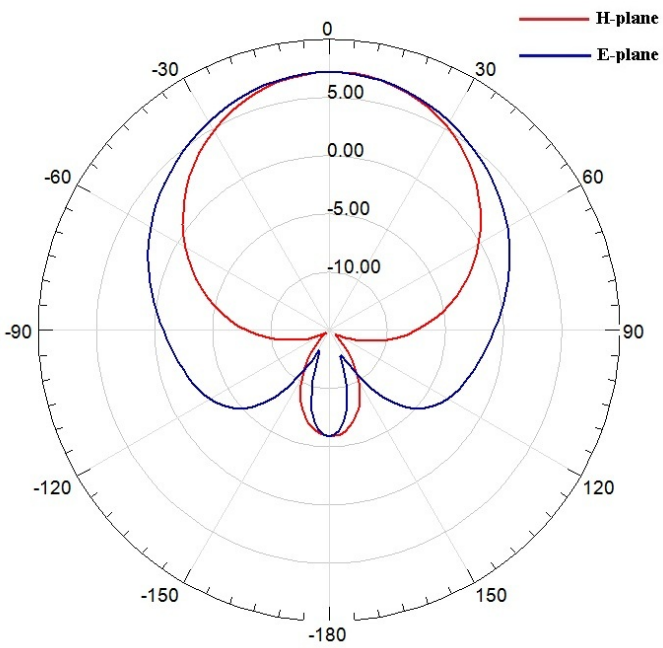

Fig. 3.23: The radiation pattern of a thin cavity-backed slot antenna.

3.5 Cavity-Backed Slot Antenna Excitation

In addition to using a stripline within the cavity structure, the dielectric-loaded cavity-backed slot antenna could also be excited using a probe as shown in Fig. 3.24. The probe could be the inner conductor of a coaxial cable whose inner conductor passes through the dielectric loading, and shorts to the top ground plane of the antenna where the slots are located. The outer coaxial conductor terminates at the bottom ground plane of the antenna. The probe would excite the cavity, which would in turn excite the slot. The probe is matched to the antenna structure by moving its position on the cavity relative to the slot. With a probe feed excitation, a single layer of dielectric is enough. The simulation result of the antenna in Fig. 3.21, with the stripline feed substituted with a probe excitation is presented in Fig. 3.25 and Fig. 3.26. At 2.5 GHz, the forward gain was 7.54 dB, the front-to-back ratio was 11.5 dB. The E-plane and H-plane beamwidths are 86 and 75 degrees, respectively.

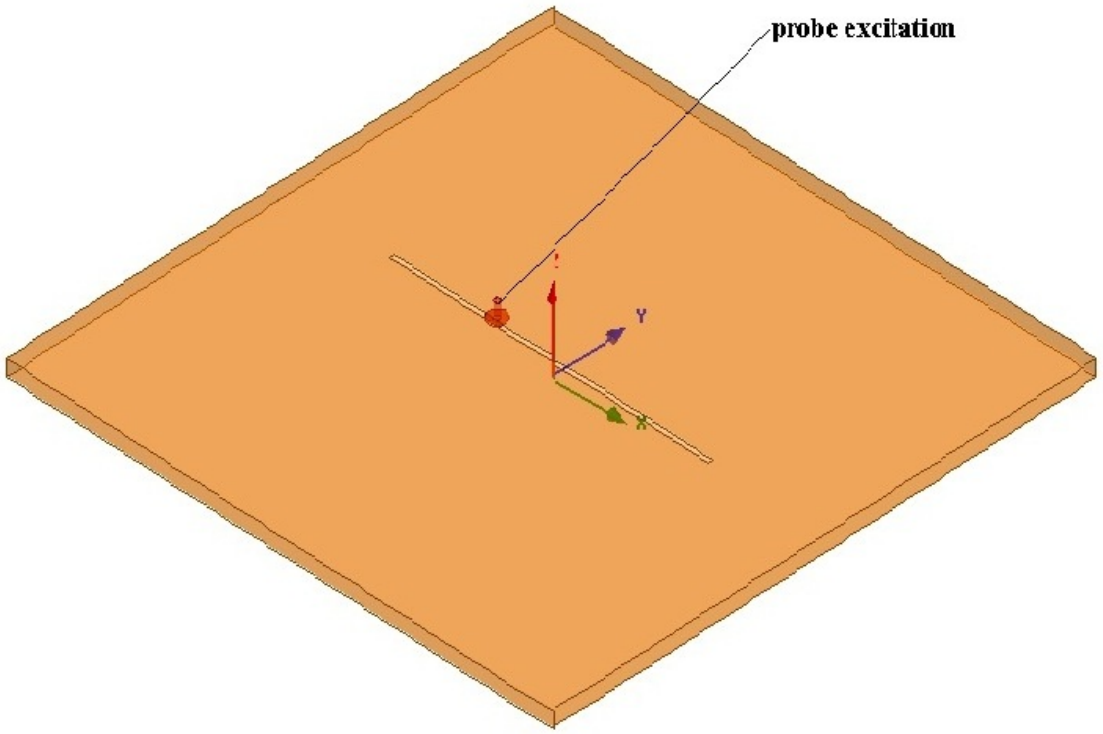

Fig. 3.24: A thin probe-excited cavity-backed slot antenna.

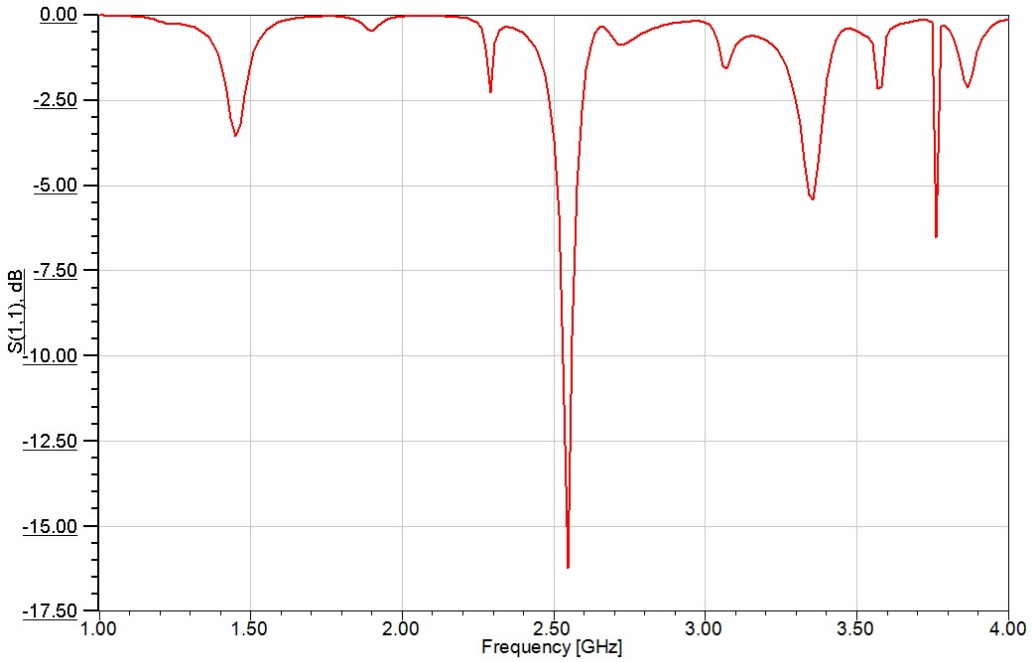

Fig. 3.25: The return loss of a thin probe-excited cavity-backed slot antenna.

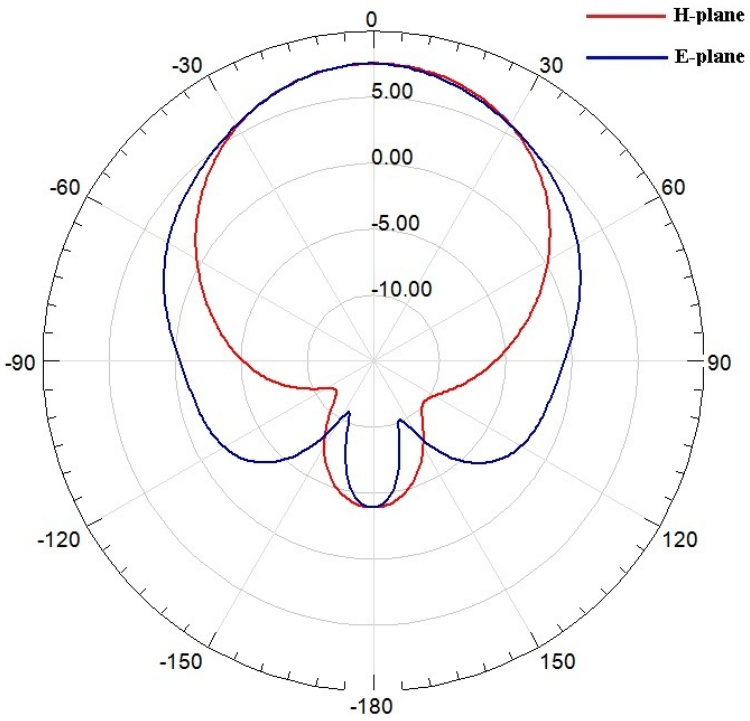

Fig. 3.26: The radiation pattern of a thin probe-excited cavity-backed slot antenna.

A hybrid of the stripline excitation and probe excitation is also possible. In this case a probe is used to excite a stripline which then excites the slots. This excitation method also requires at least two layers of dielectric material.

3.6 Physical Parameters that Affect Slot Antenna Electrical Properties

Hadidi and Hamid [34] gave a detailed analysis of the physical parameters that affect the field and circuit parameters of the cavity-backed slot antenna. The paper established that changing the material loading a cavity-backed slot antenna to one with a higher dielectric constant increases the resonance frequency for the cavity-backed slot antenna, and vice versa. In addition, higher dielectric constant of material loading decreases the antenna bandwidth. Furthermore, the resonance of a cavity-backed slot antenna changes if the position of the slot relative to the cavity changes.

3.7 Multiple Slots on a Cavity

By cutting out multiple slots out of the ground plane of a metallic cavity, different kind of the cavity-backed antenna, each with different funtion, can be realized. This design approach is different from an array of cavity-backed slot antenna in which each slot is backed by its individual cavity as presented by Eldesouki et al. [35]. In the case of multiple slots with each slot having its own cavity, there is minimal interaction between the slots. However, this kind of antenna will be difficult to fabricate. An antenna with multiple slots sharing the same cavity is easily fabricated. The slots in this antenna type will interact strongly with each other. Some of the radiation possibilities of using multiple slots on the same cavity are listed below.

3.7.1 Array Setup

Multiple slots can be etched on a single cavity of the cavity-backed antenna to form an antenna exhibiting array antenna properties like high gain and beam steering. For example, Li and Shen [36] presented an antenna in which slots in a 2 x 4 slot array were fed using a network of microstrip line feed. This antenna setup achieved a gain of more than 14 dBi.

3.7.2 Dual-Band Cavity-Backed Slot Antenna

Mahmoud and Baktur [37] presented a dual-band cavity-backed slot antenna. The antenna consists of two close slots in series. The two slots shared the same cavity, and were excited together using a stripline. Due to mutual coupling, the slots resonate at a secondary frequency, in addition to their fundamental frequency. The upper frequency was 5.2 GHz, and the lower frequency 4.22 GHz. This paper specified that the ratio between the secondary (lower) resonance and fundamental (upper) resonance for this antenna setup was 1.25. The measured upper band gain was 4.2 dB, and the lower band gain was 3.5 dB, and the polarizations were linear. This dual-band antenna, whose design is one of the bases structure for the multifunctional antenna in this thesis, is further investigated in this thesis below.

Figure 3.27 shows a dual-band antenna which achieves dual-band operation by mutual coupling between proximal slots. The antenna consists of two slots each of length 55 mm. The slots are separated by a distance of 6 mm. The two slots, which are symmetric with the center of the cavity, are etched on a 180 mm x 180 mm cavity that is 3.15 mm deep. The cavity is filled with two layers of Rogers RT/duroid 5880 laminate each of thickness 1.575 mm. A stripline was sandwiched between the two layers of dielectric material. The stripline started as a 50 Ohm line of width 2.3 mm, extended for 10 mm, and then tapered exponentially into a 25 Ohm line. The 25 Ohm line had a width of 5.8 mm. The taper length was 60 mm [38]. The 25 Ohm line extended for 10 mm, and then divided at a t-junction into two 50 Ohm lines that excited the slots. The slot feed offset position (dop) and offset length (dol) shown in Fig. 3.28 were 8.15 mm and 9.1 mm, respectively. The simulated upper frequency was 2.79 GHz, while the lower frequency was 1.95 GHz as shown in Fig. 3.29. The upper band and lower band radiation pattern are presented in Fig. 3.30. The upper band forward gain was 4.5 dB, with front-to-back ratio of 9.7 dB. The upperband E- and H- plane beamwidth are 177 degrees and 45 degrees, respectively. The lower band forward gain was 7.7 dB, with front-to-back ratio of 10.2 dB. The lower band E- and H-plane half-power beamwidths are 120 degrees and 60 degrees, respectively.

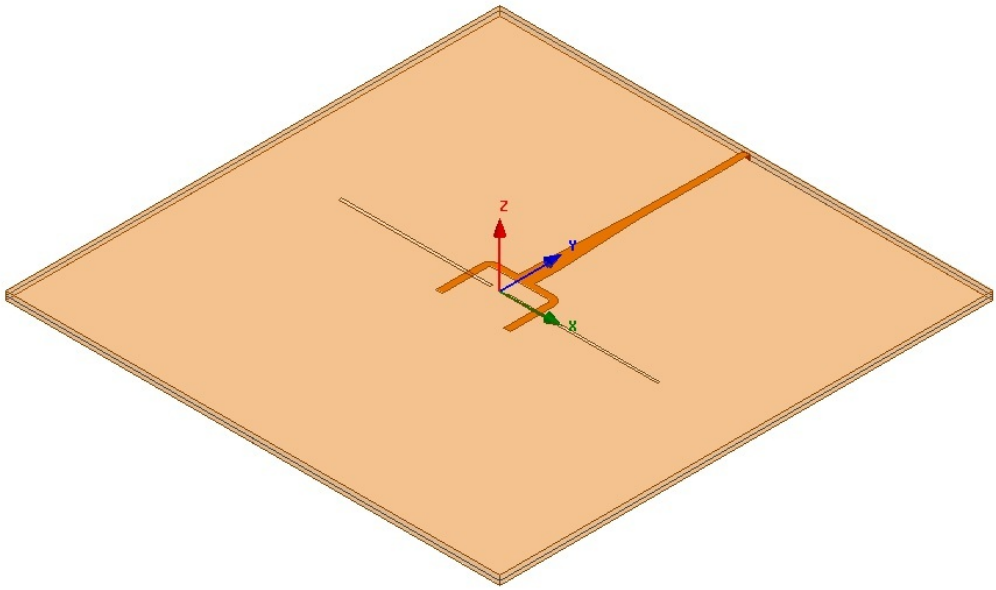

Fig. 3.27: A simple dual-band cavity-backed slot antenna.

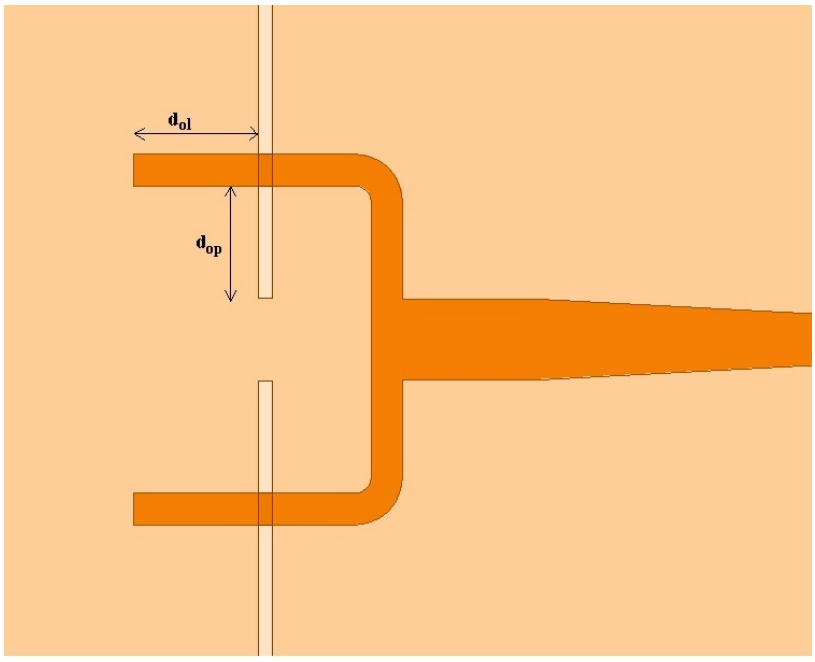

Fig. 3.28: A annotated feed structure for a dual-band cavity-backed slot antenna.

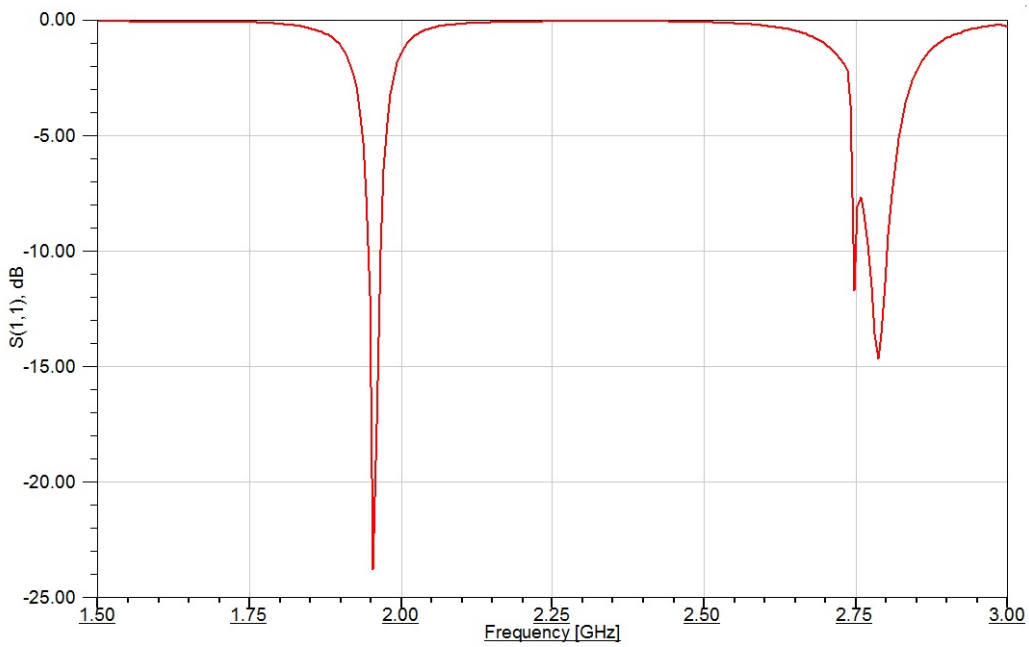

Fig. 3.29: The return loss simple dual-band cavity-backed slot antenna.

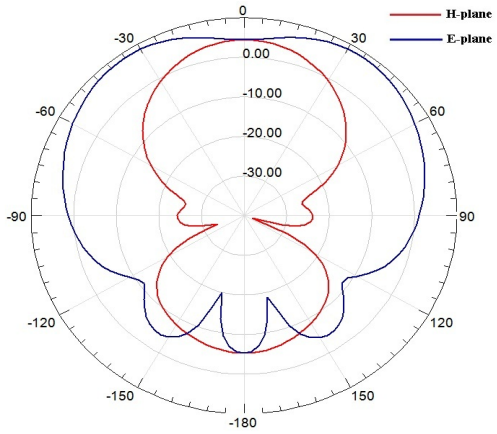

(a) The upper band radiation pattern of a simple dual-band cavity-backed slot antenna.

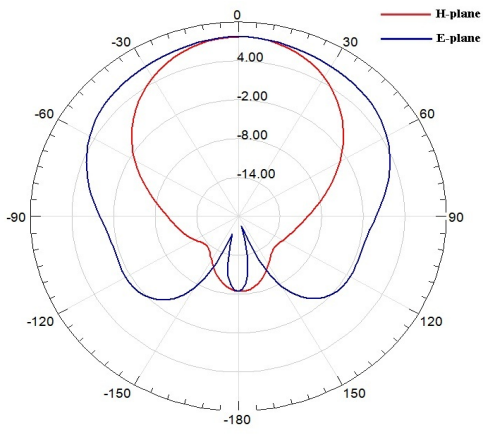

(b) The lower band radiation pattern of a simple dual-band cavity-backed slot antenna.

Fig. 3.30: The dual-band radiation patterns.

An array of dual-band cavity-backed antennas was also investigated. It consists of two dual-band (four slots) antenna placed some distance apart as shown in Fig. 3.31. The slots all have lengths of 41 mm and widths 1 mm, and the spacing between the two slots in each dual-band subarray is 4 mm. The cavity of the slots has a dimension of 83 mm x 340 mm and it is 3.15 mm deep. The cavity is loaded with two layers of Rogers RT Duroid 5880 each of thickness 1.575 mm. A stripline is sandwiched between the two layers of dielectric material. The stripline starts as a 50 Ohm line, then branches at a t-junction into two 100 Ohm lines. The width for a 100 Ohm line is 0.53 mm. Each 100 Ohm line tapers exponentially into a 25 Ohm line. The taper length is 72 mm. Each 25 Ohm line then divides at a t-junction into two 50 Ohm lines that feeds the two slots of a dual-band sub-array. The offset length (dol) and offset positions(dop1 and dop2) shown in Fig. 3.32 for the antenna in which the spacing between center of each dual-band sub-array is 250 mm are 20 mm, 29.15 mm and 1.15 mm, respectively. dfb is 9.135 mm. The upper band frequency is 2.46 GHz and the lower band frequency is 2.11 GHz as shown in Fig. 3.33. The upper band radiation pattern and the lower band radiation pattern are shown in Fig. 3.34.

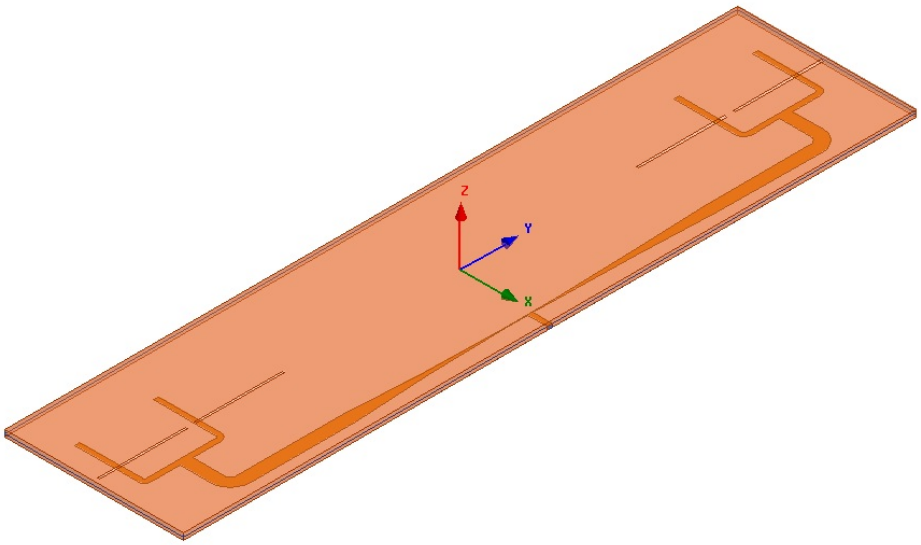

Fig. 3.31: An array of two dual-band cavity-backed slot antenna.

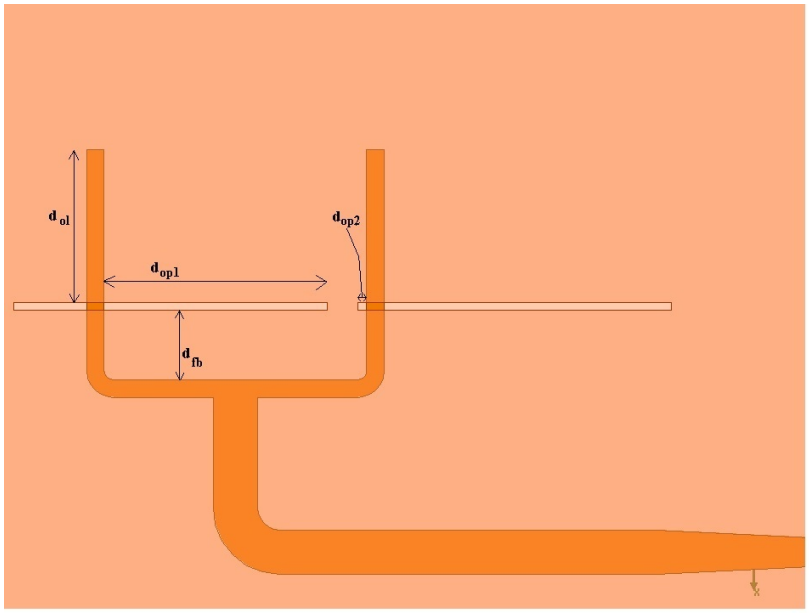

Fig. 3.32: Feed matching of an array of two dual-band cavity-backed slot antennas.

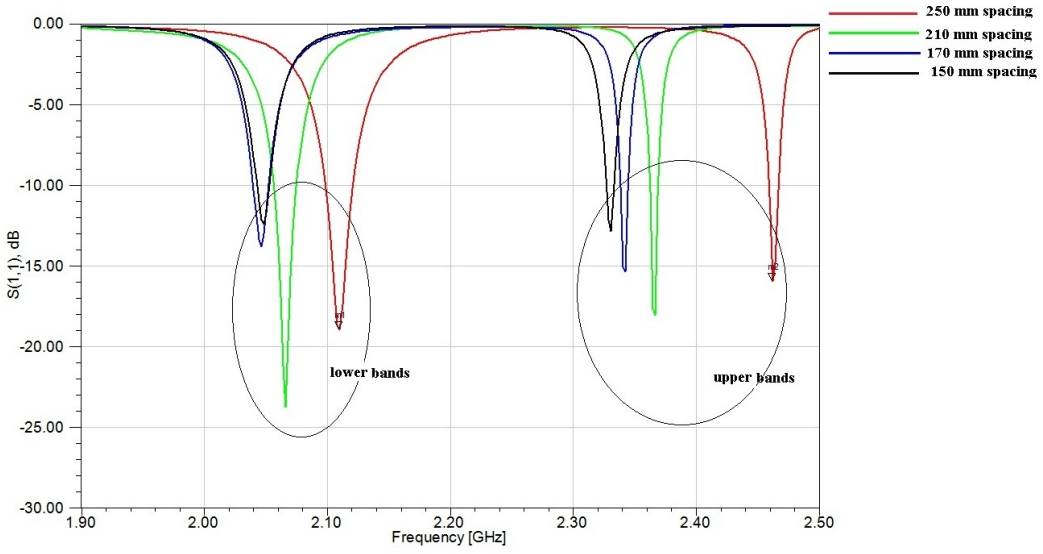

Fig. 3.33: The return losses of a dual-band cavity-backed slot antenna array with different spacings.

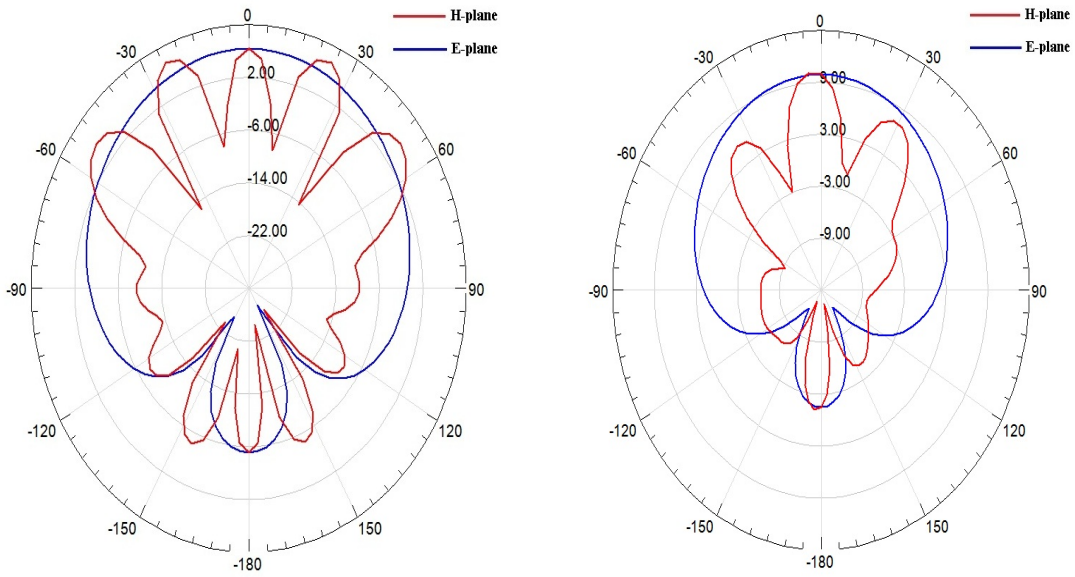

(a) The upper band radiation pattern of an array of dual-band cavity-backed slot antenna with 250 mm spacing.

(b) The lower band radiation pattern of an array of dual-band cavity-backed slot antenna with 250 mm spacing.

Fig. 3.34: The dual-band radiation patterns.

A study was performed to investigate the effect of the spacing between the two dual-band antenna subarrays on the antenna impedance and radiation properties. For the array with spacing of 150 mm shown in Fig. 3.35, the upper frequency is 2.33 GHz, and the lower frequency is 2.05 GHz as shown in Fig. 3.33. The upper and lower frequency radiation pattern are shown in Fig. 3.36. Two other spacings between the subarrays were also investigated. The impedance plots, overlayed on each other are presented in Fig. 3.33, while Table 3.1 gives the gain and sidelobe levels.

3.7.3 Circularly Polarized Cavity-Backed Slot Antenna

Multiple slots can be integrated on the same cavity of a cavity-backed antenna for circular polarization as demonstrated by Li and Shen [39] in a design that used a subarray of four slots fed by a microstrip line to generate the phase differences between the slots needed for circular polarization. The measured antenna gain for right-hand circular polarization (RHCP) for this antenna was 8.7 dBi at 6.0 GHz.

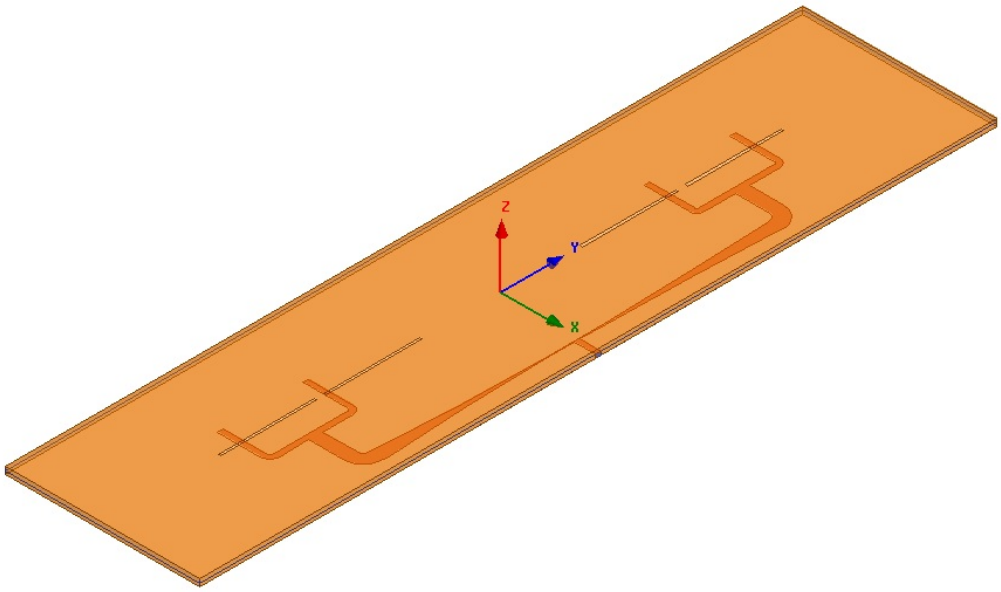

Fig. 3.35: An array of two dual-band cavity-backed slot antenna with 150 mm spacing.

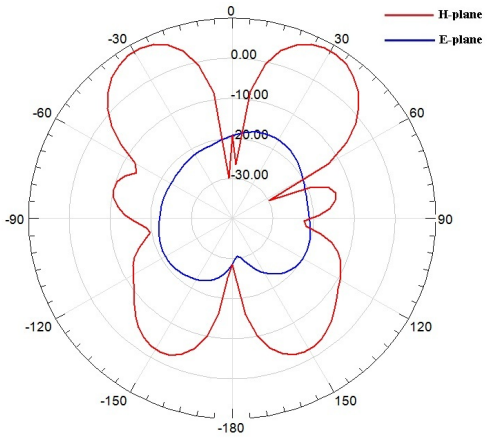

(a) The upper band radiation pattern of an array of dual-band cavity-backed slot antenna with 150 mm spacing.

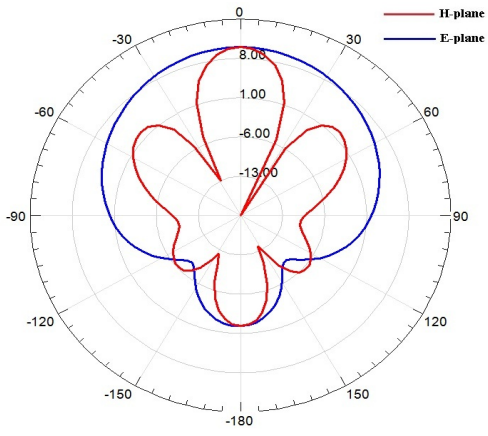

(b) The lower band radiation pattern of an array of dual-band cavity-backed slot antenna with 150 mm spacing.

Fig. 3.36: The dual-band radiation patterns.

Table 3.1: Varying the spacing between dual-band antenna array.

array space (mm)	dol (mm)	dop1 (mm)	dop2 (mm)	upper band gain(dB)	lower band gain(dB)	upper band side lobe gain(dB)	upper band side lobe angle(°)	lower side lobe gain(dB)	lower side lobe angle(°)
250	20	29.15	1.15	6.4	9.9	7.4	24	7.3	30
210	10	31.15	1.15	-3.2	10.6	8.15	25	5.2	39
170	10	31.15	1.15	-12	10.6	7	26	2.7	45
150	10	31.15	1.15	-19.3	10	8.4	30	2.3	48

Furthermore, two crossed slots have been shown to be capable of generating circular polarization. According to Sievenpiper et al. [40], when two unequal length cross-slots on a cavity are excited by exciting the cavity with a probe, the differential radiation from the two slots combine in the far-field to give a circularly polarized wave. The antenna presented in this paper was left-handed circularly polarized (LHCP). However, the paper suggested that a right-handed circularly polarized antenna could be achieved by changing the region of location of the probe feed as show in Fig. 3.37 [40] below.

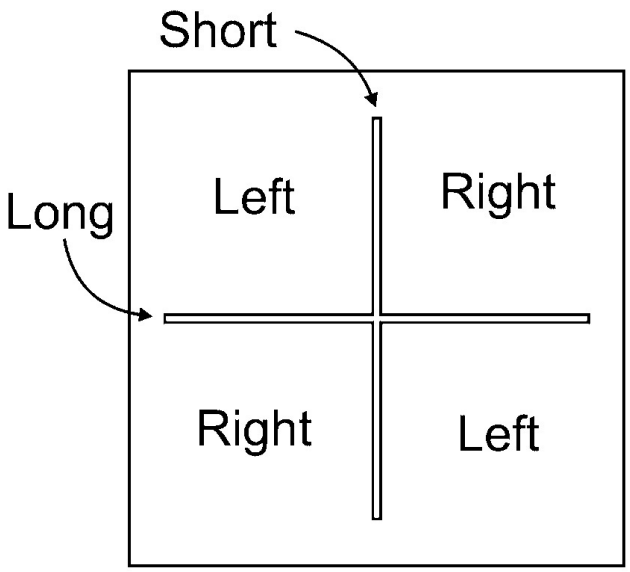

Fig. 3.37: Location of the probe feed excitation for different senses of circular polarization.

Using the idea of differential radiation from unequal length slots for circular polarization, the design in Fig. 3.37 was extended as shown in Fig. 3.38. In this extension, two feed points were placed on the same antenna structure, each feed for alternate sense of circular polarization. In this design, when the port for feed 1 is excited, with the port for feed 2 terminated with a matched load, the antenna would function as a right-handed circularly polarized antenna. On the other hand, when the port for feed point 2 is excited, and the port for feed point 1 is terminated with a matched load, the antenna would function as a left-handed circularly polarized antenna. Slot 1 and 2 has lengths 52 mm and 56 mm, respectively. The cavity is a 65 mm square of thickness 3 mm. The cavity is loaded with Rogers RT duroid 5880. Probe feed 1 has a x displacement of -16 mm and y displacement of 16 mm from the center of the cavity. Probe feed 2 has a x displacement of 16 mm and a y displacement of 16 mm from the center of the cavity. The return loss plots for both feed ports (s11, s22) are presented in Fig. 3.39. It can be seen that the return loss port for port 1 is similar to that of port 2, likewise are the mutual coupling plots. It can be seen from the mutual coupling plots that there is high isolation between port 1 and port 2. Figure 3.40(a) shows the radiation pattern for the antenna when port 1 is excited and port 2 terminated. The radiation is RHCP. Figure 3.40(b) shows the radiation pattern for the antenna when port 2 is excited and port 1 terminated. The radiation is LHCP. In both cases, the axial ratio at 2.3 GHz is below 2 dB, and the gain is 5.5 dB.

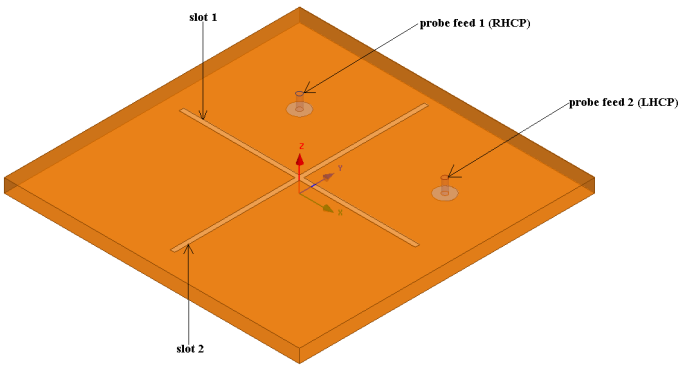

Fig. 3.38: A dual-fed, dual circularly-polarized cavity-backed slot antenna.

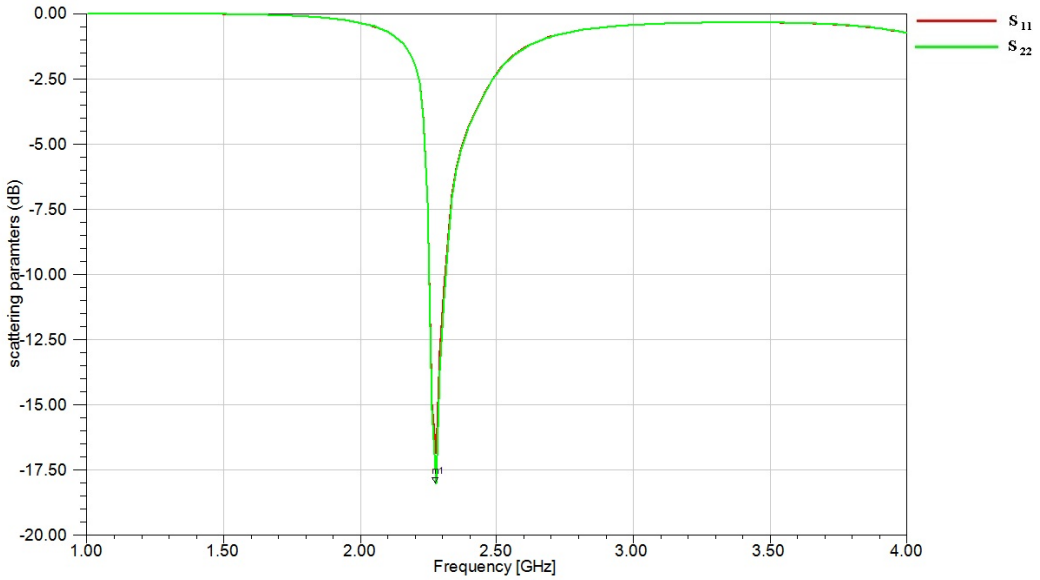

Fig. 3.39: Return loss and mutual coupling plots for the dual-fed antenna.

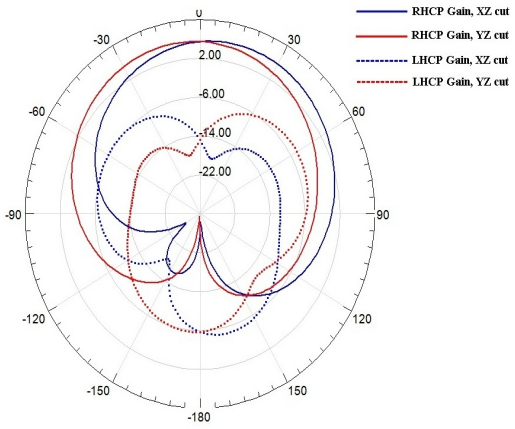

(a) Radiation pattern for port 1.

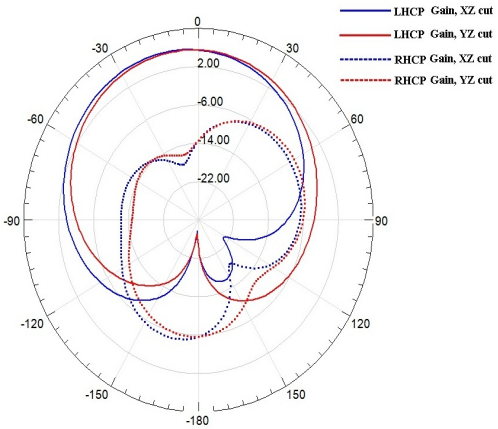

(b) Radiation pattern for port 2.

Fig. 3.40: The circular polarization radiation patterns for a simple dual-sense CP antenna.

Another investigation was performed to see the possiblity of achieving a circularly polarized antenna on a cavity which has the same size as a face of a 3U CubeSat, using a flexible slot layout. One of the design is shown in Fig. 3.41. It consisted of a 83 mm x 340 mm metallic cavity of thickness 3.15 mm. The cavity is loaded with two layers of Rogers Duroid 5880 each of thickness 1.575 mm. On top of the cavity were etched 14 slots, each slot assigned a number for easy reference as shown in the figure. The x displacement and y displacement of the center of each slot from the center of the cavity, and the length for some of the slots are given in Table 3.2. The parameters for others slot can easily be inferred from the table since each of the remaining slots is a mirror image of a slot given in the table. Probe 1 has an x displacement of -13.5 mm and a y displacement 5 mm, and it gives RHCP. Probe 2 has a x displacement of 13.5 mm and a y displacement of 5 mm, and it gives LHCP. The scattering parameter plots for excitation port 1 (s11) and port 2 (s22) are given in Fig. 3.42. Figure 3.43(a) shows the radiation pattern for the antenna when port 1 is excited and port 2 terminated. The radiation is RHCP. Figure 3.43(b) shows the radiation pattern for the antenna when port 2 is excited and port 1 terminated. The radiation is LHCP. In both cases, the axial ratio at 2.54 GHz is below 3 dB, and the gain is around 5 dB.

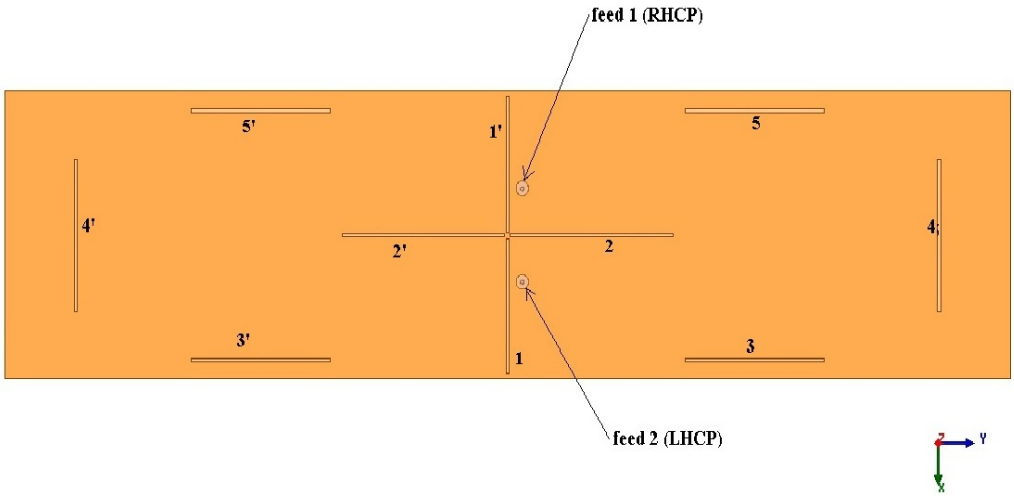

Fig. 3.41: A 3U dual-fed, dual circularly-polarized cavity-backed slot antenna.

Table 3.2: Slot position on cavity.

slot	length (mm)	x (mm)	y (mm)
1	39	20.5	0
2	55	0	28.5
3	47	40	88.5
4	44	0	146
5	47	-40	88.5

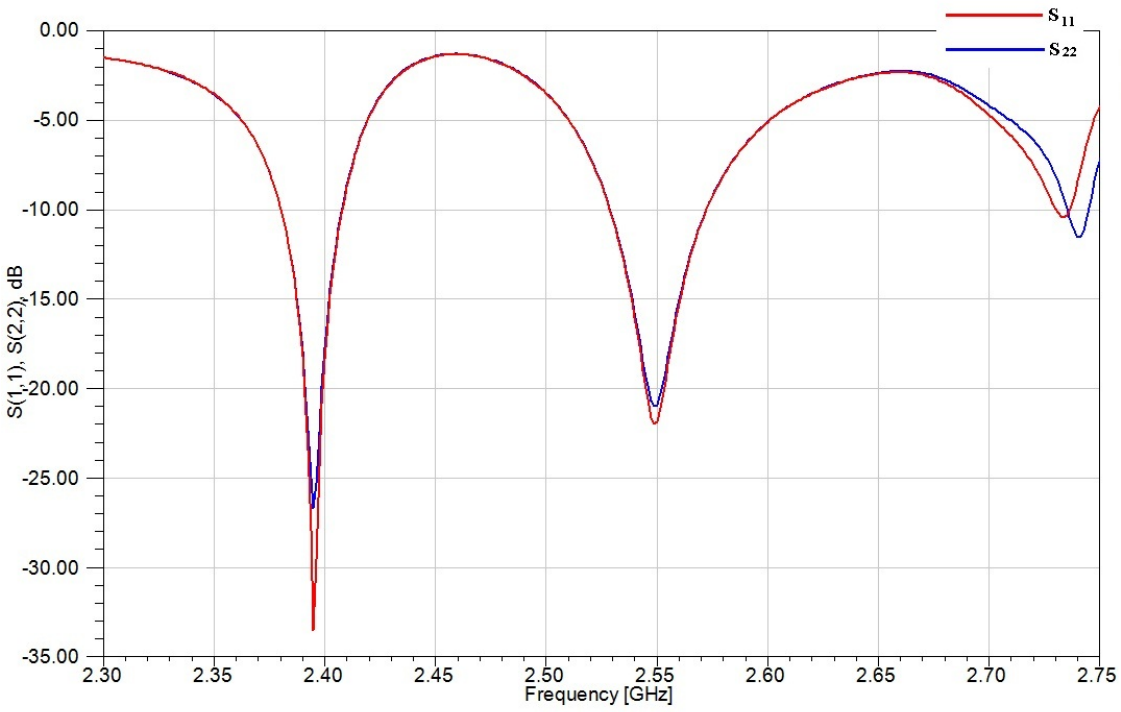

Fig. 3.42: Return loss plots for the 3U dual-fed antenna.

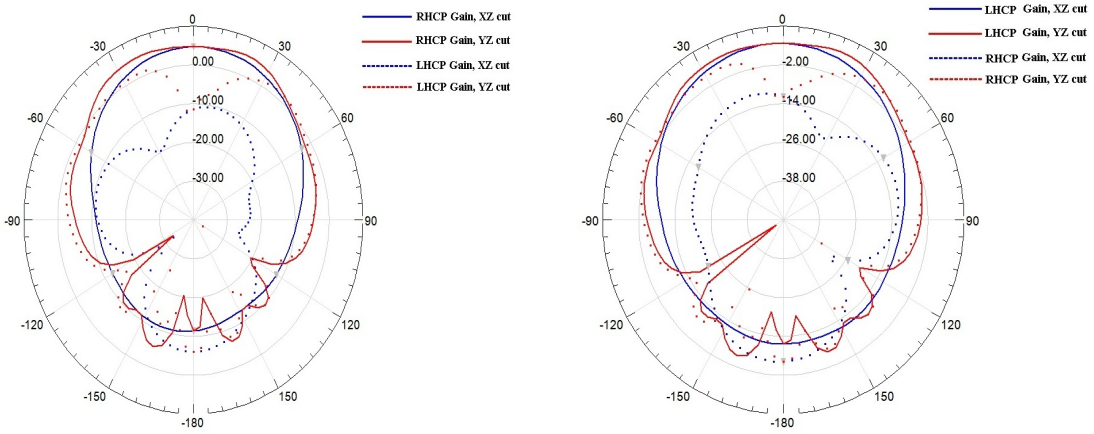

(a) Radiation pattern for port 1.

(b) Radiation pattern for port 2.

Fig. 3.43: The circular polarization radiation patterns for a size 3U CP antenna.

Figure 3.44 shows an alternate CP antenna design on a 3U surface. This 13 slot design has a different slot pattern from the design of Fig. 3.41, but the cavity parameters are the same in both designs. The x displacement and y displacement of the center of each slot from the center of the cavity, and the length for some of the slots are given in Table 3.3. The parameters for others slot can be easily inferred. Probe 1 has an x displacement of -14.5 mm and a y displacement 3 mm and it gives RHCP. Probe 2 has a x displacement of 14.5 mm and a y displacement of 3 mm, and it gives LHCP. The scattering parameter plots for excitation port 1 (s11) and port 2 (s22) are given in Fig. 3.45. Figure 3.46(a) shows the radiation pattern for the antenna when port 1 is excited and port 2 terminated. The radiation is RHCP. Figure 3.46(b) shows the radiation pattern for the antenna when port 2 is excited and port 1 terminated. The radiation is LHCP. In both cases, the axial ratio at 2.18 GHz is below 3 dB, and the gain is about 5.7 dB.

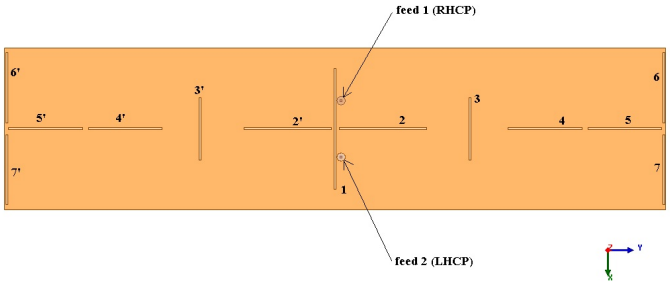

Fig. 3.44: A 3U dual-fed, dual circularly-polarized cavity-backed slot antenna.

Table 3.3: Slot position on cavity.

slot	length (mm)	x (mm)	y (mm)
1	62	0	0
2	45	0	24.5
3	32	0	69.5
4	38	0	108
5	38	0	108
6	36	-21	169
7	36	21	169

Although both the designs in Fig. 3.41 and Fig. 3.44 gave circular polarization, it is important to note that the radiation patterns in each case are different due to the different slot pattern in each. Therefore, it is possible to design a circularly polarized antenna with different radiation pattern by different slot layout. Furthermore the gain of a 3U CP antenna is comparable to the smaller 65 mm square antenna presented in Fig. 3.38. This is unusally given the bigger size of the 3U antenna, and the higher number of radiating slots. This lower gain is due to the constraint in the size of the 3U antenna which must be maintained at the standard 83 mm x 340 mm size of a CubeSat surface, which is a sub-optimal dimension. To design a high gain antenna using probe feeds, the cavity and the slots need to be tuned together. To illustrate this, another antenna with the same number of slots, and similar slot layout, as in the design in Fig. 3.44, was investigated, but now with a cavity size of 100 mm x 300 mm. This antenna achieved a gain of about 9 dB, with axial ratio less than 2 dB for both LHCP and RHCP.

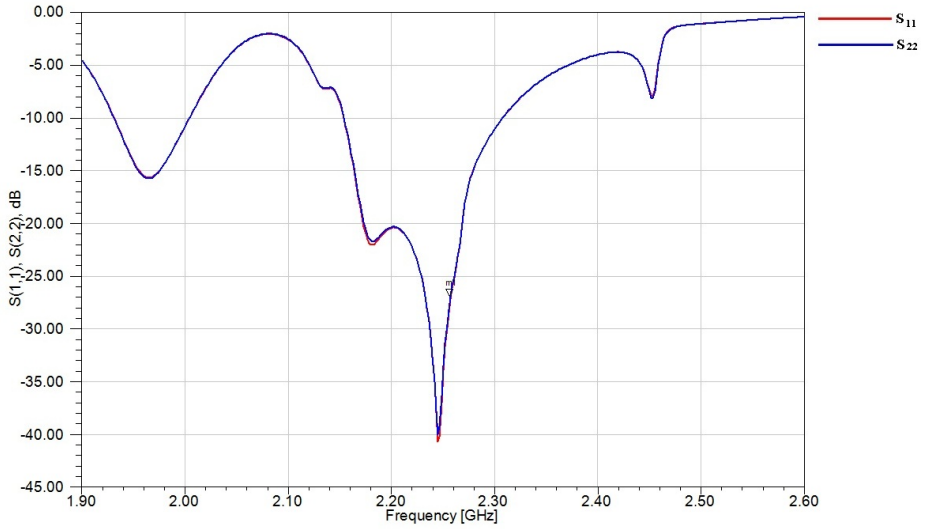

Fig. 3.45: Return loss plots for the 3U dual-fed antenna.

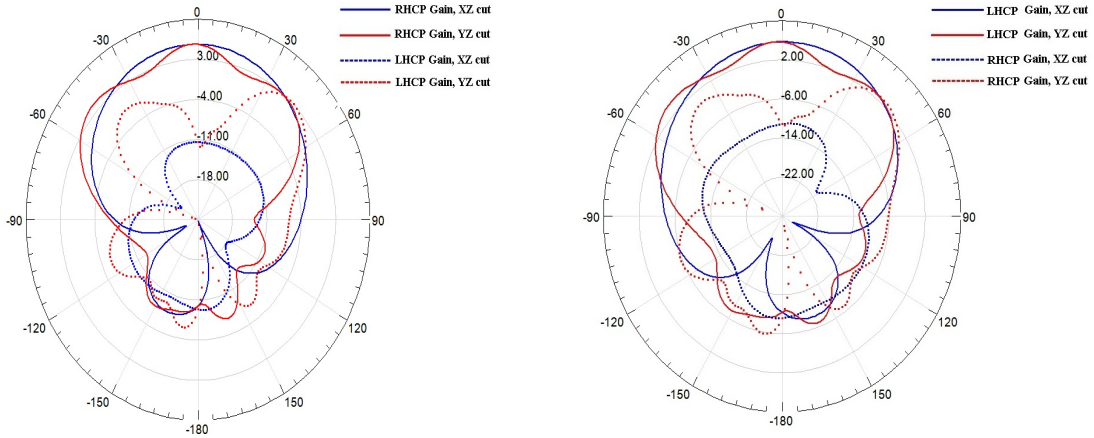

(a) Radiation pattern for port 1.

(b) Radiation pattern for port 2.

Fig. 3.46: The circular polarization radiation patterns for a size 3U CP antenna.

Chapter 4

The Multifunctional Antenna

4.1 Reconfigurable and Multifunctional Antennas

Reconfigurability, when used in the context of antennas, is the capacity to change an individual radiators fundamental operating characteristics through electrical, mechanical, or other means [41]. The ability of a radiating structure to change its fundamental property in a flexible manner to accommodate changing operating environment improves the overall performance of a communication system. The fundamental properties of an antenna that are usually configured are the resonance (working) frequency, the radiation pattern, the bandwidth, and the polarization. For example, the working frequency of a frequency reconfigurable antenna can be switched to another frequency to avoid interference present at a particular frequency. Or, the radiation pattern of a pattern reconfigurable antenna can be switched to a beam which provides maximum reception from a transmitting source. These switching for different antenna properties will improve the performance of a communication system.

The frequency of an antenna could be reconfigured discretely or continuously. Switches are usually employed to reconfigure the resonance frequency of an antenna in a discrete fashion. For example, since the resonance frequency of wire antennas and slot antennas depend on the length of such antennas, switches could be located on a wire antennas such that some length of the wire could be cut off to yield an effectively shorter length with higher resonance frequency when the switches are turned off as illustrated by Bernhard [41]. Continuous frequency reconfiguration is achieved by integrating reactive elements whose reactances could be varied continuously in an antenna system.

The polarization of an antenna could also be reconfigured by integrating switches in the structure of the antenna. The switches are located on the radiation structure in such

a way that the turning the switch on and off will switch the current distribution, and therefore the polarization of the antenna. Bernhard [41] presented a microstrip antenna which reconfigures between RHCP and LHCP was presented. Furthermore, the radiation pattern of an antenna could be reconfigured by changing the current distribution of an antenna by electronic means.

In the radiating structure presented in this thesis, all of the above mentioned objectives of reconfigurability are achieved in a single structure.

A multifunctional antenna is desired because it can enhance the capacity of a communication system. Furthermore, integrating multiple antennas on one structure will translate to savings in space. In addition, an antenna that can dynamically switch between function electronically means less moving parts which equals less points for failure.

The multifunctional antenna presented in this thesis extends the work of Sievenpiper et al. [40] and the work of Mahmoud and Baktur [37], and then combines these two independent works together. The extension of the each work was presented in the previous chapter. This chapter presented the hamonization of these two extensions to realize the multifunctional antenna. The multifunctional antenna presented could be integrated easily with solar cells on the solar panel of a 3U CubeSat.

It has been demonstrated that multiple slots on a cavity can give circular polarizations when the cavity is excited by probes, and dual-band linear polarization when some close slots are excited with a stripline. Therefore it is possible to design, through thoughtful layout of multiple slots, and multiple feed ports, an antenna that provides left-handed circular polarization or right-handed circular polarization function at a frequency, or dual-band linearly polarized function. Also, to suit the antenna design for integration of solar cells for CubeSat application, these multiple slots on the cavity of the multifunctional antennas need to be laid out such that there is ample space for the placement of solar cells.

Basically, in all multifunctional antenna designs presented, there is a port for LHCP, another port for RHCP, and at least one port for dual-band operation. When a port for a particular function is excited, the other ports will be terminated with matched loads or left

open, depending on the design.

One major challenge in the realization of these designs is how to isolate the functionalities such that trying to achieve a particular function will not interfere negatively with another function, such that antennas can be switched from one function to another neatly.

4.2 Multifunctional Antenna Design One

The first designed multifunctional antenna is shown Fig. 4.1 below. The antenna is designed for LHCP at 2.47 GHz, within the S-band, or RHCP at 2.47 GHz, within the S-band, or dual-band LP operation at 2.43 GHz and 2.1 GHz. The design consisted of nine slots on a dielectric-loaded cavity. The cavity is excited with two probes, and the stripline sandwiched between the two layers o the cavity is exicited by another probe. The slots are laid out such that when the first probe is excited through port 1, the differential radiation from all the slots combine together to give a RHCP. Furthermore, when the second probe is excited through port 2, the differential radiations from the slots combine to give LHCP. Furthermore, when the feed line between the cavity is excited through port 3, the feed line couples energy to slots 4 and 5 for dual band operation, also slots 4' and 5', which were also excited by the same feedline, provided dual band operation simultaneously.

Table 4.1 gives the dimensions and positions on the cavity of the slots of design 1. All slots have width of 1 mm. The cavity has a size of 340 mm x 83 mm, the standard size of a face of a 3U CubeSat. The cavity has a depth of 3.15 mm and it is loaded with two layers of Rogers Duroid 5880 of relative permittivity of 2.2. Each dielectric substrate has a thickness of 1.575 mm. The slots on the surface area on top of the cavity were laid out with enough spaces between them such that standard space grade 26 cm squared solar cells could fit on the cavity without the solar cells covering the slots or getting too close to the edges of the slots. Eight of these solar cells can fit conveniently on this design.

The stripline for the dual-band excitation of the slots, between the substrate layers, started as a 50 Ohm line 4 mm from the edge of the cavity, extends for 4 mm, and then branches into two 100 Ohm line that extends for 7 mm and then tapers exponentially into a 25 Ohm line. The taper length is 72 mm. The 25 Ohm line extends in a straight line for

47.5 mm, bends in a quater circle of radius 5.8 mm and the extends for 18 mm. The 25 mm line then divides at a t-junction into two 50 Ohm lines. The 50 Ohm line are the matched to the slots for dual-band excitation. In this design, the offset length (dol) and offset positions (dop1 and dop2) annotated in Fig. 3.32 are 14 mm, 32.65 mm, and 0.65 mm, respectively. dfb is 6.635 mm. The width for a 100 Ohm, 50 Ohm, and 25 Ohm stripline are 0.53 mm, 2.3 mm, and 5.8 mm, respectively.

For circular polarization excitations, probe 1 has an x displacement of -10 mm and a y displacement 2.5 mm and it gives RHCP, probe 2 has a x displacement of 10 mm and a y displacement of 2.5 mm, and it gives LHCP. In this design, a probe feed is modelled as the inner conductor of a 50 Ohm coaxial cable of radius 0.6272 mm whose outer radius 2.1 mm.

For RHCP operation of the multifunctional antenna, port 1 is excited with port 2 and port 3 terminated with matched loads. Similarly for LHCP operation, port 2 is excited with port 1 and port 3 terminated with matched loads. For dual-band LP operation, port 3 is excited, with port 1 and port 2 terminated with matched loads.

The simulation results for the antenna are presented below in Figs. 4.2 - 4.6.

Table 4.1: Slot position on cavity.

slot	length (mm)	x (mm)	y (mm)
1	58	0	0
2	62	0	34
3	10	0	70.5
4	41	0	93.5
5	41	0	139.5

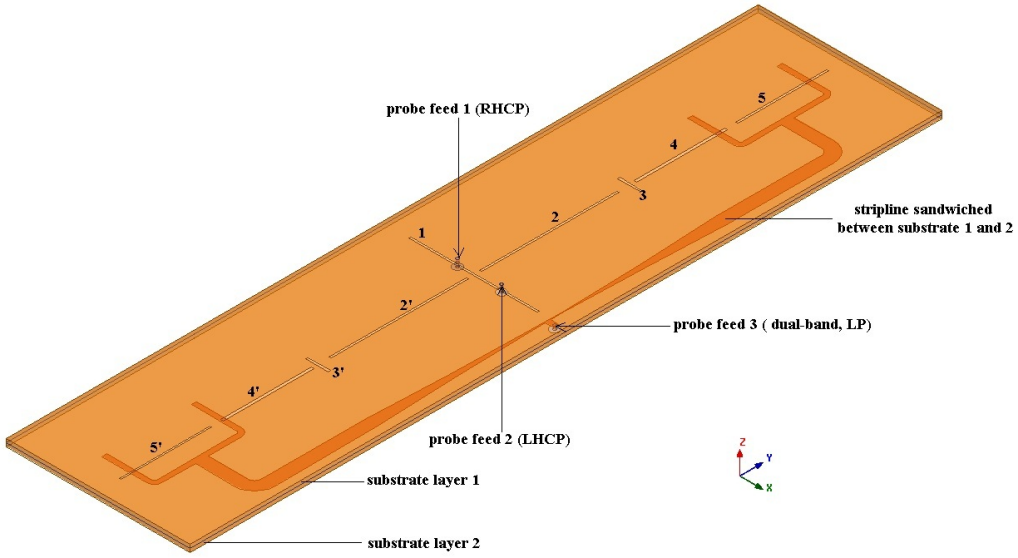

Fig. 4.1: A 3U multifunctional antenna.

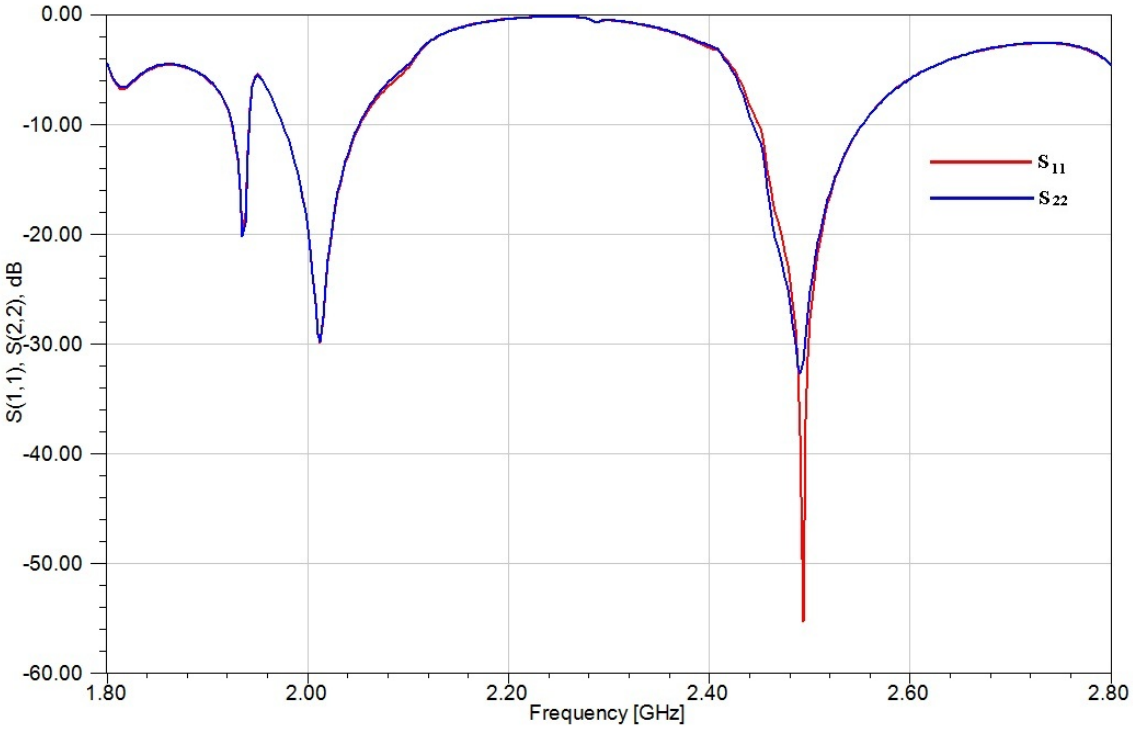

Fig. 4.2: Return loss for the CP ports.

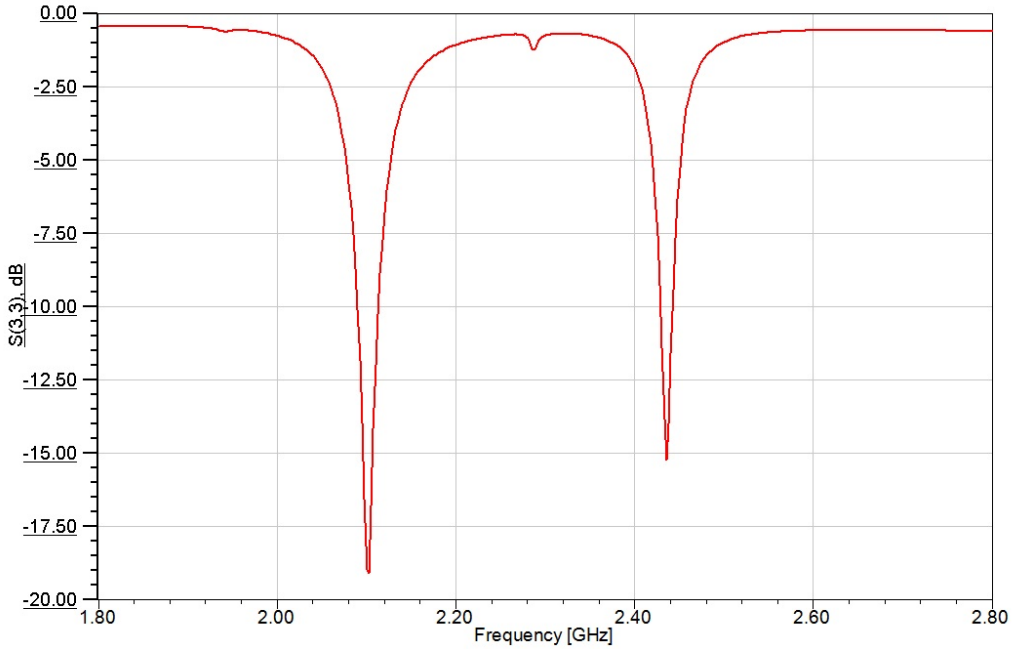

Fig. 4.3: Return loss for the LP port.

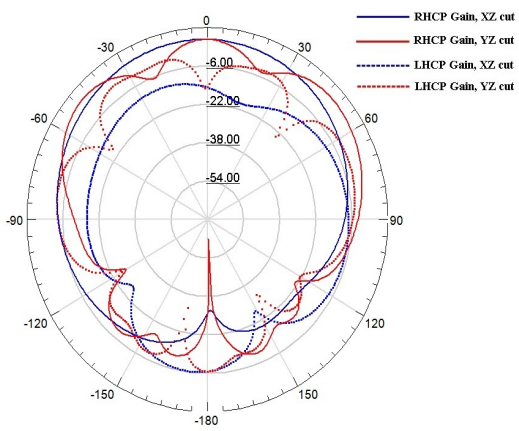

(a) RHCP radiation pattern at 2.47 GHz.

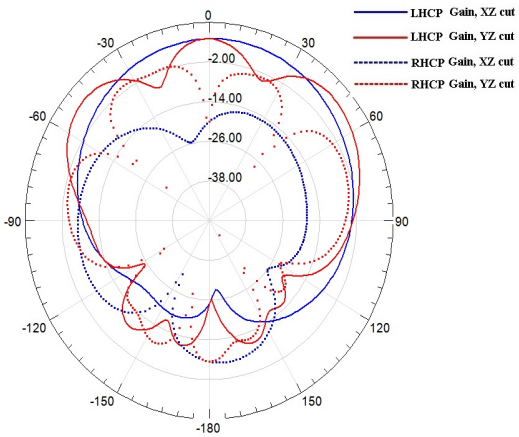

(b) LHCP radiation pattern at 2.47 GHz.

Fig. 4.4: The circular polarization radiation patterns.

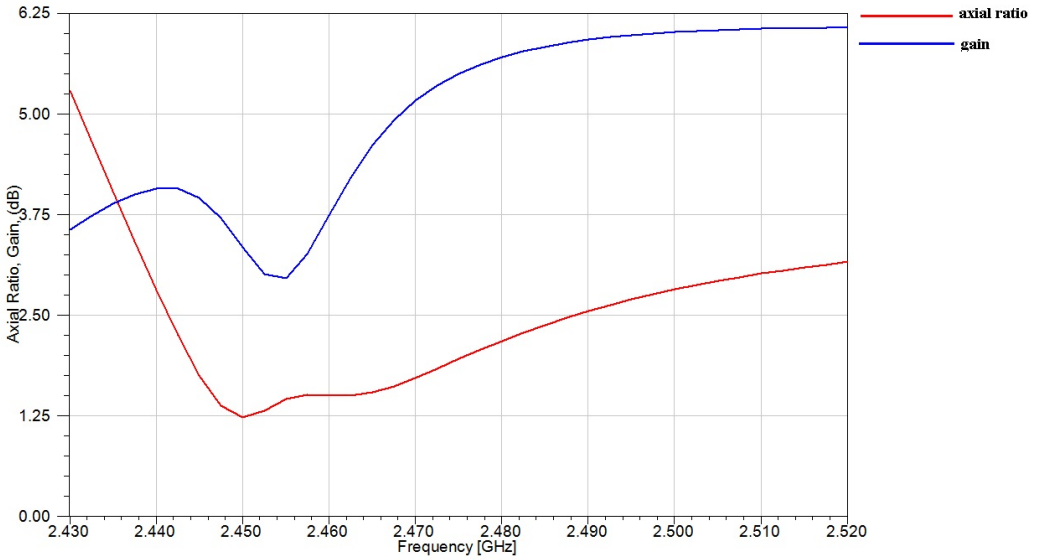

Fig. 4.5: CP axial ratio and gain sweep.

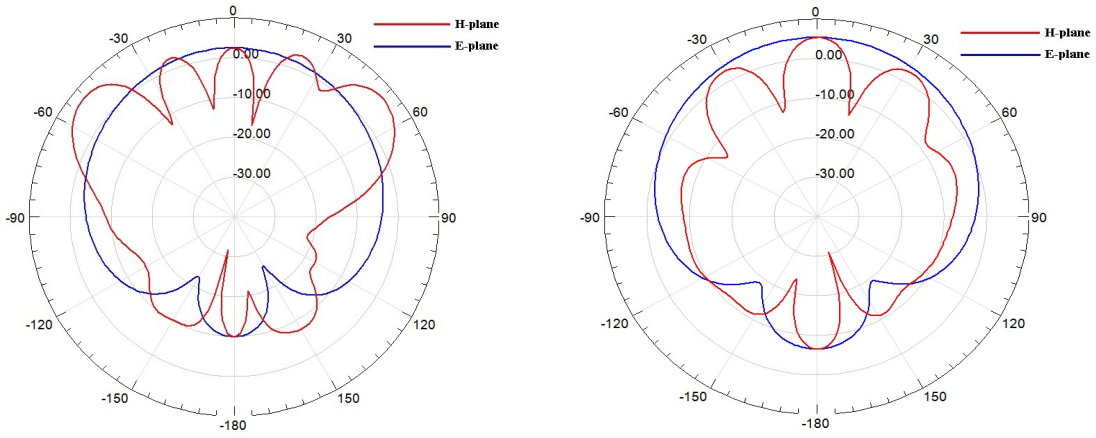

(a) Upper band LP radiation pattern at 2.435 GHz.

(b) Lower band LP radiation pattern at 2.1 GHz.

Fig. 4.6: The dual-band linear polarization radiation patterns.

4.3 Multifunctional Antenna Design Two

The second designed multifunctional antenna is shown Fig. 4.7 below. The antenna is designed for LHCP at 2.22 GHz, within the S-band, or RHCP at 2.22 GHz, within the S-band, or dual-band LP operation at 1.945 GHz and 2.42 GHz. The design consisted of eight slots on a dielectric-loaded cavity. The cavity is excited with two probes, and two stripline sandwiched between the two layers of the cavity are exicited by a lumped. The slots are laid out such that when the first probe is excited through port 1, the differential radiation from all the slots combine together to give a RHCP. Furthermore, when the second probe is excited through port 2, the differential radiations from the slots combine to give LHCP. Furthermore, when the feed line between the cavity is excited through port 3, the feed line couples energy to slots 3 and 4 for dual band operation, also when slots 4' and 5'which are excited by the second feed line, the structure provides dual-band operation.

Table 4.2 gives the dimensions and positions on the cavity of the slots of design 1. Slots 1, 2, 1', and 2' have width of 1 mm. Slots 3, 4, 3' and 4' have widths 3 mm. The cavity has a size of 340 mm x 83 mm, the standard size of a face of a 3U CubeSat. The cavity has a depth of 2.54 mm and it is loaded with two layers of Rogers Duroid 5880LZ of relative permittivity of 1.96. Each dielectric substrate has a thickness of 1.27 mm. The slots on the surface area on top of the cavity were laid out with enough spaces between them such that standard space grade 26 cm squared solar cells could fit on the cavity without the solar cells covering the slots or getting too close to the edges of the slots. Eight of these solar cells can fit conveniently on this design.

Each stripline for the dual-band excitation of the slots, between the substrate layers, started as a 50 Ohm line from a edge of the cavity, extends for 2 mm, and then tapers exponentially into a 25 Ohm line. The taper length is 60 mm. The 25 Ohm line extends in a straight line for 16 mm. The 25 mm line then divides at a t-junction into two 50 Ohm lines. The 50 Ohm line are the matched to the slots for dual-band excitation. In this design, the offset length (dol) and offset positions (dop1 and dop2) annotated in Fig. 3.32 are 20.1 mm, 9.65 mm and 9.65 mm, respectively. dfb is 5.2 mm.

For circular polarization excitations, probe 1 has an x displacement of -14.5 mm and a y displacement 8 mm and it gives RHCP, probe 2 has a x displacement of 14.5 mm and a y displacement of 8 mm, and it gives LHCP. In this design, a probe feed is modelled as the inner conductor of a 50 Ohm coaxial cable of radius 0.6272 mm whose outer radius 2.1 mm.

In this design, for RHCP operation of the multifunctional antenna, port 1 is excited with port 2 terminated with a matched loads, and port 3 and 4 left open. Similarly for LHCP operation, port 2 is excited with port 1 is terminated with a matched load, and port 3 and 4 left open. For one dual-band operation port 3 is excited, and port 4 is terminated with a matched and port 1 and port 2 left open.

The simulation results for the antenna are presented below in Figs. 4.8 - 4.13.

4.4 Multifunctional Antenna Design Three

In this design, the ground size of the cavity was increased for the standard 3U size of 83 mm x 340 mm to 100 mm x 300 mm as shown in Fig. 4.14 below. The simulation results are shown in Figs. 4.15 - 4.18. The CP gain properties of this antenna improved substantially. This is because the size constraint dictacted by a 3U cavity size leads to an antenna design with suboptimal performances. To tune the gain of the CP antenna for optimal performance, the cavity and the slots should be tuned together [40].

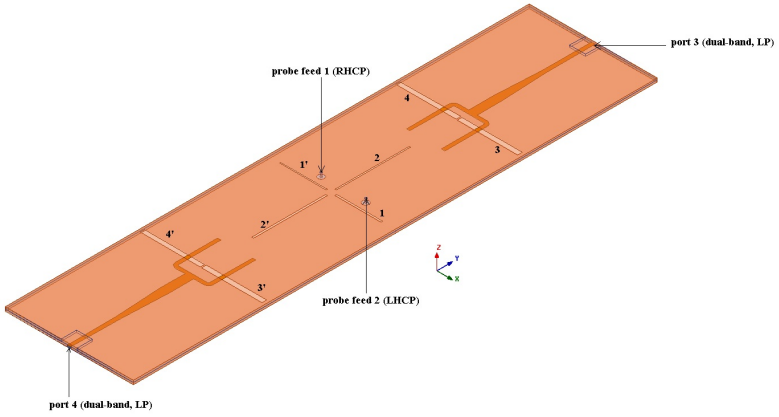

Fig. 4.7: A 3U multifunctional antenna.

Table 4.2: Slot position on cavity.

slot	length (mm)	x (mm)	y (mm)
1	30	18	0
2	48	0	27
3	39	20	83
4	39	-20	83

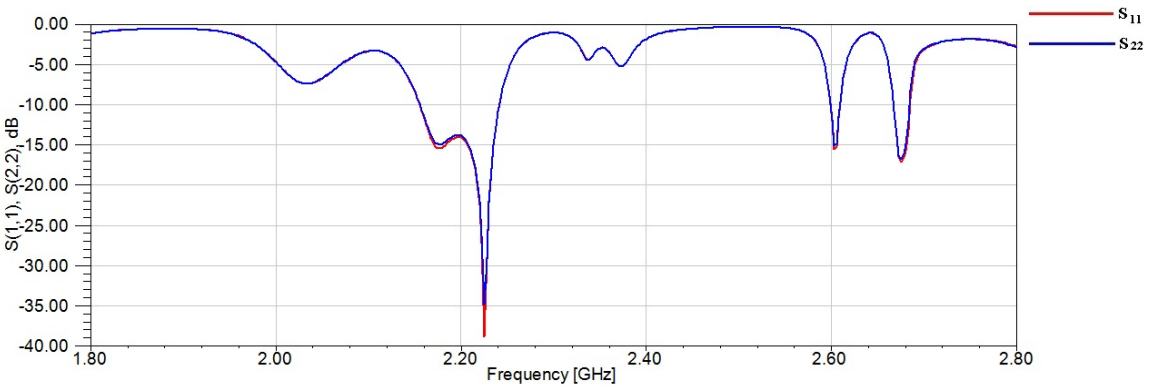

Fig. 4.8: Return loss for the CP ports.

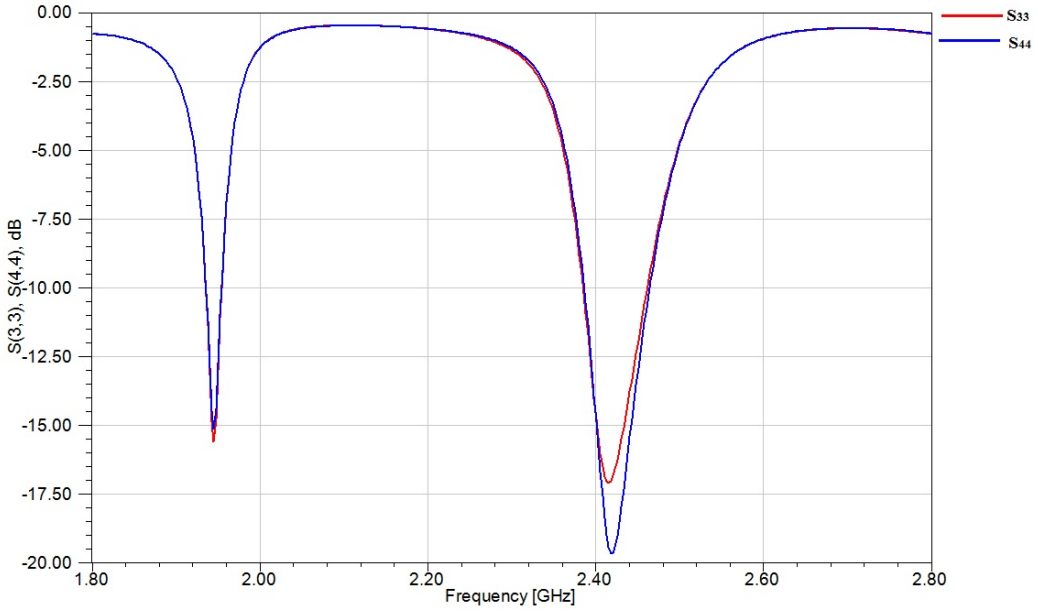

Fig. 4.9: Return loss for the LP ports.

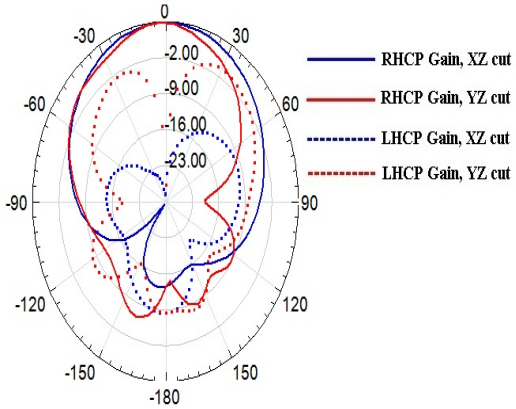

(a) RHCP radiation pattern at 2.22 GHz.

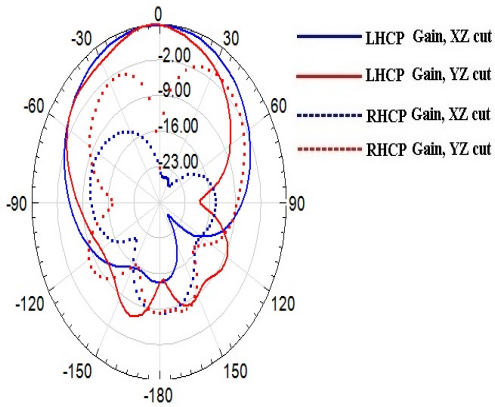

(b) LHCP radiation pattern at 2.22 GHz.

Fig. 4.10: The circular polarization radiation patterns.

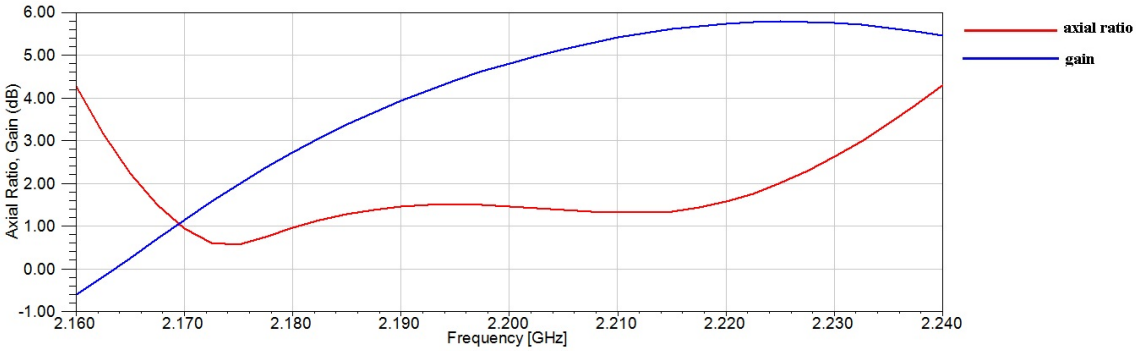

Fig. 4.11: CP axial ratio and gain sweep.

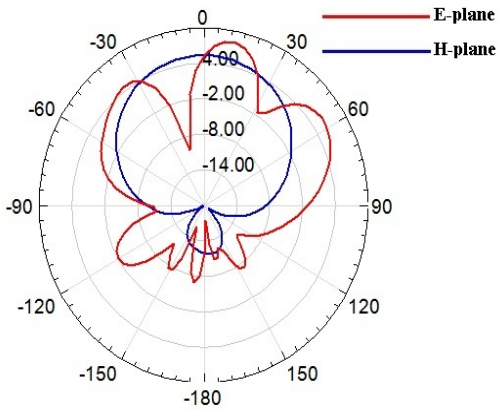

(a) Upper band LP radiation pattern at 2.415 GHz from port 3.

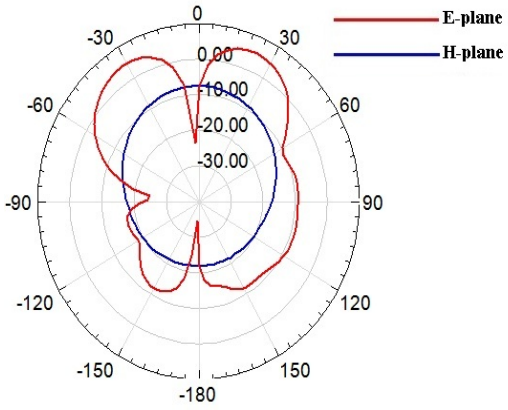

(b) Lower band LP radiation pattern at 1.945 GHz from port 3.

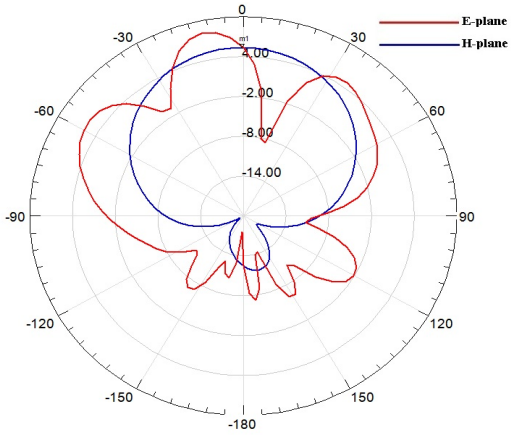

(c) Upper band LP radiation pattern at 2.415 GHz from port 4.

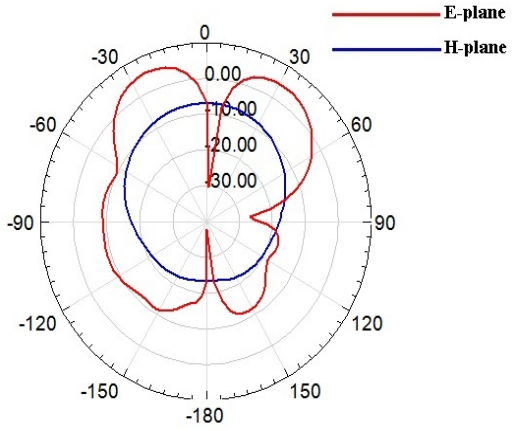

(d) Lower band LP radiation pattern at 1.945 GHz from port 4.

Fig. 4.12: The dual-band linear polarization radiation patterns.

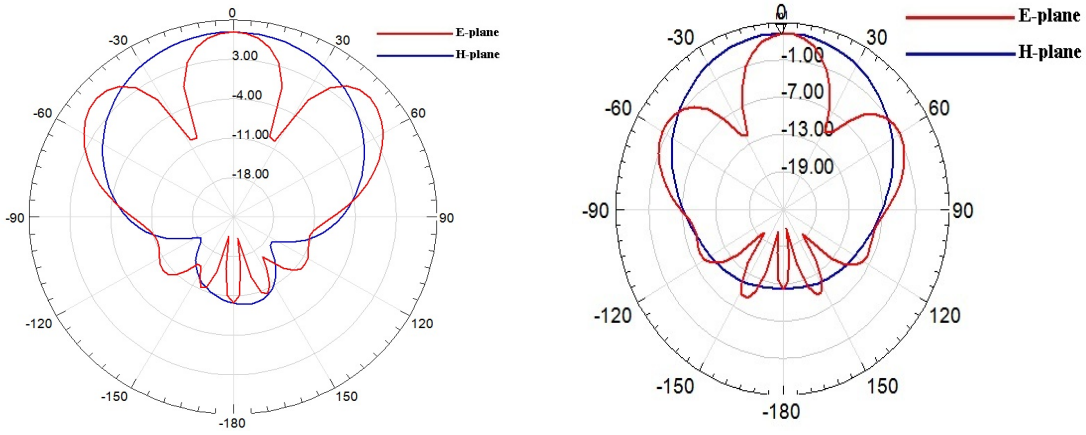

(a) Upper band LP radiation pattern at 2.415 GHz from port 3 and port 4 with 180 degrees phase difference.

(b) Lower band LP radiation pattern at 1.945 GHz from port 3 and port 4 with 180 degrees phase difference.

Fig. 4.13: The dual-band LP radiation patterns with phase shifts.

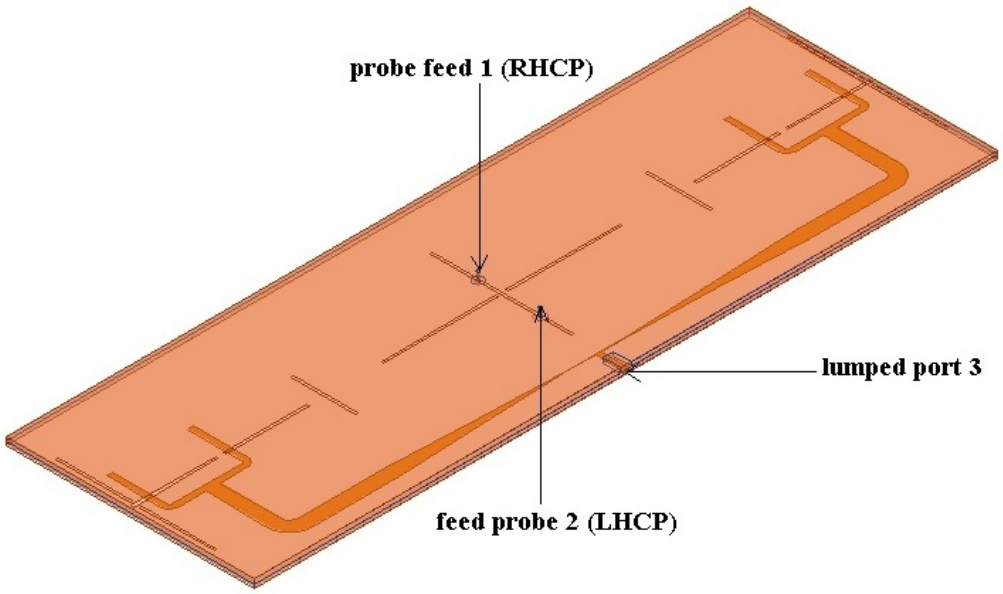

Fig. 4.14: A non-3U multifunctional antenna.

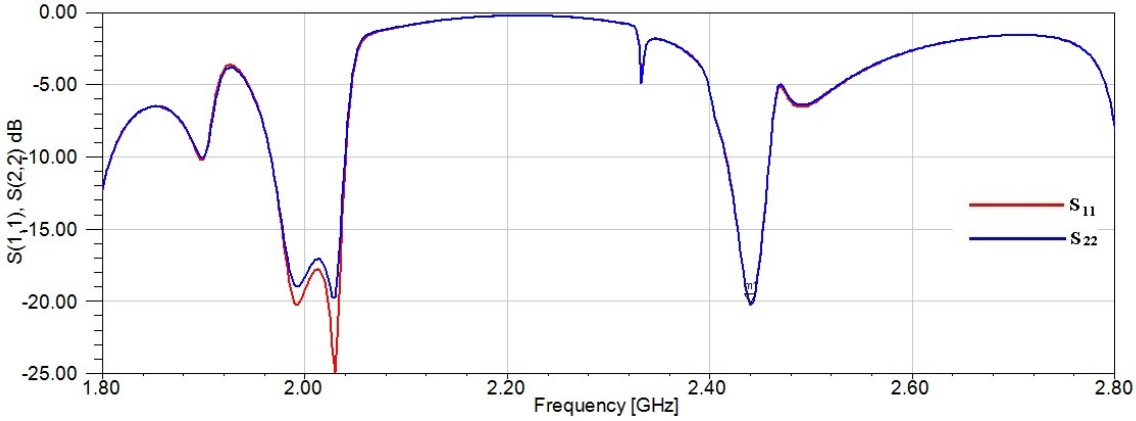

Fig. 4.15: Return loss for the CP ports.

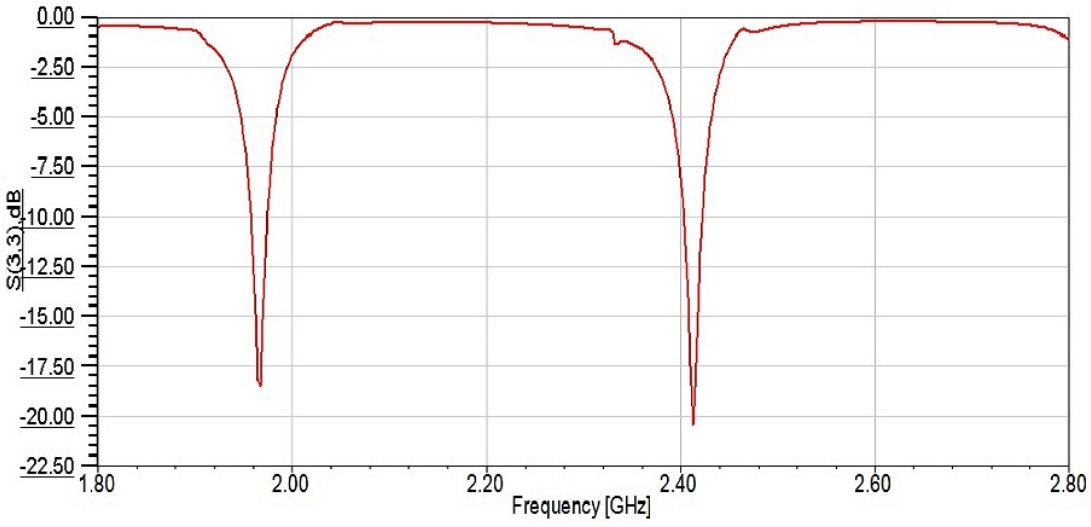

Fig. 4.16: Return loss for the LP port.

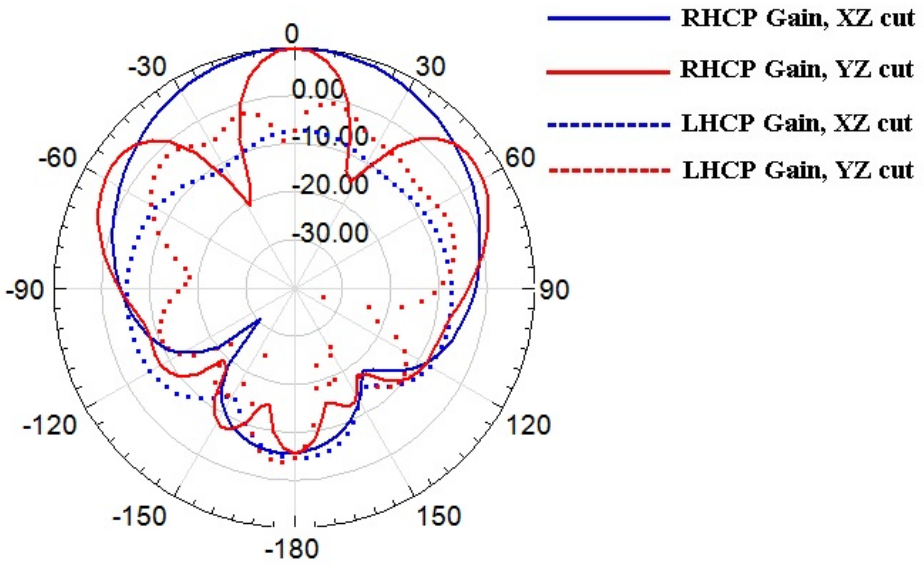

Fig. 4.17: RHCP radiation pattern at 2.43 GHz.

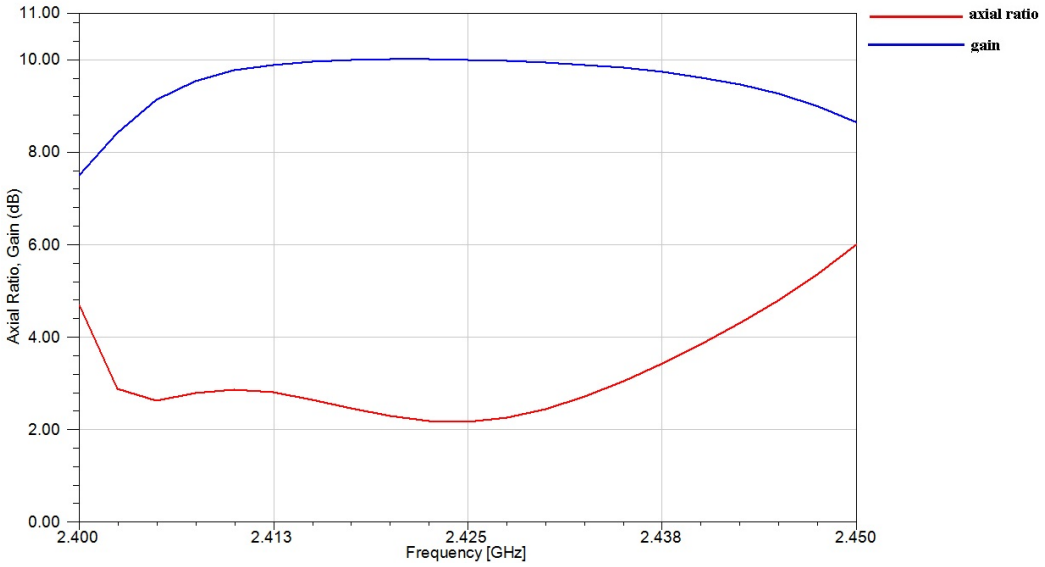

Fig. 4.18: CP axial ratio and gain sweep.

Chapter 5

Antenna Fabrication, Measurement, and Integration with CubeSat

5.1 Fabrication One

A variation of the antenna in Fig. 4.1 was manufactured using PCB technology. This variation is shown in Fig. 5.1 with the the exploded view shown in Fig. 5.2. The design consists of a cavity with an area of the size of a face of a 3U CubeSat (83 mm x 340 mm), loaded with two layers of Rogers Duroid 5880 as shown in the figure. Each Rogers substrate has a thickness of 1.575 mm. The slots are etched on the top copper surface of the first substrate, and a stripline feed is printed on the top surface of the second substrate. To ensure that no gap exists between the two substrates, a FR4 substrate bonding layer was introduced between the two substrates to join them together. The FR4 material has a dielectric constant of 4.3 at 1 MHz, and it has a thickness of 0.127 mm. The sidewalls of the cavity were made using conductive copper tape. The positions and dimensions of the slots are given in Table 5.1.

The stripline for the dual-band excitation of the slots, between the substrate layers, started as a 50 Ohm line 4 mm from the edge of the cavity, extends for 4 mm, and then branches into two 100 Ohm line that extends for 7 mm and then tapers exponentially into a 25 Ohm line. The taper length is 72 mm. The 25 Ohm line extends in a straight line for 47.7 mm, bends in a quater circle of radius 5.8 mm and the extends for 18 mm. The 25 mm line then divides at a t-junction into two 50 Ohm lines. The 50 Ohm line are then matched to the slots for dual-band excitation. In this design, the offset length (dol) and offset positions (dop1 and dop2) annotated in Fig. 3.32 are 14 mm, 32.65 mm, and 0.65 mm, respectively. dfb is 6.635 mm. The width for a 100 Ohm, 50 Ohm, and 25 Ohm stripline

are 0.53 mm, 2.3 mm, and 5.8 mm, respectively.

For the circular polarization excitations, probe 1 has an x displacement of -10 mm, and a y displacement 2.5 mm, and it gives RHCP, probe 2 has a x displacement of 10 mm, and a y displacement of 2.5 mm, and it gives LHCP. In this design, a probe feed is modelled as the inner conductor of a 50 Ohm coaxial cable of radius 0.6272 mm whose outer radius 2.1 mm.

Table 5.1: Slot position on cavity.

slot	length (mm)	x (mm)	y (mm)
1	58	0	0
2	62	0	34
3	10	0	70.5
4	41	0	93.5
5	41	0	139.5

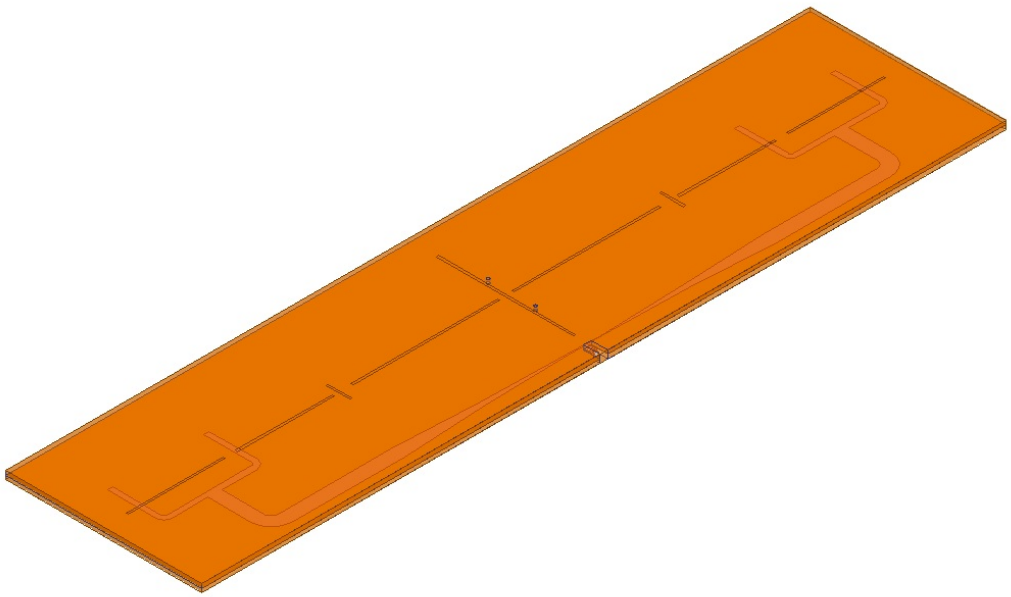

Fig. 5.1: A model of the multifunctional antenna to be manufactured using PCB technology.

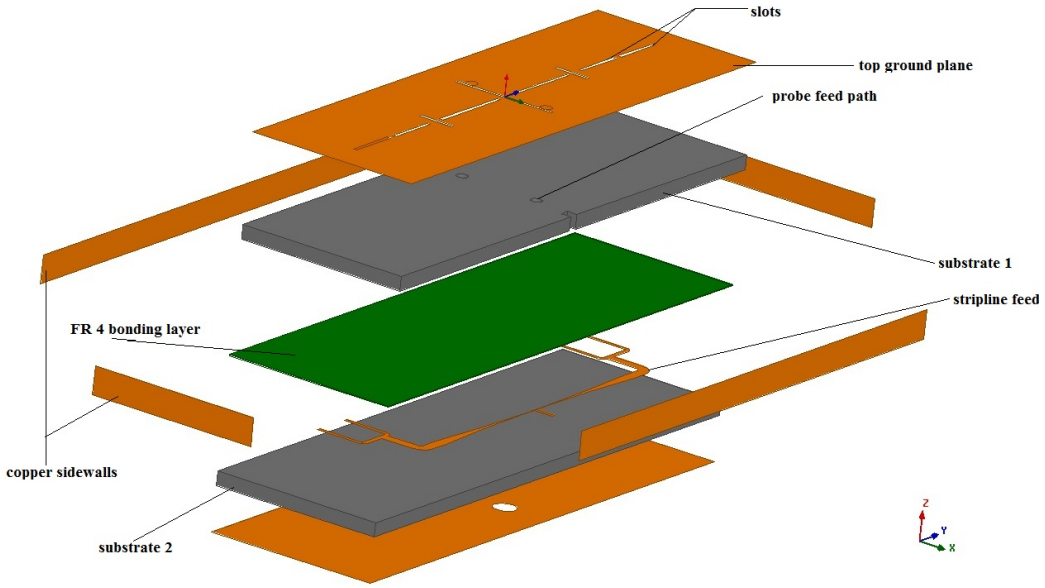

Fig. 5.2: The exploded view of the multifunctional antenna to be manufactured using PCB technology.

After acceptable results in simulation, the design was sent to a PCB manufacturing compamy for fabrication. The fabricated antenna is shown in Fig. 5.3 after the SMA connectors have been soldered. The fabricated antenna was then measured in the Millimeter Wave Lab and the Anderson Wireless lab at Utah State University. The return losses were measured using a Vector Network Analyzer as shown in Fig. 5.4, and the radiation properties measured in an in-house anechoic chamber as shown in Fig. 5.5.

The simulation and measured results for this multifunctional antenna are presented in Figs. 5.6 - 5.10 below. The measured axial ratio for both senses of circular polarization is about 2 dB at 2.46 GHz as shown in Fig. 5.8.

5.2 Fabrication Two

Another variation of the antenna in Fig. 4.1 was manufactured using a milling machine. This design has solar cells incorporated into it. The solar cells are commercial cells from solarbotics [42]. The design consists of a cavity with the size of a face of a 3U CubeSat (83 mm x 340 mm) loaded with two layers of Rogers Duroid 5880 as shown in the figure. Each substrate has a thickness of 1.575 mm. The slots are etched on the top copper surface of the

first substrate, and a stripline feed is printed on the top surface of the second substrate. To ensure that no gap exists between the two substrates, eight plastic screws were used to join the two substrate layers together. The sidewalls of the cavity were made using conductive copper tape. The model of the antenna is shown in Fig. 5.11. The positions and dimensions of the slots are given in Table 5.2.

The stripline for the dual-band excitation of the slots, between the substrate layers, started as a 50 Ohm line from the edge of the cavity, extends for 11 mm, and then branches into two 100 Ohm line that extends for 15 mm and then tapers exponentially into a 25 Ohm line. The taper length is 72 mm. The 25 Ohm line extends in a straight line for 41.95 mm, bends in a quater circle of radius 5.8 mm and then extends for 14.5 mm. The 25 mm line then divides at a t-junction into two 50 Ohm lines. The 50 Ohm line are the matched to the slots for dual-band excitation. In this design, the offset length (dol) and offset positions (dop1 and dop2) annotated in Fig. 3.32 are 26 mm, 32.15 mm, and 0.65 mm, respectively. dfb is 6.9 mm. The width for a 100 Ohm, 50 Ohm, and 25 Ohm stripline are 0.53 mm, 2.3 mm, and 5.8 mm, respectively.

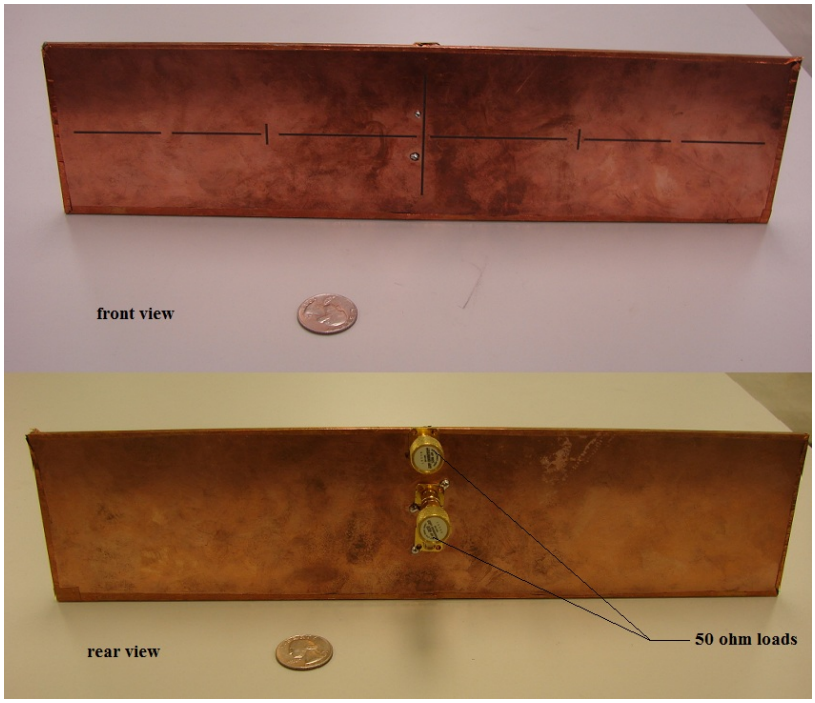

Fig. 5.3: The assembled antenna after PCB manufacture.

Fig. 5.4: Measuring the antenna return loss with a Vector Network Analyzer.

For circular polarization excitations, probe 1 has an x displacement of -11.5 mm and a y displacement 2 mm and it gives RHCP probe 2 has a x displacement of 11.5 mm and a y displacement of 2 mm and it gives LHCP. In this design, a probe feed is modelled as the inner conductor of a 50 Ohm coaxial cable of radius 0.6272 mm whose outer radius 2.1 mm.

After acceptable results were obtained in simulation, the design was fabricated in-house using a milling machine. The assembled fabricated antenna with the solar cells integrated is shown in Fig. 5.12. The fabricated antenna was then measured in the labs at Utah State University. The return losses were measured using a Vector Network Analyzer and the radiation properties measured in an in-house anechoic chamber.

The simulation and measured results for this multifunctional antenna are presented in Figs. 5.13 - 5.17.

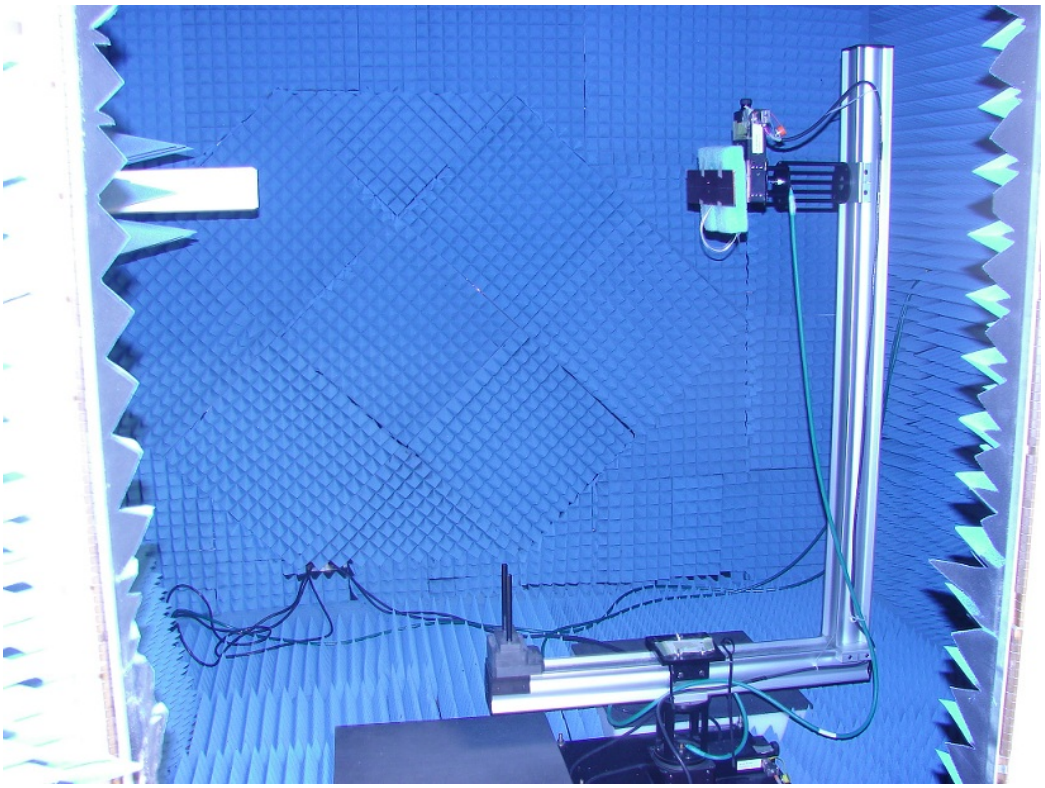

Fig. 5.5: Measuring the antenna radiation properties in an anechoic chamber.

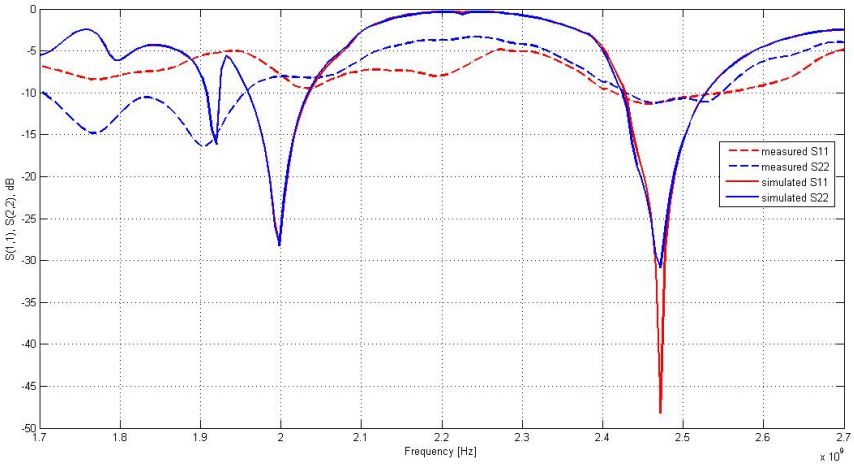

Fig. 5.6: Measured and simulated return loss for the CP ports.

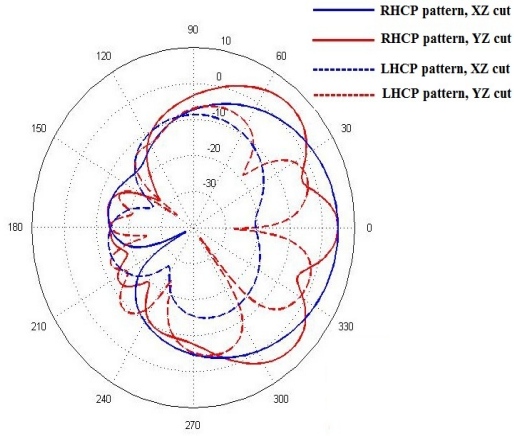

(a) Simulated RHCP radiation pattern for port 1.

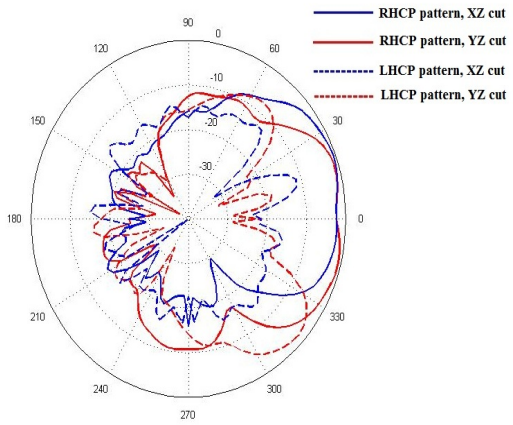

(b) Measured RHCP radiation pattern for port 1.

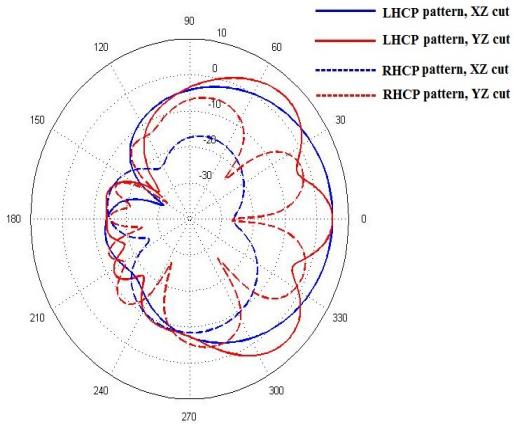

(c) Simulated LHCP radiation pattern for port 2.

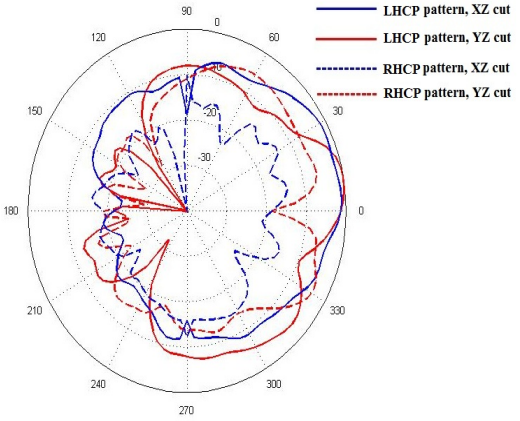

(d) Measured LHCP radiation pattern for port 2.

Fig. 5.7: The simulated and measured circular polarization radiation patterns.

5.3 On the Measured Efficiency and Gain of the Fabricated Antenna

The simulated and measured efficiency and gain of the multifunctional antenna are given in Tables 5.3 and 5.4 shown below. It was observed that despite the high efficiency shown by HFSS in simulation, and the similarities between simulated and measured radiation patterns, the measured efficiency is very low. This low efficiency could be due to the losses incured in the way the antenna was fabricated, and also mutual coupling between the ports. An investigation of how the efficiency and gain of the fabricated antenna can be improved will be left for future work.

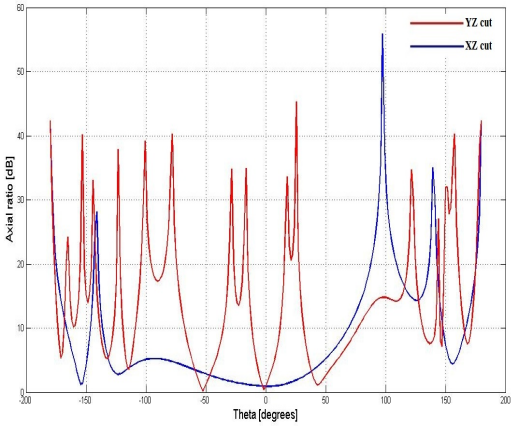

(a) Simulated RHCP axial ratio for port 1.

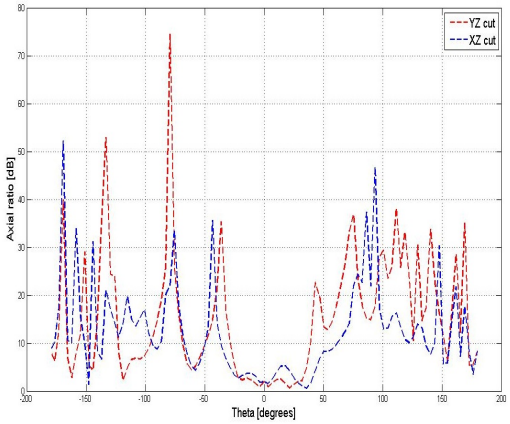

(b) Measured RHCP axial ratio for port 1.

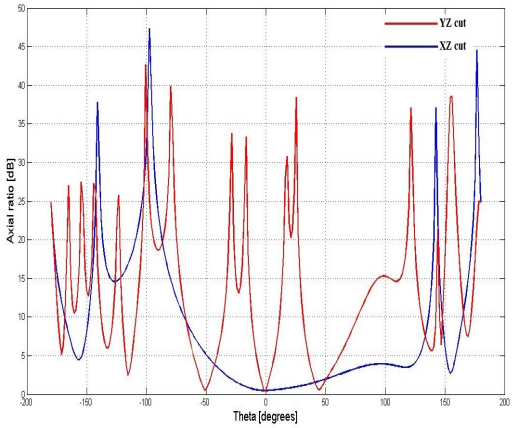

(c) Simulated LHCP axial ratio for port 2.

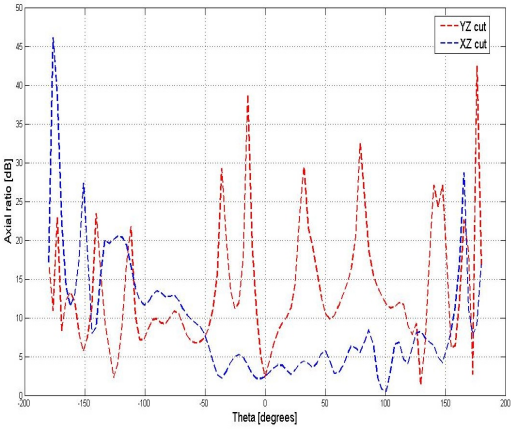

(d) Measured LHCP axial ratio for port 2.

Fig. 5.8: The simulated and measured circular polarization axial ratios.

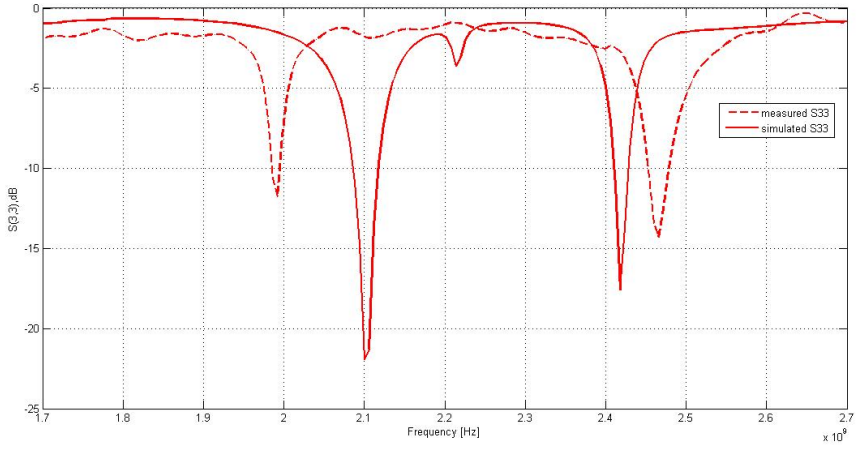

Fig. 5.9: Measured and simulated return loss for the LP port.

5.4 Multifunctional Antennas on CubeSat

Finally, the design above was placed on the surfaces of a CubeSat in simulation as shown in Fig. 5.18. The CubeSat is a 3U CubeSat, and the four of its long faces were fitted with 4 multifuntional antennas. The return losses for all the four RHCP ports of the eight CP ports of the setup are given in Fig. 5.19. The remaining four LHCP ports will have the similar return loss plots as had been seen in previous studies. The radiation pattern when one (RHCP) of the CP ports is excited, with all other ports terminated with matched loads, is given in Fig. 5.20. Furthermore, the return loss plots for all the LP ports are given in Fig. 5.21. Furthermore, the upper band and lower band radiation patterns when one LP port is excited is given in Fig. 5.22. Similar results are obtained when any other port is excited with the others terminated with matched loads. From these simulation results, it can be seen that placing the multifunctional antennas on the CubeSat did not deteriorate the performance of the antenna.

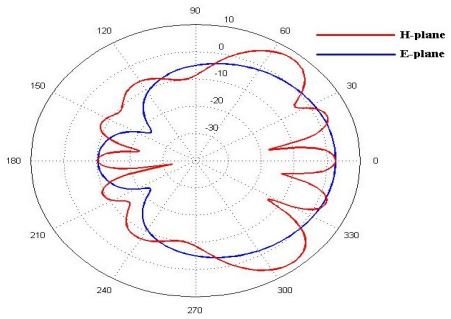

(a) Simulated upper band radiation pattern for port 3.

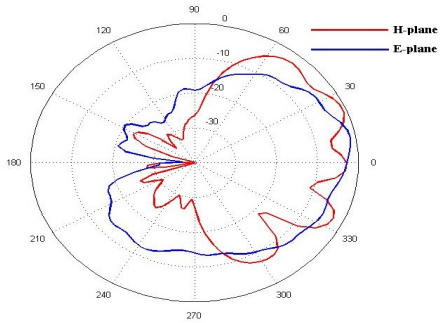

(b) Measured upper band radiation pattern for port 3.

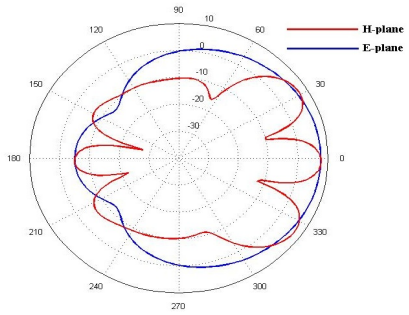

(c) Simulated lower band radiation pattern for port 3.

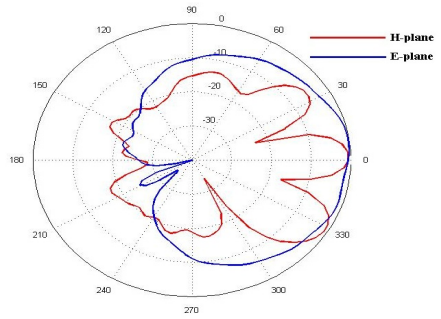

(d) Measured lower band radiation pattern for port 3.

Fig. 5.10: The simulated and measured linear polarization radiation patterns.

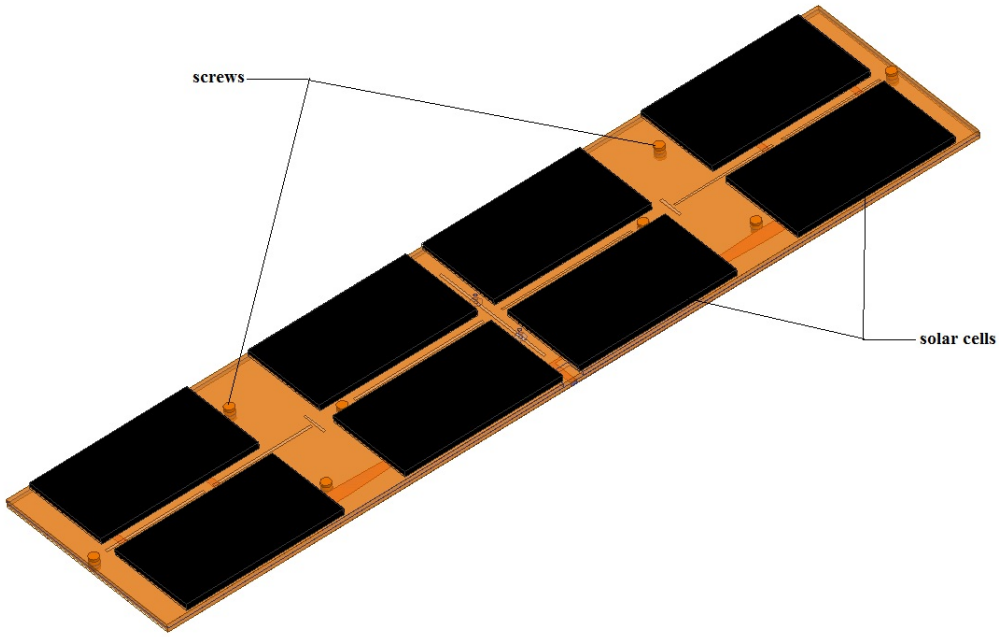

Fig. 5.11: The model of the the multifunctional antenna for milling machine fabrication.

Table 5.2: Slot position on cavity.

slot	length (mm)	x (mm)	y (mm)
1	54	0	0
2	54	0	31
3	10	0	74.5
4	41	0	96.5
5	41	0	141.5

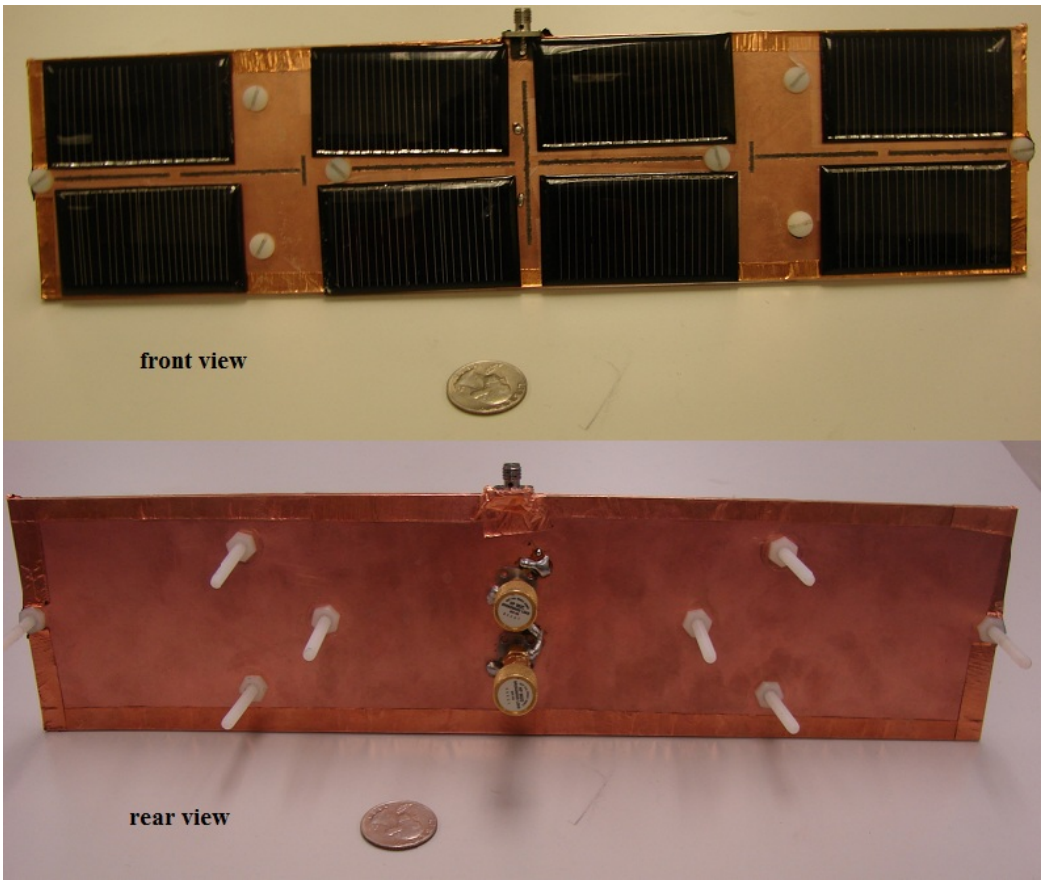

Fig. 5.12: The multifunctional antenna with solar cells integrated.

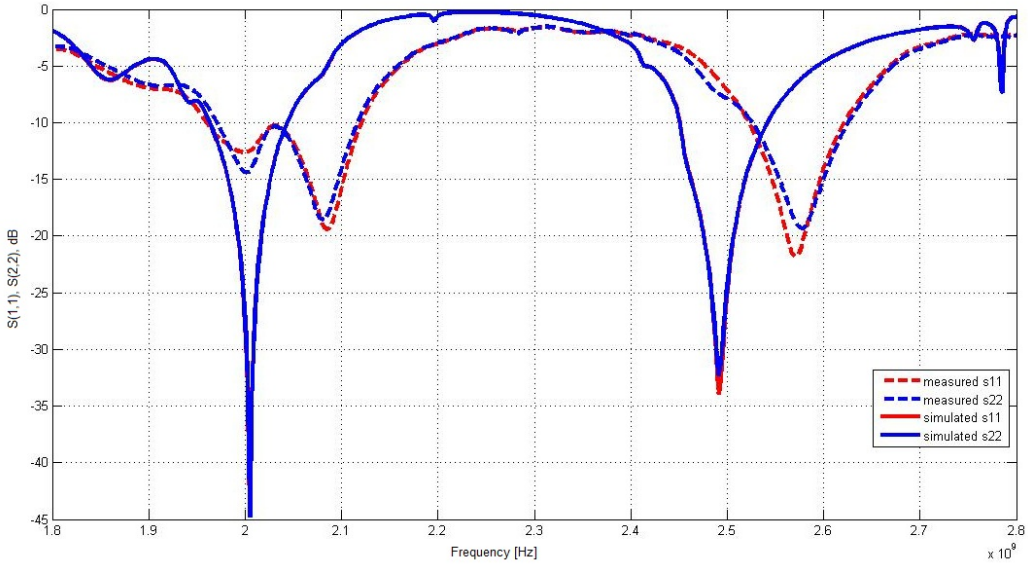

Fig. 5.13: Measured and simulated return loss for the CP ports.

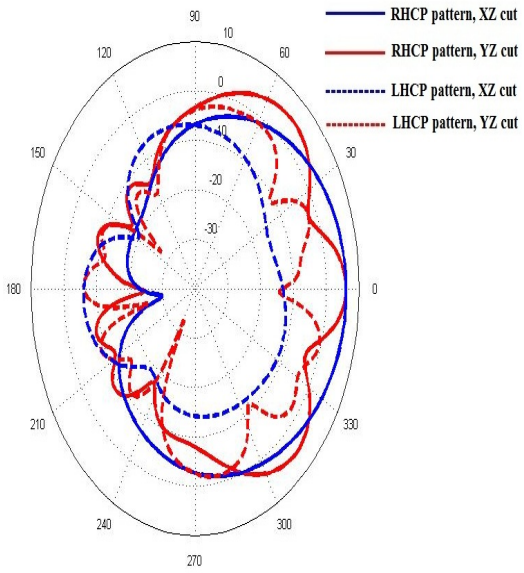

(a) Simulated RHCP radiation pattern for port 1.

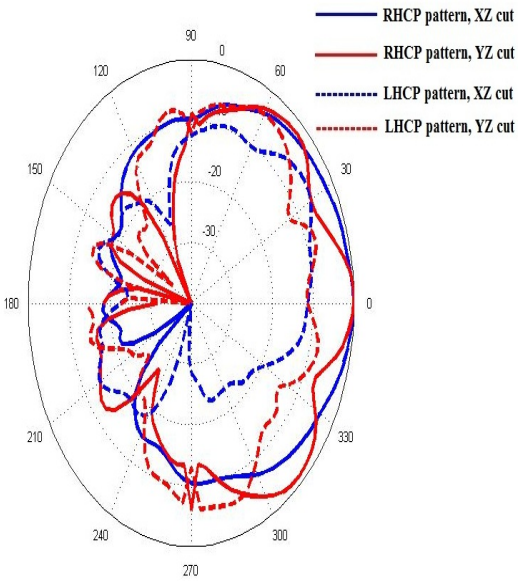

(b) Measured RHCP radiation pattern for port 1.

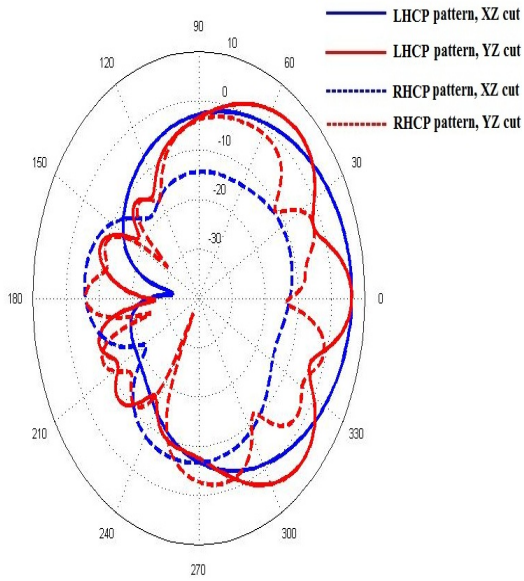

(c) Simulated LHCP radiation pattern for port 2.

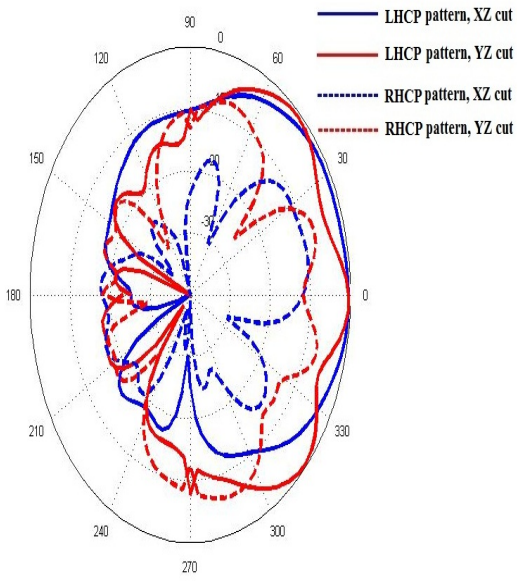

(d) Measured LHCP radiation pattern for port 2.

Fig. 5.14: The measured and simulated circular polarization radiation patterns.

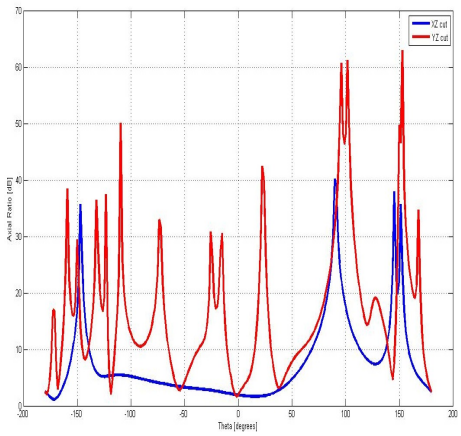

(a) Simulated RHCP axial ratio for port 1.

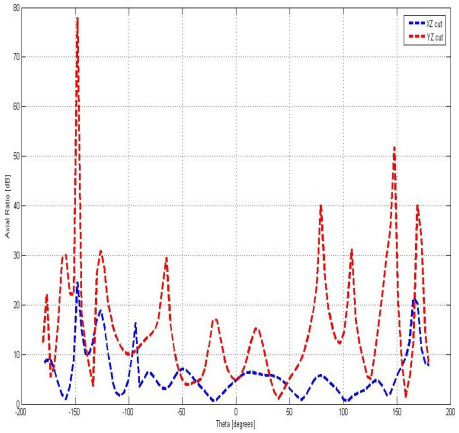

(b) Measured RHCP axial ratio for port 1.

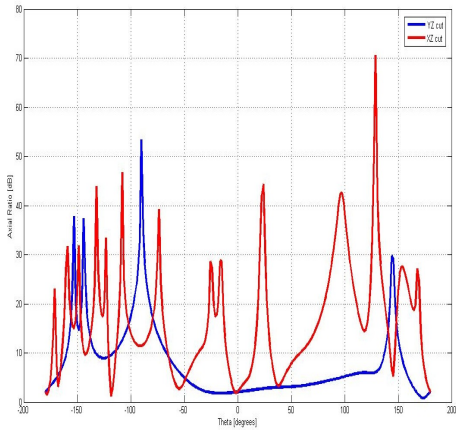

(c) Simulated LHCP axial ratio for port 2.

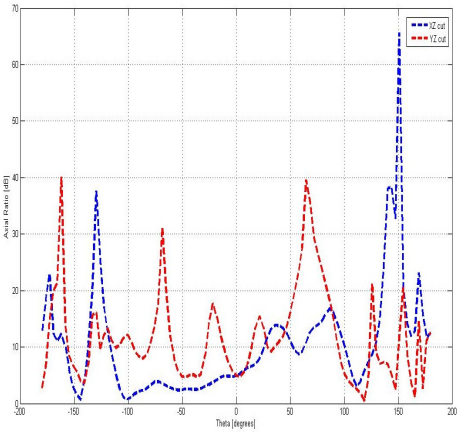

(d) Measured LHCP axial ratio for port 2.

Fig. 5.15: The simulated and measured circular polarization axial ratios.

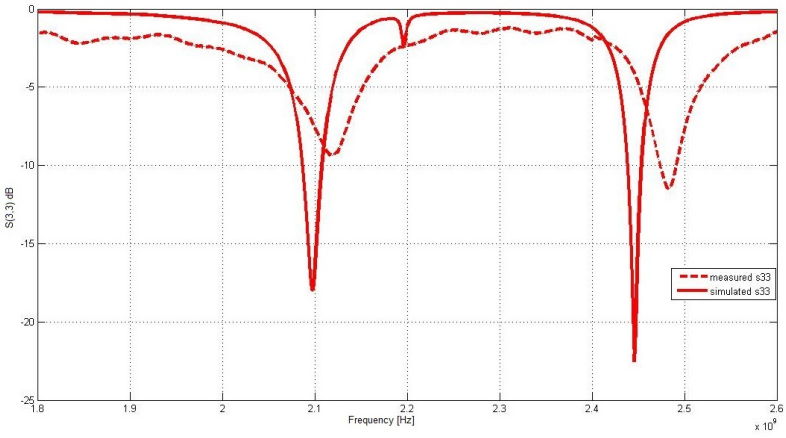

Fig. 5.16: Measured and simulated return loss for the LP port.

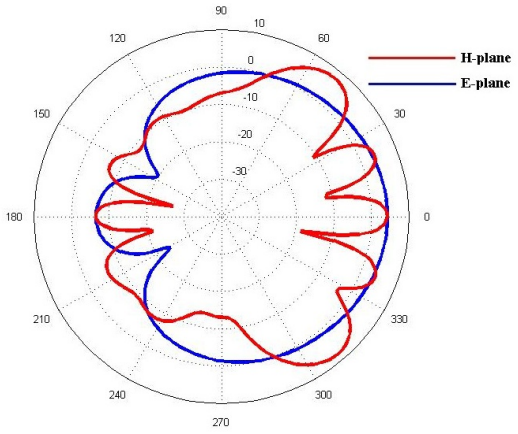

(a) Simulated upper band radiation pattern for port 3.

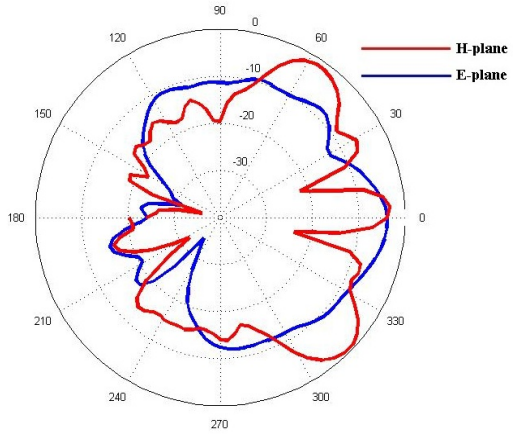

(b) Measured upper band radiation pattern for port 3.

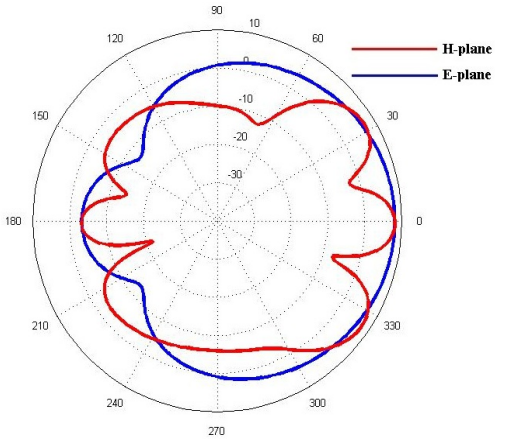

(c) Simulated lower band radiation pattern for port 3.

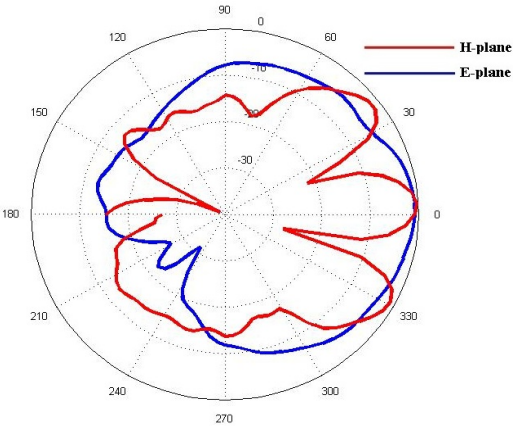

(d) Measured lower band radiation pattern for port 3.

Fig. 5.17: The measured and simulated circular polarization radiation patterns.

Table 5.3: The simulated and measured gains of antenna one.

Port	Simulated Gain (dB)	Simulated Efficiency (%)	Measured Gain (dB)	Measured Efficiency (%)
port 1	5.0	80	-5.0	5
port 2	5.0	80	-5.7	4
port 3 (upper band)	2.6	80	1.4	16
port 3 (lower band)	7.7	88	0.53	10

Table 5.4: The simulated and measured gains of antenna two.

Port	Simulated Gain (dB)	Simulated Efficiency (%)	Measured Gain (dB)	Measured Efficiency (%)
port 1	6	90	-3.1	12
port 2	6	90	-2.7	13
port 3 (upper band)	4.3	90	3.3	26
port 3 (lower band)	8.2	99	3.5	26

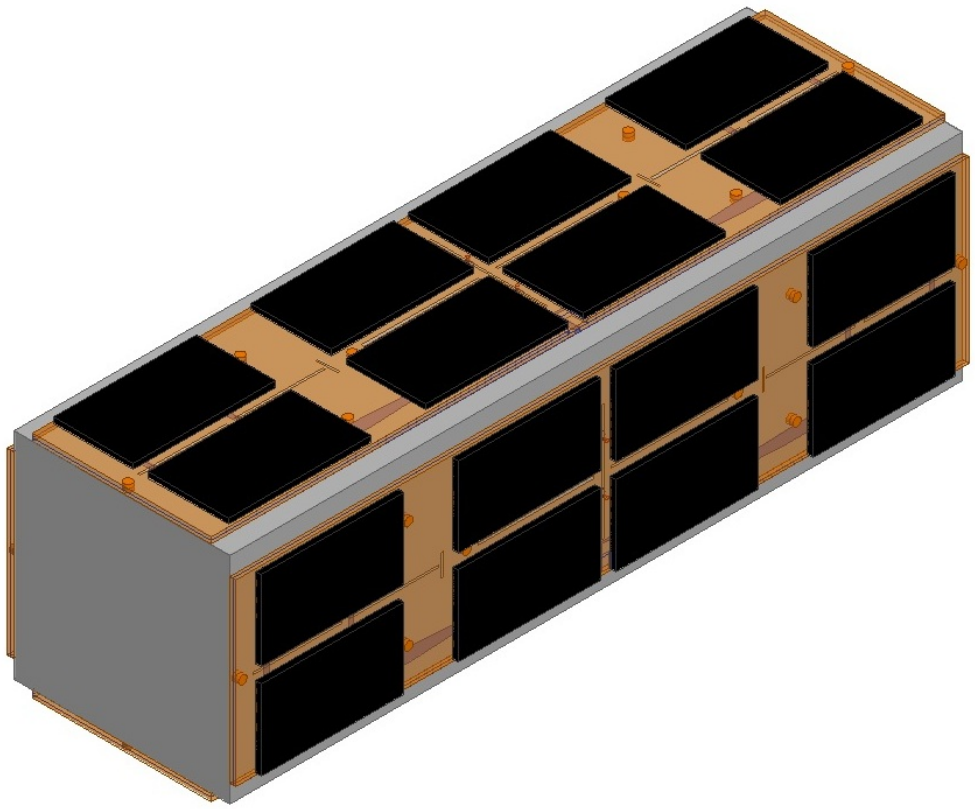

Fig. 5.18: The multifunctional antennas with solar cells integrated placed on a 3U CubeSat.

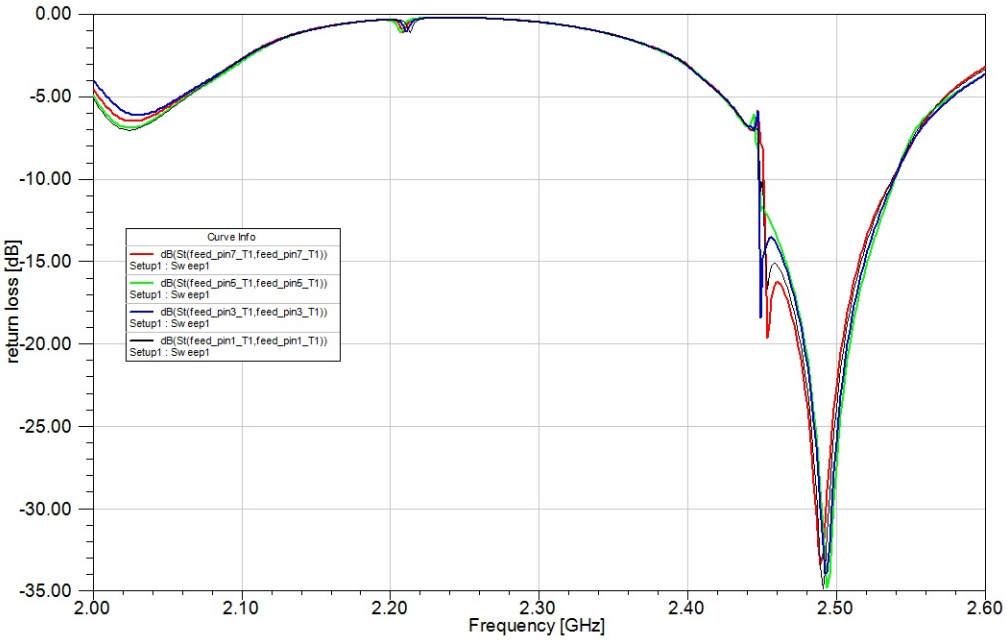

Fig. 5.19: RHCP port return losses for the four multifunctional antenna on a 3U CubeSat.

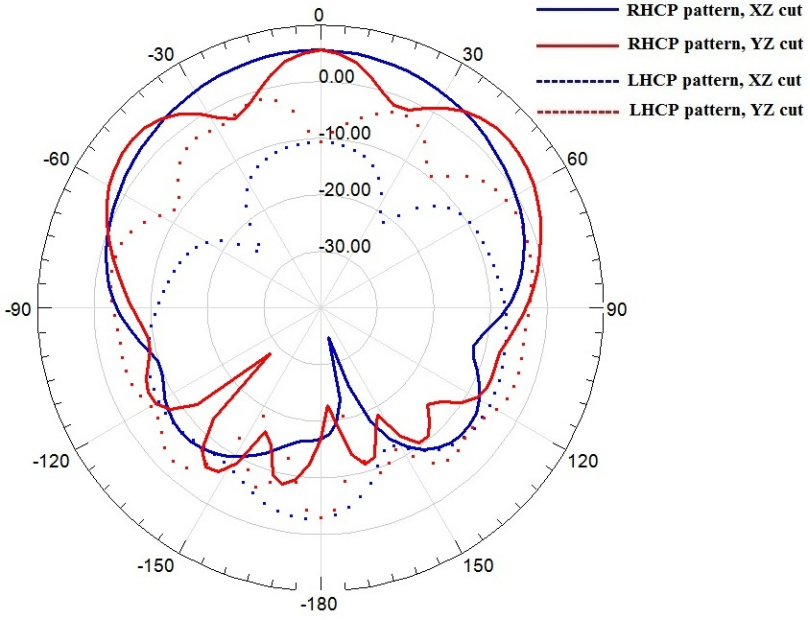

Fig. 5.20: The radiation pattern from a RHCP port.

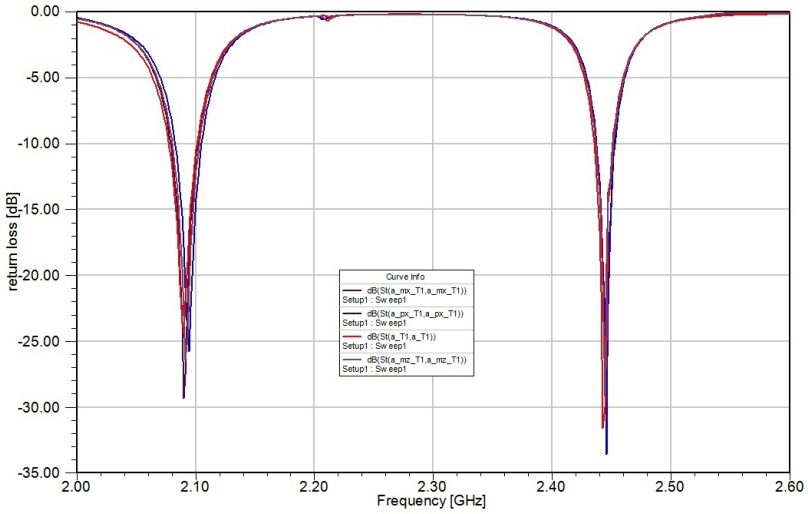

Fig. 5.21: LP dual-band port return losses for the four multifunctional antenna on a 3U CubeSat.

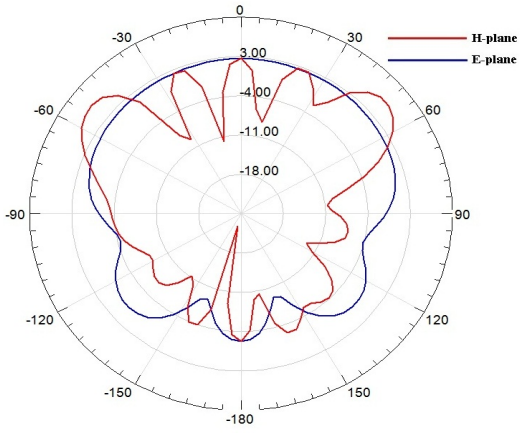

(a) Upper band radiation pattern for one LP port on the four multifunctional antenna on a 3U CubeSat.

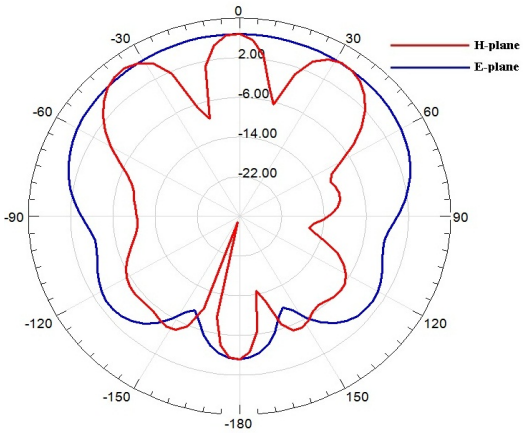

(b) Lower band radiation pattern for one LP port on the four multifunctional antenna on a 3U CubeSat.

Fig. 5.22: The dual-band linear polarization radiation patterns of four multifunctional antennas on a 3U CubeSat.

Chapter 6

Conclusions and Future Work

In this thesis, it has been demonstrated how a cavity-backed slot antenna can be used to realize and antenna that exhibits multiple impedance and radiation properties by using multiple slots which are selectively excited. Different CP radiation pattern can be realized by a playing with the layout of the slots on the cavity. Furthermore, alternate sense of CP can be realized by the location of the excitation probe feed. In addition, to achieve optimum gain for CP radiation, the slots and the cavity need to be tuned together. Dual-band linearly polarized function can be realized by two proximal slots in series excited by a strip line. The radiation pattern of the dual-band LP in a antenna having two or more dual-band subarray can be controlled by adjusting the spacing between the subarrays. In short, a single struture which provides multiple frequencies, multiple radiation patterns, and multiple polarizations can be realized by selectively exciting the multiple slots etched on a metallic cavity.

The fabricated multifunctional antenna, in spite of its attractive properies, has a low efficiency, and therefore a low gain. The reason why the fabricated antenna has low efficiency should also be investigated for improved design in future.

In future, a systematic relationship between the layout of the slot on the cavity, and the resulting circular polarization radiation pattern may be established, such that when a particular CP radiation pattern is dictated, the slot layout for this pattern could easily be derived. Furthermore, since the slots in the multifunctional antenna in this thesis are selectively excited manually (exciting a port, and maually loading the ports with matched load), it will be desired in future to introduce an the external electronic switching circuits for selective excitation of the slots. This external switching circuitry could be developed and integrated with the antenna design, eliminating the neeed for manual switching used in this

design in this thesis. Finally, the design in Fig. 5.18, where four multifuctional antennas are placed on a CubeSat, can be further investigated for the case in which two or more ports are excited simultaneously. In such a case, ports on different faces of the CubeSat can be excited together, and phase shifted to see the radiation pattern possibilites. With the three different types of port on each of the four CubeSat surfaces, the radiation possibilites are many.

References

[1] K. Woellert, P. Ehrenfreund, A. Ricco, and H. Hertzfeld, "Cubesats: Cost-effective science and technology platforms for emerging and developing nations," *Advances in Space Research*, vol. 47, no. 4, pp. 663–684, 2011.

[2] Small Satellite Home Page. [Online]. Available: http://centaur.sstl.co.uk/SSHP/sshp_classify.html.

[3] "Cubesat design specification, rev 12," *California Polytechnic State University, San Luis Obispo*, 2009.

[4] Gunter's Space Webpage. [Online]. Available: http://space.skyrocket.de/doc_sdat/perseus-000.htm.

[5] Clyde Space Webpage. [Online]. Available: http://www.clyde-space.com/cubesat_shop/solar_panels

[6] A. Toorian, K. Diaz, and S. Lee, "The cubesat approach to space access," in *Aerospace Conference*. IEEE, 2008, pp. 1–14.

[7] Spectrolab Webpage. [Online]. Available: http://www.spectrolab.com/solarcells.htm

[8] Emcore Webpage. [Online]. Available: http://www.emcore.com/solar_photovoltaics/space_solar_cells

[9] Spectrolab Webpage. [Online]. Available: http://www.spectrolab.com/DataSheets/PV/PV_NM_TASC_ITJ.pdf

[10] Ultra Triple Junction (UTJ) Solar Cells Data Sheet. [Online]. Available: http://www.spectrolab.com/DataSheets/cells/PV%20UTJ%20Cell%205-20-10.pdf.

[11] Spectrolab Webpage. [Online]. Available: http://www.spectrolab.com/faq.htm

[12] Space Dynamics Laboratory Webpage. [Online]. Available: http://www.sdl.usu.edu/news/press/2011/oct29-dice-launch-hj

[13] Small Satellite Home Page. [Online]. Available: http://www.smallsat.org/

[14] S. Vaccaro, J. Mosig, and P. de Maagt, "Two advanced solar antenna solant designs for satellite and terrestrial communications," *Antennas and Propagation, IEEE Transactions*, vol. 51, no. 8, pp. 2028–2034, 2003.

[15] S. Gao, K. Clark, M. Unwin, J. Zackrisson, W. Shiroma, J. Akagi, K. Maynard, P. Garner, L. Boccia, G. Amendola *et al.*, "Antennas for modern small satellites," *Antennas and Propagation Magazine, IEEE*, vol. 51, no. 4, pp. 40–56, 2009.

[16] A. Eatchel, R. Fevig, C. Cooper, J. Gruenenfelder, J. Wallace, U. Fink, L. Schooley, and A. Hudor, "Development of a baseline telemetry system for the cubesat program at the university of arizona," in *International Telemetry Conference*, 2002.

[17] D. Kuester and P. Radhakrishna. (2007) A 2.4 ghz high speed communications system for cubesat applications. Colorado University. [Online]. Available: http://spacegrant.colorado.edu/COSGC_Projects/symposium_archive/2007/papers/S07_02_HSCOM_presentation.pdf

[18] Colorado space grant consortium. [Online]. Available: http://spacegrant.colorado.edu/index.php/current-projects/255-hermesobjectives.

[19] W. Alomar, J. Degnan, S. Mancewicz, M. Sidley, J. Cutler, and B. Gilchrist, "An extendable solar array integrated yagi-uda uhf antenna for cubesat platforms," in *Antennas and Propagation (APSURSI), 2011 IEEE International Symposium*. IEEE, pp. 3022–3024, 2011.

[20] K. Doerksen, J. Levesque, and I. Mas, "Design, modeling and evaluation of a 2.4 ghz fhss communications system for narcissat," in *17th AIAA/USU Conference on Small Satellites*, 2003.

[21] R. Mathur, R. Haupt, and C. Swenson, "Student antenna design for a nanosatellite," in *Aerospace Conference, IEEE Proceedings*, vol. 7, pp. 7–3688, 2001.

[22] T. Turpin and R. Baktur, "Meshed patch antennas integrated on solar cells," *Antennas and Wireless Propagation Letters, IEEE*, vol. 8, pp. 693–696, 2009.

[23] A. Genc, T. Turpin, T. Yasin, and R. Baktur, "Active integrated meshed patch antennas for small satellites," *Microwave and Optical Technology Letters*, vol. 54, no. 7, pp. 1593–1595, 2012.

[24] P. Muri, O. Challa, and J. McNair, "Enhancing small satellite communication through effective antenna system design," in *MILITARY COMMUNICATIONS CONFERENCE*. IEEE, pp. 347–352, 2010.

[25] M. Mahmoud, "Integrated solar panel antennas for cube satellites," Master's thesis, Utah State University, Logan, 2010.

[26] C. A. Balanis, *Antenna Theory: Analysis and Design, 3rd Edition*, 3rd ed. New York: Wiley-Interscience, Apr. 2005.

[27] H. Booker, "Slot aerials and their relation to complementary wire aerials (babinet's principle)," *Electrical Engineers-Part IIIA: Radiolocation, Journal of the Institution of*, vol. 93, no. 4, pp. 620–626, 1946.

[28] J. Yun and R. Vaughan, "Open slot antenna in a small ground plane," *Microwaves, Antennas & Propagation, IET*, vol. 5, no. 2, pp. 200–213, 2011.

[29] High Frequency Structural Simulator. [Online]. Available: www.ansys.com.

[30] R. Garg, *Microstrip Antenna Design Handbook*. Boston, MA: Artech house publishers, 2001.

[31] *RT/duroid 5880 Datasheet*, Rogers Corporation, www.rogerscorp.com.

[32] Advanced Design System (ADS), www.agilent.com.

[33] Y. Yoshimura, "A microstripline slot antenna (short papers)," *Microwave Theory and Techniques, IEEE Transactions*, vol. 20, no. 11, pp. 760–762, 1972.

[34] A. Hadidi and M. Hamid, "Aperture field and circuit parameters of cavity-backed slot radiator," in *Microwaves, Antennas and Propagation, IEE Proceedings H*, vol. 136, no. 2, IET, pp. 139–146, 1989.

[35] E. Eldesouki, K. Hussein, and A. El-Nadi, "Circularly polarized arrays of cavity-backed slot antennas for x-band satellite communications," *Progress In Electromagnetics Research*, vol. 9, pp. 179–198, 2008.

[36] Q. Li and Z. Shen, "Inverted microstrip-fed cavity-backed slot antennas," *Antennas and Wireless Propagation Letters, IEEE*, vol. 1, no. 1, pp. 98–101, 2002.

[37] M. Mahmoud and R. Baktur, "A dual band microstrip fed slot antenna," *Antennas and Propagation, IEEE Transactions*, no. 99, pp. 1–1, 2011.

[38] D. Pozar, *Microwave Engineering*. New York: John Wiley and Sons, 2005.

[39] Q. Li and Z. Shen, "An inverted microstrip-fed cavity-backed slot antenna for circular polarization," *Antennas and Wireless Propagation Letters, IEEE*, vol. 1, no. 1, pp. 190–192, 2002.

[40] D. Sievenpiper, H. Hsu, and R. Riley, "Low-profile cavity-backed crossed-slot antenna with a single-probe feed designed for 2.34-ghz satellite radio applications," *Antennas and Propagation, IEEE Transactions*, vol. 52, no. 3, pp. 873–879, 2004.

[41] J. Bernhard, "Reconfigurable antennas," *Synthesis Lectures on Antennas*, vol. 2, no. 1, pp. 1–66, 2007.

[42] 37 x 66 mm monocrystalline solar cell. Solarbotics Ltd. [Online]. Available: http://www.solarbotics.com/product/scc3766.